**UNIVERSIDADE DE BRASÍLIA - UNB**

**INSTITUTO DE GEOCIÊNCIAS - IG**

**PROGRAMA DE PÓS-GRADUAÇÃO EM GEOLOGIA**

# Coberturas lateríticas do SW do cráton amazônico: aspectos geofísicos e geoquímicos.

Edgar Romeo Herrera de Figueiredo Iza

**Tese de Doutorado Nº 140**

**Brasília, 9 de outubro de 2017.**

**UNIVERSIDADE DE BRASÍLIA - UNB**

**INSTITUTO DE GEOCIÊNCIAS - IG**

**PROGRAMA DE PÓS-GRADUAÇÃO EM GEOLOGIA**

# Coberturas lateríticas do SW do cráton amazônico: aspectos geofísicos e geoquímicos.

**DISCENTE**

Edgar Romeo Herrera de Figueiredo Iza

**Banca Examinadora:**

**Dra. Adriana Maria Coimbra Horbe (Orientadora)**

**Dr. Álvaro Penteado Crósta**

**Dr. Augusto César Bittencourt Pires**

**Dr. Rômulo Angélica Simões**

**Brasília, 9 de outubro de 2017.**

**UNIVERSIDADE DE BRASÍLIA - UNB**

**INSTITUTO DE GEOCIÊNCIAS - IG**

**PROGRAMA DE PÓS-GRADUAÇÃO EM GEOLOGIA**

Tese de doutorado apresentada ao Programa de Pós Graduação em Geologia do Instituto de Geociências da Universidade de Brasília em cumprimento ao requisito parcial para a obtenção do Título de Doutor em Geologia, área de concentração geologia regional.

A Tese foi julgada adequada e aprovada em sua forma final.

**Autor:**

Edgar Romeo Herrera de Figueiredo Iza

**Banca Examinadora**

**Dra. Adriana Maria Coimbra Horbe**

**(Orientadora)**

**Dr Augusto César Bittencourt Pires**

**Examinador Interno**

**Dr. Álvaro Penteado Crosta**

**Examinador Externo**

**Dr. Rômulo Angélica Simões**

**Examinador Externo**

**Brasília, DF, 9 outubro de 2017.**

**DEDICATÓRIA**

A Isabel Iza Echeverria Herrera,

Ana Júlia Iza Herrera e Matheus Iza Herrera.

## Agradecimentos

Agradeço inicialmente ao grande arquiteto do universo.

A minha paciente esposa Isabel Leonor Iza E. Herrera pelas noites acordadas e pelo suporte técnico ao longo de todo o trabalho.

Aos meus pais Gilvan Assunção de Figueiredo, Rosilda Carvalho de Figueiredo e Giovanna Rósula de Figueiredo pelo incentivo e palavras de apoio ao longo de toda a caminhada.

Ao amigo e guia espiritual, Roberto Nascimento.

Ao amigo Cassiano Costa e Castro pelo apoio inclusive nas etapas de campo.

A minha orientadora Adriana Maria Coimbra Horbe pela confiança e orientação.

Ao Serviço Geológico do Brasil/Companhia de Pesquisa de Recursos Minerais – CPRM pelo apoio nas etapas de campo, cessão das imagens aerogeofísicas e análises químicas.

A todos que contribuíram de alguma forma com a elaboração desta tese de doutorado.

**Resumo**

O estudo do regolito laterítico provê informações geológicas, metalogenéticas e pedogenéticas importantes, especialmente quando integrado com estudos geomorfológicos, geoquímicos, geofísicos e técnicas matemáticas. Os próprios lateritos são considerados excelentes testemunhos paleoambientais. Desse modo, realizaram-se estudos geofísicos e geoquímicos, na porção sudoeste do cráton amazônico, com o fim de desenvolver métodos para cartografar o regolito laterítico e os lateritos, assim como compreender a evolução da paisagem.

A área principal de pesquisa deste trabalho (área sul) está localizada na porção sul do estado de Rondônia (sudoeste do cráton amazônico) e tem aproximadamente 17.000 km$^2$. Nesta área foram coletados os dados da pesquisa assim como desenvolvidas todas as técnicas. A área secundária ou de comparação (área norte), está localizada na porção norte do estado de Rondônia e tem aproximadamente 4000 km$^2$ e foi utilizada com o objetivo de avaliar a eficiência das técnicas desenvolvidas na área sul. Dentre os principais resultados obtidos destacam-se a existência de lateritos imaturos em grande parte colunares, pisolíticos/nodulares e celulares compostos principalmente por goethita, hematita, caulinita e secundariamente gibbsita e quartzo. Os perfis lateríticos da área podem ser completos ou truncados. Os lateritos ocorrem em duas principais superfícies de aplanamento, sendo que a superior (SAS) ocorre no intervalo altimétrico entre 500 e 627 m e a inferior ocorrendo abaixo de 300 m.

A integração multifonte (altimetria e aerogeofísica - gamaespectrometria) utilizando as lógicas booleana e *fuzzy*, permitiu a definição de áreas potenciais para a presença de lateritos. Estas áreas foram averiguadas com trabalhos de campo o que possibilitou a comprovação da eficiência do modelo de detecção de áreas potenciais para presença de lateritos.

Na etapa seguinte criou-se o índice de intensidade de intemperismo (WII) no intuito de mapear/delimitar as áreas mais ou menos intemperizadas. O WII foi desenvolvido a partir da integração e correlação de dados aerogeofísicos (gamaespectrometria) e altimétricos, utilizando-se para tanto, uma regressão múltipla de dados. O WII destacou pelo menos 4 domínios com distintos níveis intempéricos, variando de intensamente intemperizado a pouco intemperizado. Os domínios mais intemperizados mostraram excelente correlação com os dados do modelo de detecção de áreas potenciais para a presença de lateritos. As áreas menos intemperizadas do WII coincidiram com domínios com maior frequência de exposição de saprolito e rocha sã (dados de campo). Desse modo, o referido índice mostrou-se robusto, constituindo-se em uma importante ferramenta de apoio ao mapeamento do regolito/geológico, além de ter contribuído com as interpretações dos dados geoquímicos. O índice laterítico (LI)

foi desenvolvido, neste trabalho, como ferramenta de suporte ao mapeamento do regolito e de lateritos. Na sua concepção considerou-se apenas dados gamaespectrométricos, especialmente as razões Th/K e U/K. Os resultados mostraram-se coerentes e ratificaram os dados apresentados no WII e no modelo de detecção de áreas potenciais para a presença de lateritos.

O índice máfico (IM) foi aplicado com o objetivo de averiguar as possíveis fontes dos lateritos. Na superfície inferior e na porção norte da área, os resultados mostraram que tanto rochas mais magnéticas (máficas) quanto menos magnéticas são as possíveis fontes dos lateritos. No domínio centro-sudeste há maior influência de rochas menos magnéticas (félsicas).

As principais associações geoquímicas do regolito foram avaliadas por meio de dados de solo, sedimento de corrente e litoquímica dos lateritos. Os resultados geoquímicos não evidenciaram anomalias importantes no que diz respeito ao seu aproveitamento econômico (metalogenético). Em todo caso, as principais associações geoquímicas foram identificadas e correlacionadas com os padrões geofísicos observados no WII. As áreas mais intemperizadas (WII) evidenciaram forte associação com os elementos Al-Ce-Ga-Hf-La-Tb-Th-U-Y e Zr, enquanto áreas menos intemperizadas evidenciaram forte associação com Ba-Be-Ca-Cs-K-Li-Mg-Na-Rb-Sr. A geoquímica também ratificou os resultados do índice máfico na medida que destacou associações máficas e félsicas relacionadas aos lateritos.

O mapa do regolito da área foi elaborado por meio de dados de campo e apoiado com os resultados obtidos pelo WII, IL e IM, e permitiram a reinterpretação das áreas anteriormente mapeadas como coberturas sedimentares indiferenciadas. Nesse aspecto, as áreas associadas a processos supergênicos/pedogenéticos/residuais foram significativamente ampliadas, o que pode contribuir para a abertura de novas fronteiras prospectivas. Na etapa final, os métodos de identificação dos lateritos desenvolvidos para a área deste trabalho foram comparados com os métodos desenvolvidos no norte do Estado de Rondônia. Ambos mostraram-se eficientes, entretanto, ficou claro que cada área possui características específicas (altitudes distintas, diferentes intervalos de ocorrência, contexto geomorfológico distintos, etc.) que implicam na necessidade de adaptações dos referidos modelos para cada área. Em todo caso, a integração multifonte, assim como o modelo previsional para a presença de lateritos, os índices WII, IL e IM mostraram-se robustos para sua finalidade. Portanto, recomenda-se suas aplicações como ferramentas pré, sin e pós campo no intuito de incrementar as interpretações e as próprias atividades operacionais inerentes aos mapeamentos geológico, geomorfológico e pedológico.

**Palavras-chave**: regolito, Th/K, crostas lateríticas, WII, índice laterítico.

**Abstract**

The study of the lateritic regolith provides important geologic, metallogenic and pedogenetic information, especially when integrated with geomorphologic, geochemical, geophysical studies and mathematical techniques. The lateritic duricrusts are considered excellent paleoenvironmental testimonies. In this sense, geophysical and geochemical studies were developed, in the southwest of the Amazon craton, aiming to develop methods of mapping lateritic regolith and lateritic duricrusts, as well as to understand the evolution of the landscape.

The main study area of this work (southern area) is located in the southern portion of the Rondônia State (southwest of the Amazon craton) and has approximately 17,000 km$^2$. In the area all data were collected, all the techniques were developed and the principal results were obtained. The secondary area or comparison area (northern area), is located in the north side of the Rondônia State and has about 4000 km$^2$. This area was used aiming to evaluate the efficiency of the techniques developed in the southern area. Among the main results obtained, it can be highlighted the existence of immature lateritic crusts, mainly columnar, pisolithic/nodular and cellular, consisting majorly of goethite, hematite, kaolinite, and secondarily gibbsite and quartz. The lateritic profiles of the area can be complete or truncated. The lateritic duricrusts occur mainly on two major planation surfaces, the upper surface (UPS) on altitudes between 500 and 627 m and the lower planation surface (LPS) on altitudes below 300 m.

The multisource integration (altimetry, aerogeophysics – gamma-ray spectrometry) using the Boolean and fuzzy logics, allowed the definition of potential areas for the occurrence of lateritic duricrusts. These areas were checked with field words, which made possible the verification of the efficiency of the predictability model for the occurrence of lateritic duricrusts for the study area.

On the next stage, it was created the weathering intensity index (WII) in order to map/delimit the areas more or less weathered. The WII was developed from the integration and correlation of aerogeophysical (gamma-ray spectrometry) and altimetric data, using a multiple regression. The WII highlighted at least 4 domains with different weathering levels, varying from intensely weathered to weakly weathered. The more intensely weathered domains showed an excellent correlation with the data from the predictability model of the occurrence of lateritic duricrusts. The less weathered area coincided with domains dominated by saprolite and rocky outcrops (field data). Therefore, the referred index showed to be robust, becoming an important support tool for the regolith/geologic mapping, besides having contributed with the

geochemical interpretations. The lateritic index was developed in this work as a support tool for the regolith and lateritic duricrusts mapping. In its conception, it was considered only gamma-ray spectrometric data, especially the Th/K and U/K ratios. The results were coherent and ratified the results presented on the WII and on the predictability model for the occurrence of lateritic duricrusts.

The mafic index (MI) was applied to verify the possible sources of the lateritic duricrusts. On the LPS and on the north side of the area, the results showed that both, magnetic rocks (mafic) and less magnetic rocks are the possible sources of the lateritic duricrusts. On the central-southeast of the area, there is a greater influence of less magnetic rocks (felsic).

The main geochemical associations of the regolith were evaluated from soil, stream sediments and lithochemistry of the lateritic duricrusts data. The geochemical results did not evidence important anomalies regarding the economic exploitation (metallogenic). The main geochemical associations were identified and correlated with the geophysical patterns observed on the WII. The more intensely weathered areas (WII) evidenced strong association with Al-Ce-Ga-Hf-La-Tb-Th-U-Y and Zr, while less weathered areas evidenced strong association with Ba-Be-Ca-Cs-K-Li-Mg-Na-Rb-Sr. The geochemistry also ratified the results of the mafic index, as it highlighted mafic and felsic associations related to lateritic duricrusts.

The regolith map of the area was prepared from field data and supported with the results obtained in the previous stages (WII, LI, MI), and allowed the reinterpretation of the areas previously mapped as undifferentiated sedimentary covers. In this sense, the areas associated with supergene/pedogenetic/residual processes were significantly expanded, which can contribute with the opening of new prospective frontiers. On the final stage, the methods for the identification of lateritic duricrusts developed for the study area were compared with techniques developed in an area on the northern portion of the state of Rondônia. Both showed to be efficient, however, it is clear that each area has specific characteristics (different altitudes and intervals of occurrence of lateritic duricrusts, different relief and geomorphologic features, etc.) that imply the necessity of adaptation of the referred models for each area. In a general view, the integration of multisource data, as well as the predictability model for the occurrence of lateritic duricrusts, the WII, LI and MI indexes showed to be robust tools for the regolith and lateritic duricrusts cartography. Therefore, it is suggested their application as tools to be used pre, syn and post field, in order to expand the interpretations and the operational activities related to the geologic, geomorphologic and pedologic mapping.

**Keywords**: regolith, Th/K, lateritic duricrusts, WII, lateritic index.

# LISTA DE FIGURAS

# LISTA DE TABELAS

# SUMÁRIO

# CAPÍTULO 1 - INTRODUÇÃO

# 1 INTRODUÇÃO E ESTRUTURA DA TESE

Esta tese de doutorado apresenta um estudo da integração de dados multi-fonte (gamaespectrometria, magnetometria, altimetria, geoquímica de solo e sedimento de corrente) e tem como foco o regolito laterítico e os próprios lateritos. Os estudos foram desenvolvidos principalmente em uma área localizada no sudoeste da Amazônia brasileira, mais especificamente na porção sul do estado de Rondônia (área sul), onde ambos têm ampla ocorrência. Partes das técnicas desenvolvidas foram aplicadas em uma área localizada na porção norte do estado de Rondônia (área norte) com o intuito de testar e avaliar a eficiência dos resultados obtidos na área sul.

A tese foi organizada em 5 capítulos principais sendo o primeiro a introdução, onde serão abordados: a estrutura da tese, os lateritos e a importância do seu estudo, justificativa e referencial teórico, objetivos, localização e acessos, e por fim serão apresentados os materiais e métodos de forma resumida. O segundo capítulo constitui-se no artigo científico intitulado: *Boolean and fuzzy methods for identifying lateritic regoliths in the Brazilian Amazon using gamma-ray spectrometric and topographic data*, publicado na revista Geoderma, versão online em fevereiro de 2016 e na revista física no Volume 269, p 27-38, em maio do mesmo ano. O terceiro capítulo trata da gamaespectrometria, magnetometria e geoquímica aplicada ao estudo do regolito laterítico, intitulado *Integration of geochemical and geophysical data to characterize and map lateritic regolith: an example in the Brazilian Amazon.* Está na forma de artigo científico e foi submetido na revista Chemical Geology em julho de 2017. O quarto constitui-se na comparação entre a metodologia apresentada neste trabalho e os resultados apresentados por Herrera (2016). Por fim o quinto capítulo corresponde às considerações finais.

Desse modo os artigos foram concatenados de forma a destacar inicialmente a aplicação de dados aerogeofísicos (gamaespectrometria) e SRTM com ênfase a cartografia das crostas lateríticas (capítulo 2). O segundo artigo corroborou os resultados do primeiro, mas avançou no sentido de aprofundar as técnicas de cartografia, ampliando-as e complementando-as com a integração de dados geoquímicos e com o desenvolvimento de ferramentas, tais como, o índice de intensidade do intemperismo (WII) e o índice laterítico (LI) (capítulo 3). A etapa seguinte (capítulo 4) destacou aspectos da aplicação das técnicas de cartografia das crostas evidenciando sua eficiência em duas áreas distintas (comparação entre as áreas norte e sul). Na etapa final (considerações finais) destacaram-se, além de outros resultados, a aplicabilidade das técnicas desenvolvidas nesta tese de doutorado.

## 1.1 OS LATERITOS E A IMPORTÂNCIA DO SEU ESTUDO

O estudo do regolito tem permitido a compreensão dos processos supergênicos, pedológicos, geomorfológicos e contribuído para prospecção mineral. A lateritização é um dos importantes processos envolvidos na formação do regolito (formação de solos, formação de platôs lateríticos, etc.) no enriquecimento supergênico e no modelamento da paisagem, ocorrendo em condição de clima tropical (Anand e Paine, 2002). Neste processo há decomposição de grande parte dos minerais primários, formação de novos minerais, lixiviação de elementos químicos mais solúveis e/ou concentração dos minerais resistatos e dos elementos menos solúveis (Freyssinet *et al.*, 2005).

Christofoletti (1980) destaca que o estudo das formas de relevo, construídas pelos processos geológicos, contribui para uma maior compreensão da dinâmica geomorfológica sob diversas condições climáticas. Para Bigarella *et al.* (1996), os processos lateríticos estão relacionados à geomorfologia quando interessada em aspectos do relevo (platôs). No caso da pedologia o foco é especificamente o aproveitamento agrícola e no caso da geologia a ênfase principal é nos recursos minerais.

Em todo caso, os lateritos se formam a partir da alternância de períodos secos e úmidos (clima tropical) e mostram, segundo Moss (1965) e Thomas (1974), íntima relação com diversas formas de relevo tais como, chapadas e mesas, escarpas na margem de planaltos, terraços, paleo-pavimentos detríticos, etc. Nesse contexto, autores como Thomas, (1974); Penteado (1978), Büdel, (1982), entre outros, destacam a afinidade dos lateritos com os processos geomorfológicos, seu papel na manutenção das paleosuperfícies e geração das superfícies aplanadas. Thomas (1974) avalia os processos químicos e físicos de desenvolvimento dos lateritos e sua relação com questões climáticas (tropicais) e geomorfológicas. O autor enfatiza, entre outros resultados, que a erosão de terrenos lateríticos pode produzir inversão de relevo, ou seja, desenvolvimento de paleosuperfícies de erosão. Essas últimas permanecem preservadas nas cimeiras devido ao consequente rebaixamento erosivo diferencial de áreas não protegidas pelo capeamento laterítico.

A relação dos lateritos com o desenvolvimento do relevo e sua influência na preservação e formação das superfícies aplanadas é também discutida por Penteado (1978). A autora destaca que os lateritos conservam paleosuperfícies originadas em ambientes tropicais de savana e complementa afirmando que elas reduzem a erosão, facilitam o escoamento superficial impedindo a infiltração, proporcionado assim o desenvolvimento de uma paisagem aplanada.

Por outro lado, Costa *et al.* (1996), ao abordar os aspectos da neotectônica na Amazônia, destacam o papel dos lateritos como horizontes de referência para os estudos neotectônicos. Os autores sugerem a ação de uma neotectônica especialmente marcada no Mioceno sobre os lateritos maturos e no Pleistoceno sobre os imaturos, estendendo-se até os tempos atuais.

Smith *et al.* (2000) discutem o uso e implicações das superfícies de aplanamento na exploração mineral na Austrália. Os autores destacam que o mapeamento do regolito e/ou controle do relevo são importantes para a compreensão dos processos supergênicos; e ressaltaram que pelo menos 13 depósitos de ouro foram descobertos na Austrália entre 1983 e 1994, por meio de estudos geoquímicos dos perfis lateríticos integrados ao mapeamento do regolito.

A importância entre as diversas áreas de estudo relacionadas ao regolito e sua associação com a paisagem é destacada por Taylor e Eggleton (2001). Outro aspecto discutido pelos autores é o da exploração dos regolitos, especialmente como fonte de minerais metálicos (Al, Fe, Mn, Ni, Cu, Pb, Au), além de agregados para construção civil.

Em todo caso, áreas com presença significativa de crostas lateríticas são conhecidas em várias partes do mundo, especialmente associadas ao cinturão intertropical (latitudes menores que 30º). No Brasil, o estudo do regolito laterítico com ênfase aos aspectos geofísicos e geocronológicos ainda é pouco difundido, apesar dos lateritos serem a fonte principal de Al (bauxita) e do processo laterítico aumentar a concentração de vários elementos como Sn, Au, Mn, Ni, P, muitas vezes viabilizando sua explotação econômica (Costa 1997, Costa *et al.* 2005 e Costa 2008). Em Rondônia há diversas ocorrências minerais, garimpos e minas associadas a perfis lateríticos, notadamente aqueles vinculados ao Sn, Mn e áreas potenciais para ETR e Au, entre outros (Costa 1991). Por exemplo, Costa (2008) destaca que o forte potencial mineral da Amazônia está relacionado a províncias lateríticas, em especial a de Carajás.

O estudo do regolito laterítico provê, portanto, informações geológicas, metalogenéticas e pedogenéticas importantes, sobretudo quando integrado com estudos geomorfológicos, geoquímicos, geofísicos e métodos matemáticos (Thomas, 1974; Büdel, 1982; Beauvais, 1999; Tardy e Roquin, 1998; Butt e Zeegers, 1992; Taylor e Eggleton, 2001; Anand e Paine, 2002; Moreira *et al.,* 2003; McBratney *et al.,* 2003; Carranza, 2009; Carrino *et al.,* 2011; Wilford, 2012; Vasconcelos *et al.,* 2015; Arhin *et al.,* 2015, Iza *et al.,* 2016b, Herrera, 2016, entre outros).

## 1.2 JUSTIFICATIVA E REFERENCIAL TEÓRICO

No sudoeste da Amazônia há poucos trabalhos relacionados ao tema lateritos e apenas os mais recentes integram dados multifonte, (Guerra, 1952 e 1953; McNeil, 1978; Costa, 1991; Della-Justina, 1994; Costa *et al.* 1996; Quadros e Rizzotto, 2007; Adamy, 2010; Nascimento, 2011; Nascimento *et al.* 2012; Oliveira e Filho, 2013; Castro, 2015; Herrera *et al.* 2016a; e Iza *et al.,* 2016b).

Os estudos pioneiros de Guerra (1952 e 1953) registraram lateritos em Rondônia com ênfase a Guajará-Mirim e Porto Velho. O autor discute os lateritos abordando aspectos geoquímicos, mineralógicos e suas respectivas ocorrências. Entre suas discussões, Guerra (1953) evidencia a existência de uma pequena cachoeira na cidade de Porto Velho situada sobre lateritos. Essa e outras evidencias geomorfológicas são utilizadas como argumento de um possível afundamento recente da rede hidrográfica fazendo, portanto, clara referência à atuação neotectônica na região, assim como discutido por Costa *et al.* (1996).

Os processos lateríticos nas proximidades de Guajará-Mirim/RO, mais exatamente, na região do Iata foram discutidos por McNeil (1978). A autora aborda questões relacionadas ao avançado nível de lateritização da região e a presença de platôs enfatizando a falta de planejamento da colonização e a fertilidade restrita dos lateritos.

A exploração de lateritos em Porto Velho foi estudada por Della-Justina (1994), que enfatizou os aspectos sócio-econômicos-ambientais relacionados e, entre outros resultados, cartografou os lateritos, cadastrando as principais frentes de lavra associadas. Adamy (2010), entre outras avaliações, destaca a importância dos lateritos como insumos para construção civil, além do potencial metalogenético associado ao ouro, ferro e manganês. O referido autor mostra ainda que a principal edificação portuguesa no território rondoniense, o forte Príncipe da Beira, foi integralmente construída com blocos de lateritos e é atualmente um dos principais pontos turísticos do Estado.

Nascimento *et al.* (2012) discutiram questões referentes ao uso/aplicação dos lateritos localizados em Porto Velho e entorno. Além de outros resultados, os autores enfatizaram a relação de relevo jovem colinoso e platôs relacionados a perfis lateríticos imaturos.

Na região sudoeste do cráton amazônico, apesar de não destacarem especificamente a cartografia dos lateritos, os trabalhos de Quadros e Rizzotto (2007), Rizzotto (2010), Quadros *et al.* (2011), Rizzotto (2012), Oliveira e Filho (2013), entre outros, representam os primeiros mapeamentos geológicos sistemáticos com ampla cartografia dos lateritos disponibilizados em

ambiente SIG (sistema de informações geográficas), mas sem nenhuma ênfase aos aspectos geomorfológicos, geoquímicos, geofísicos e geocronológicos.

O mapeamento geológico de Rondônia realizado na escala 1:1.000.000, por Quadros e Rizzotto (2007), destacou, entre outras unidades, as coberturas detrito-lateríticas. Neste trabalho ficou clara a marcante presença de lateritos em todo o Estado. As coberturas sedimentares indiferenciadas também foram mapeadas e descritas como constituídas por produtos sedimentares (argila, silte, areia, cascalho) e produtos derivados de processos residuais, tais como, lateritos, fragmentos resultantes de sua desagregação e solos indiscriminados.

No norte de Rondônia destaca-se o trabalho de Oliveira e Filho (2013) que teve como objetivo principal o levantamento de insumos para construção civil da Folha Porto Velho (cascalho, brita, areia, etc.) e além de outras unidades geológicas mapeou os lateritos na escala 1:100.000.

Castro (2015) estudou os aspectos lateríticos no ocidente da Amazônia baseado em características texturais, mineralógicas e geoquímicas. Em Rondônia, o autor destaca que os perfis podem ser incompletos ou completos de acordo com o nível de truncamento/evolução, e descreve lateritos colunares e vermiformes, localmente pisolíticos formados por goethita e hematita e, subordinadamente, gibbsita. Castro (2015) afirma que os perfis são remanescentes de uma fase erosiva vinculada ao esculpimento da Chapada dos Parecis e ao desenvolvimento do rio Madeira. O autor advoga que a ausência de lateritos bauxíticos e a própria estrutura dos perfis, indicam pouca evolução dos lateritos, provavelmente relacionados ao Plio-Pleistoceno.

O estudo desenvolvido por Herrera *et al.* (2016a) integra dados altimétricos, geológicos e geomorfológicos com a finalidade de melhorar as respectivas cartografias no norte de Rondônia. Os lateritos descritos são ferruginosos, pisolíticos/nodulares e podem apresentar estrutura colunar a megacolunar. Além de outros resultados a correlação dos lateritos com as feições de relevo (platôs) contribuiu significativamente com a cartografia dos mesmos.

Herrera (2016) e Herrera *et al.* (2016b) integraram dados gamaespectrométricos e altimétricos com o objetivo de identificar domínios com lateritos, melhorar a sua cartografia e compreender o padrão de resposta gamaespectrométrico. Os resultados propiciaram, a partir da aplicação do método booleano (*index overlay*), a identificação de novas áreas propícias à ocorrência de lateritos. Os domínios de favorabilidade obtidos permitiram sugerir incrementos cartográficos nos mapas geológico, geomorfológico e de aptidão agrícola em escalas entre 1:250.000 e 1:100.000.

Apesar da expressividade do regolítico laterítico e da existência de dados aerogeofísicos recentes, não há registro de caracterização e/ou estudo do regolito/intemperismo de forma sistematizada no sudoeste do cráton amazônico. A cartografia das crostas lateríticas ainda é inadequada e/ou insuficiente e não reflete a realidade geológica da região. Em muitos casos, áreas mapeadas como coberturas sedimentares indiferenciadas incluem tanto materiais de origem sedimentar quanto residuais (solos e crostas lateríticas). Além disso, a ocorrência de diversos recursos minerais nas adjacências da área, tais como ETR, Ni, Au, entre outros, credencia esta região como forte candidata a estudos relacionados ao intemperismo e processos supergênicos associados.

## 1.3 OBJETIVOS

A proposta desta pesquisa de doutorado é realizar estudos de caracterização geofísica e geoquímica do regolito laterítico na porção sudoeste do cráton amazônico, com o fim de desenvolver métodos para cartografar o regolito laterítico e os lateritos, assim como compreender aspectos da evolução da paisagem. Dentre os objetivos específicos, destacam-se:

1) Definir, no sul do estado de Rondônia, áreas potenciais para a presença de lateritos por meio da integração de dados multifonte (métodos de álgebra de mapas booleana e *fuzzy*);
2) Descrever os tipos de coberturas lateríticas (perfis completos, truncados, tipos de lateritos) na porção sul do estado de Rondônia;
3) Definir as principais associações geoquímicas do regolito, os padrões geofísicos relacionados e os níveis de intemperismo por meio de dados de solo, sedimento de corrente e litoquímica dos lateritos;
4) Desenvolver o mapa do regolito baseado em dados, altimétricos, geológicos, aerogamaespectrometricos, geomorfológicos, pedológicos e índice de intensidade de intemperismo assim como no índice laterítico; e
5) Comparar os resultados deste trabalho com áreas similares (geologia, geomorfologia, etc.) com o objetivo de averiguar a eficiência dos modelos e identificar eventuais discrepâncias.

## 1.4 LOCALIZAÇÃO E ACESSO

A área principal desta pesquisa (área sul) tem cerca de 17.000 km² e localiza-se no sul do estado de Rondônia e parte da porção noroeste do estado do Mato Grosso, próximo à fronteira

com a Bolívia. Localiza-se na Faixa Alto Guaporé com unidades do Mesoproterozoico até o Recente (figura 1.1). Outros detalhes da área podem ser observados nos capítulos 2, 3 e 4.
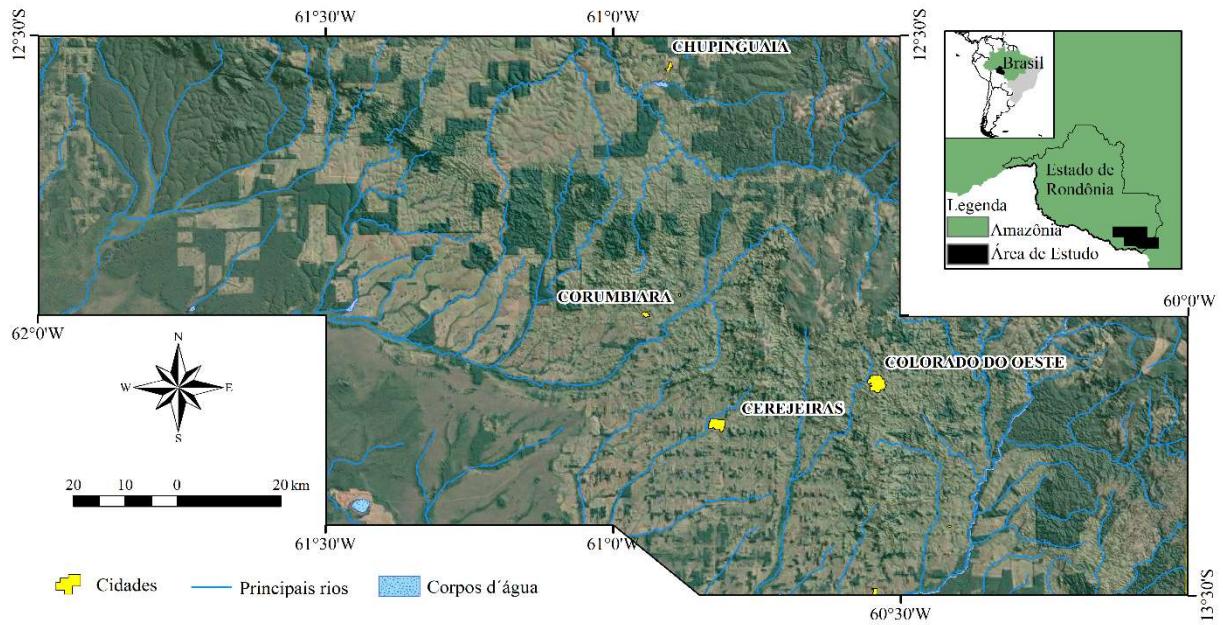


Figura 1.1– Localização da área sul.

A área secundária (área norte) tem cerca de 4000 km$^2$ e localiza-se no norte do estado de Rondônia. Está situada na Província Rondônia-Juruena Faixa Alto Guaporé com unidades do Paleoproterozoico até o Recente (figura 1.2). Detalhes da área podem ser observados no capítulo 4.
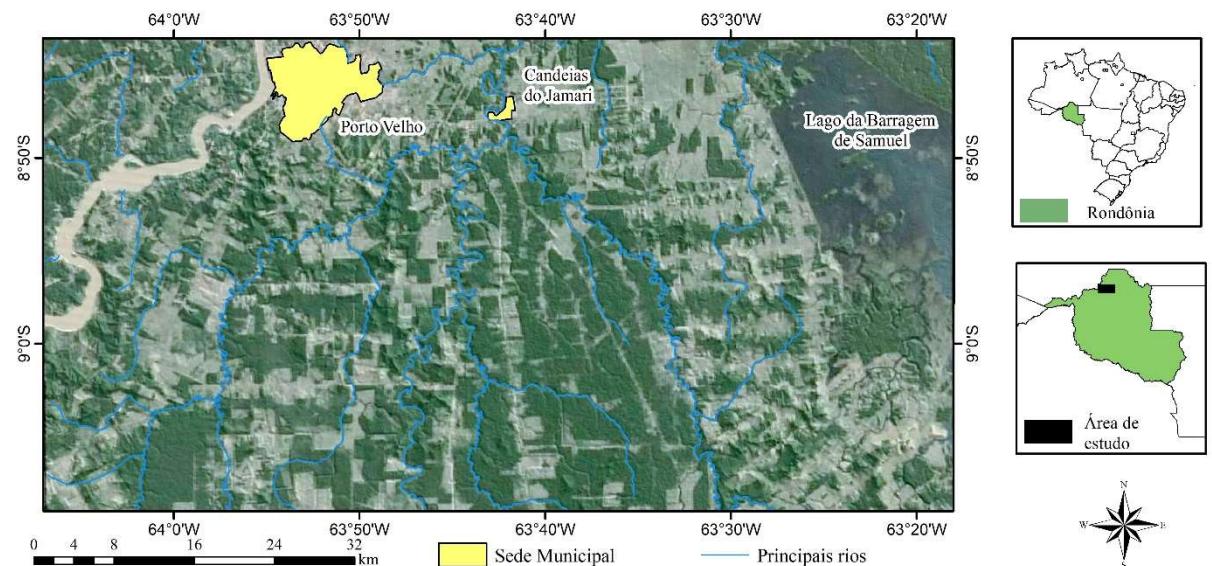


Figura 1.2– Localização da área norte, modificado de Herrera (2016).

## 1.5 MATERIAIS E MÉTODOS

O trabalho priorizou inicialmente a delimitação das áreas potenciais para a presença de lateritos com base na integração de dados digitais de elevação e gamaespectrométricos com apoio de métodos de álgebra de mapas (booleana e *fuzzy*).

A identificação dos lateritos e descrição dos aspectos geomorfológicos associados foram feitas com apoio de verificações de campo e com base em dados geomorfológicos preexistentes, cartas topográficas (IBGE) e imagens SRTM (*Shuttle Radar Topography Mission*) do ano de 2000 com 30 m de resolução espacial.

A aquisição aerogeofísica foi realizada pela FUGRO AIRBORNE SURVEYS para a CPRM/Serviço Geológico do Brasil. Os produtos analisados foram: i) imagens referentes aos canais do eTh, K, eU; ii) razões eU/K, eTh/K; e iii) composições ternárias eTh/K, SRTM, eU/K (RGB) e K, eTh, eU (RGB). Os softwares utilizados foram o Oasis Montaj 8.5 e o ArcGis 10.2 com uma extensão do *Geosoft* que permitiu o processamento das imagens aerogeofísicas e a manipulação integrada de todos os produtos.

A modelagem para o reconhecimento dos lateritos utilizou os métodos booleano e *fuzzy,* que estão embasados em informações prévias ou mesmo hipóteses obtidas por um *expert* (Bonham-Carter, 1994). As etapas de campo permitiram a verificação dos modelos apresentados e os resultados foram posteriormente comparados aos trabalhos de mapeamento prévios de Quadros e Rizzotto (2007) e Rizzotto (2010 e 2012). Detalhes sobre os parâmetros de aquisição dos dados geofísicos, dos métodos booleano e *fuzzy*, além dos resultados, podem ser observados no capítulo 2.

Em seguida, avaliaram-se os dados geoquímicos de sedimento de corrente, solo, além dos dados litoquímicos dos lateritos. O objetivo foi caracterizar quimicamente o regolito e os lateritos e comparar com os resultados geofísicos. Os resultados obtidos nesta etapa foram integrados às áreas previsionais para a presença de lateritos e aos dados de altimetria (SRTM), geomorfologia, geologia e geofísica, proporcionando uma avaliação ampla do potencial geoquímico e de outros aspectos da área (geologia, geofísica, geomorfologia, pedologia, etc.).

A etapa seguinte constou na elaboração do índice de intensidade do intemperismo (WII) que foi desenvolvido com o objetivo de destacar as diferentes intensidades de intemperismo da área. O método é similar àquele proposto por Wilford (2012) para a Austrália, entretanto, algumas alterações foram feitas no intuito de adaptar o modelo à área de estudo. Com a finalidade de identificar apenas áreas lateríticas com os dados gamaespectrométricos, criou-se o índice laterítico (LI) e para tanto utilizou-se as razões entre os elementos considerados móveis

e imóveis no processo intempérico (Th/K e U/K). Posteriormente, foi utilizado o índice máfico (MI) de Pires e Moraes (2006) com o intuito de fazer interpretações sobre as possíveis rochas fontes dos lateritos. Detalhes sobre os métodos, as técnicas estatísticas, correlação com os dados geoquímicos e demais técnicas e resultados obtidos no WII, LI, MI e mapeamento do regolito podem ser consultados, no capítulo 3.

Na fase seguinte realizou-se o mapeamento do regolito baseado na metodologia proposta por Anand e Smith (1993), que subdivide o regolito em três principais classes de regime: residual, erosional e deposicional. Os produtos utilizados na elaboração do mapa do regolito foram os dados altimétricos (SRTM), os mapas pedológicos, geomorfológicos, geológicos, o índice de intensidade do intemperismo (WII) e o índice laterítico (LI). Nesta etapa foram integrados todos os produtos em ambiente SIG (sistema de informação geográfica) e gerado o mapa preliminar do regolito, posteriormente refinado com trabalhos de campo. O produto cartográfico final contribuiu com o entendimento do regolito da área (tipos de produtos, distribuição, etc.).

Na penúltima etapa do trabalho foram comparados os modelos de detecção de áreas potenciais para a presença de lateritos e fragmentos derivados de sua desagregação, assim como latossolos, desenvolvidos por este trabalho e por Herrera (2016), nas porções sul e norte do estado de Rondônia, respectivamente. Na etapa final foram integrados todos os resultados obtidos nesta pesquisa. As atividades previstas e realizadas ao longo do doutorado foram resumidas em grandes temas que são, em parte, correspondentes às publicações científicas relacionadas a este trabalho (Figura 1.3).
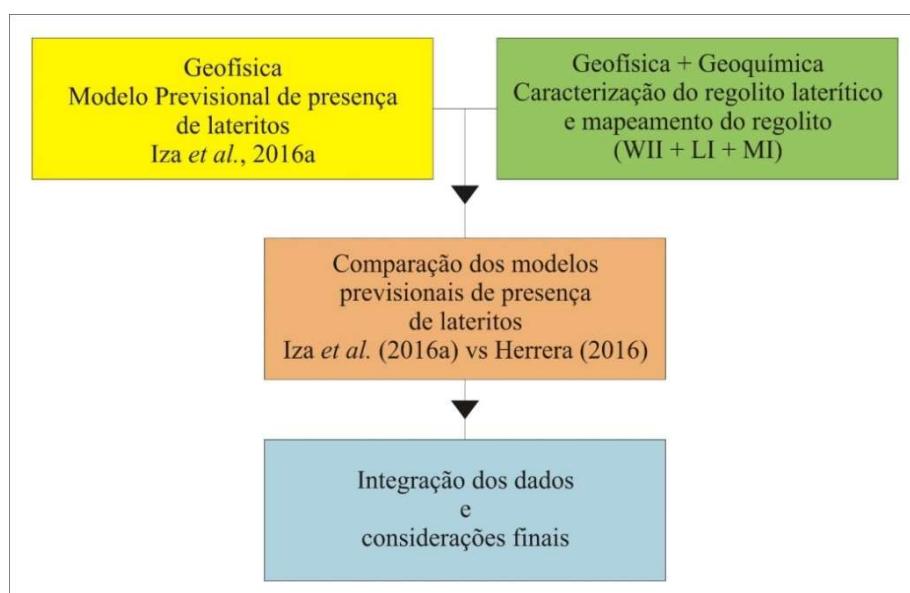


Figura 1.3 – Principais atividades previstas e realizadas ao longo da elaboração da tese. (WII – Índice de Intensidade de Intemperismo; LI – Índice Laterítico; MI – Índice Máfico).

# CAPÍTULO 2

ARTIGO CIENTÍFICO 1


# BOOLEAN AND FUZZY METHODS FOR IDENTIFYING LATERITIC REGOLITHS IN THE BRAZILIAN AMAZON USING GAMMA-RAY SPECTROMETRIC AND TOPOGRAPHIC DATA

# Boolean and fuzzy methods for identifying lateritic regoliths in the Brazilian Amazon using gamma-ray spectrometric and topographic data

CrossMark
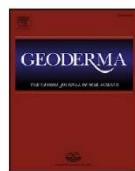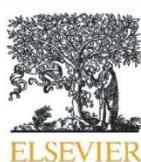
Edgar Romeo Herrera de Figueiredo Iza [a,b,*], Adriana Maria Coimbra Horbe [b], Adalene Moreira Silva [b]

[a] Serviço Geológico do Brasil-CPRM, Av. Lauro Sodré, 2561, São Sebastião, Porto Velho 76801-581, Brazil
[b] Instituto de Geociências, Universidade de Brasília, Campus Universitário Darcy Ribeiro, Brasília 70910-900, Brazil

ABSTRACT

Airborne gamma-ray spectrometry is relatively well understood when associated with rocks, but the response and radioelement distribution in weathered materials is less known. This work used airborne gamma-ray spectrometry and altimetry to identify domains with higher probability of occurrence of lateritic crust and dismantling products in an area located in the west of the Brazilian Amazon. Map algebra was used through the Boolean and fuzzy techniques to create predictability digital models highlighting favorable areas for the occurrence of lateritic crusts. The Index Overlay Method was used in the Boolean technique. The fuzzy technique used the fuzzy algebraic product operator, fuzzy algebraic sum operator, and fuzzy gamma operator. Both models showed good correlation between the favorability predicted and the presence of crusts in the field, however, the fuzzy model showed higher correlation and highlighted areas not identified by the Boolean model. In contrast, the Boolean model allowed the visualization of the areas related to the influence of each variable or its possible combinations individually on the final map. Thus, the identification of lateritic crusts based on mathematic models applied to altimetric and airborne gamma-ray spectrometric data is a new tool that will contribute significantly to geological mapping and to the understanding related to the response and radioelement distribution in weathered materials.

© 2016 Elsevier B.V. All rights reserved.

## 1. Introduction

Throughout Earth's geological history, weathering has been an important process for the modification of the landscape and formation of soils and mineral deposits and has also had a significant impact on controlling the relief and reflecting paleoclimatic variations. In humid tropical climates, lateritic crusts are the final product of weathering (Bardossy and Aleva, 1989; Tardy and Roquin, 1998). The lateritic crusts in the Amazon and along the intertropical belt are related to the Cenozoic (Lucas et al., 1989; Nahon et al., 1989; Boulangé and Carvalho, 1997; Costa, 1997; Horbe and Da Costa, 1999; Kotschoubey et al., 2005; Horbe and Da Costa, 2005).

Climate, relief, parent rock, time, and tectonics are among the main factors that affect intensity of the weathering and erosion processes; thus, these factors are strongly related to geomorphologic aspects. Thomas (1974) stated that climate is an important factor regulating weathering and therefore it determines the nature and speed of the chemical reactions on the Earth's surface. Pomerol et al. (2013) noted that the main factors related to relief evolution are tectonics and climate, whose actions are measured by long geological intervals.

Aleva (1993) and Anand and Paine (2002) noted that the lateritization process is favored by alternation between dry and wet seasons. Within this context, these authors also noted that the water table fluctuates; such fluctuations promote alternations between more or less oxidizing conditions, favor successive iron remobilization, concentrate the iron, and thus lead to the generation of ferruginous nodules. Iron accumulates during lateritization, residually forming lateritic crusts. In arid conditions, the lateritic crust tends to be preserved, thus maintaining the planation paleosurfaces, making such crusts excellent paleogeomorphologic records. In contrast, the permanent humid regime leads to intense chemical leaching and reduced water table fluctuations, thus interrupting the formation of the mottled zone and accelerating saprolite formation and degradation of the lateritic crust, which leads to the generation of oxisols. Horbe and Da Costa (2005) demonstrated the direct relationship between the lateritic crust and the overlying oxisol through textural, mineralogical, and chemical arguments and noted that the latter could be derived from the chemical alteration and consequent disaggregation of the crusts.

Taylor and Eggleton (2001) discussed climatic and topographic factors in the construction of the landscape and exploration of regoliths, particularly for Al, Fe, Mn, Ni, Cu, Pb, and Au, in addition to aggregates for civil construction. According to McFarlane (1976); Büdel (1982); Butt and Zeegers (1992), and Beauvais (1999), among others, the study of regoliths and mapping of lateritic crusts aids in the understanding of

* Corresponding author.
E-mail addresses: edgar.iza@cprm.gov.br (E.R.H.F. Iza), ahorbe@unb.br (A.M.C. Horbe), adalene@unb.br (A.M. Silva).

geomorphologic and paleoclimatic evolution and the identification of anomalous metallogenic occurrences.

The lateritic crusts in the Amazon have not been mapped at adequate scales or are located in areas with limited access. Moreover, in this region as well as other parts of Brazil, lateritic crusts have been mapped as undifferentiated sedimentary covers, which include products such as the lateritic crust itself, oxisols, nodules and pisoliths and other dismantling products. In some of these areas, there are records of several mineral occurrences, such as Ni–Co and Cu–Ni–EGP, and artisanal gold mining (Rizzotto, 2010, 2012a,b). Therefore, the identification and discrimination of lateritic crusts is essential in mineral exploration and useful for the improvement of geological mapping.

The use of the airborne gamma-ray spectrometry and altimetric data in regolith studies must be investigated, especially when applied with mathematical techniques, raster image algebra, and in the evaluation of multi-source data (e.g., Darnley and Grasty, 1971, Tucker et al., 1984, Duval, 1990, Burrough et al., 1992, Graham and Bonham-Carter, 1993, Wilford et al., 1997, Dickson and Scott, 1997, McKenzie & Ryan 1999, Zhu et al., 2010, Carrino et al., 2011, Wilford, 2012 and Dent et al., 2013).

Airborne gamma-ray spectrometry measures the concentration of potassium (K) and series of uranium (U) and thorium (Th) radioisotopes in rocks and soils at depths of 30–45 cm (Gregory and Horwood, 1961; Dickson and Scott, 1997). The intensity of gamma rays emitted from the surface depends on the mineral composition of the rock or regolith, nature and type of weathering, geological heterogeneity, distribution of allochthonous or autochthonous soils and vegetal cover, and humidity, among other factors (Wilford et al., 1997; Minty, 1997; Dickson and Scott, 1997). In general, eU, eTh, and K are the only elements that occur naturally and produce gamma rays with sufficient energy and intensity to be measured by airborne gamma-ray spectrometry (Minty, 1997).

Potassium is the most abundant radioisotope in Earth's crust; it has an average concentration of 2.4% and is generally present with high and low contents in felsic rocks and mafic rocks, respectively (Dickson and Scott, 1997, Minty, 1997). Potassium released during weathering can be partially fixed as illite. In contrast, U and Th are relatively rare compared with K, varying between 3 and 12 ppm on average. Uranium can occur as uraninite and uranothorite, whereas Th can form thorite and may be present in allanite, monazite, xenotime, and zircon at levels higher than 1000 ppm (Dickson and Scott, 1997).

During weathering, radioelements are redistributed due to geochemical reorganization. They can accumulate residually and combine to form stable to weathering minerals, such as monazite, xenotime, zircon, and thorite; alternatively, they can be incorporated into newly formed minerals, such as iron and titanium oxides and hydroxides and clay minerals, or leached. In many cases, this redistribution generates different spectrometric responses for the regolith and underlying bedrock. Dickson and Scott (1997) suggested that areas with lateritic crust tend to have low K contents and relative high Th and U contents. Moreover, Wilford et al. (1997) stated that ferruginous duricrusts, particularly those developed over greenstone, are radiometrically barren (they appear black) in a ternary RBG diagram (KThU).

Wilford et al. (1997) noted that airborne gamma-ray spectrometry is relatively well understood when associated with rocks, but the response and radioelement distribution in weathered materials is less known. Traditional geological and soil mapping can be easily performed when the area is accessible with several outcrops; otherwise, remote tools must be used to reach inaccessible areas, including Indian reservations, deep forests, areas with no roads, and areas where the lateritic crust is covered by soil. Among remote tools, remote sensing and airborne gamma-ray spectrometry can be used to provide important information that may be difficult to collect with other techniques. In accessible areas, these tools can be used as a support in the planning phase of field works, saving field time by increasing the mapping efficiency. Gamma spectrometric data are advantageous in that they provide the radioactive signatures of eTh, eU, and %K, which provide additional information for geologic mapping and can be used as a complementary tool.

The purpose of this work was to use airborne gamma-ray spectrometry and altimetry to identify geophysical and topographic parameters for the delimitation of domains with a higher probability of occurrence of lateritic crust and dismantling products. Boolean and fuzzy techniques are compared using relief and geophysical data (eTh/K, eU/K), with the aim of facilitating field work and improving the final cartographic products.

## 2. Materials and methods

The altimetric base used in this study was the Shuttle Radar Topography Mission (SRTM) performed in 2000, which had a spatial resolution of 30 m. The airborne gamma-ray spectrometric images were obtained by FUGRO AIRBORNE SURVEYS for the CPRM/Geological Survey of Brazil in the 2005–2006 period (refer to the airborne geophysical survey "Sudeste de Rondônia — RO" CPRM, 2006 for further information). The data were processed by LASA Prospecções S.A. and involved the application of routines in Oasis Montaj software, version 8.2.0.5, with minimum curvature interpolators and grid cells of 125 m. The main products generated from the interpolation were individual images of the eU, eTh, and K channels and the ratios eU/K and eTh/K. These products allowed for the generation of the ternary composition of K, eTh, and eU (RGB) as well as eTh/K, SRTM and eU/K (RGB) images. The software used to integrate the data was ArcGIS 10.2 with the Geosoft extension that allowed the processing of the airborne geophysical images and the integrated handling of all of the products. The statistic data were processed and interpreted using Statistica 12 software.

The method developed in this work used airborne geophysical (gamma-ray spectrometric), and elevation (SRTM) images, which were analyzed using Boolean and fuzzy mathematical modeling techniques to create predictability maps for the occurrence of lateritic crusts and verify which of the techniques is more efficient. The theoretical base was extracted from An et al. (1991); Zimmermann (1985); Bonham-Carter (1994); Moreira et al. (2003); McBratney et al. (2003); Lagacherie (2005); Carranza (2008); Carrino et al. (2011) and da Silva et al. (2015). However, some modifications were performed to improve the results.

The modeling process consisted of a series of procedures to obtain a simplified hypothetical vision of the studied attributes and the Boolean and fuzzy techniques were used. These techniques are closely related to knowledge-driven models, i.e., models based on previous information or even hypotheses obtained by an expert (Bonham-Carter, 1994 and Carranza, 2008). Field work was performed to verify and calibrate the models presented, and the geologic maps from Quadros and Rizzotto (2007) and Rizzotto (2010, 2012a) and the map of soils from the Brazilian Institute of Geography and Statistic (IBGE — Instituto Brasileiro de Geografia e Estatística) were used as support.

The kappa coefficient ($\kappa$) was computed to determine the concordance intensity between the models (predictability maps) and field data. The data used consist of information collected during field work for this research, as well as files stored in the GEOBANK (Geological Survey of Brazil database) available online at www.cprm.gov.br. To calculate the coefficient, 875 checkpoints were considered, classified as lateritic crust and non-lateritic materials.

The kappa coefficient is defined as $\kappa = (n \sum_{i=1}^{c} x_{ii} - \sum_{i=1}^{c} x_{i+} x_{+i}) / (n^2 - \sum_{i=1}^{c} x_{i+} x_{+i})$, where $x_{ii}$ is the value on line i and column i, $x_{i+}$ is the sum of line i, $x_{+i}$ is the sum of column i of the confusion matrix, n is the total number of samples and c is the number of classes (Cohen, 1960). According to Landis and Koch (1977), kappa is considered to have a nearly perfect agreement when it is above 0.81 and reaches 1. Substantial agreement is obtained when kappa lies within the interval 0.61–0.80. Kappa values below 0.60 are classified as moderate agreement, with values near zero indicating poor agreement.

## 2.1. Boolean logic

Boolean logic is a mathematical system used to create logic rules or expressions to select, analyze, and process data. Bonham-Carter (1994) improved the Boolean technique through the index overlay method (IOM), which consists of granting different weights to each input map considering the level of importance according to the hypothesis. The outcomes include scores appropriate for mapping. The objective is to produce a map showing areas that are arranged according to the score, with a greater spectrum of results (Bonham-Carter, 1994).

Maps in binary format (0 and 1) were obtained in the Boolean analysis (algebraic binary map technique) and use the ratios eTh/K and eU/K as well as the altimetric intervals (obtained from the SRTM image). The ratios were used to emphasize the discrepancies and highlight favorable areas associated with ferruginous crusts. Higher values of eTh/K and eU/K (equal or higher than the average plus one and a half times the standard deviation) are associated with a higher probability of the occurrence of lateritic crusts and were therefore transformed into "1"; in contrast, the lower values were transformed into "0", generating new reclassified images (0 and 1) for both ratios.

In contrast, the procedure with the SRTM elevation model (relief) used a value of "1" for elevations lower than 300 m and higher than 500 m and a value of "0" for elevations between 301 and 499 m. The first altimetric interval (<300 m) is associated with the domain where the geological unit called undifferentiated sedimentary covers is predominant and some lateritic outcrops are found. The second altimetric interval (>500 m), where the major lateritic bodies are mapped, is mainly associated with the sandstones of the Parecis Basin.

### 2.1.1. Weight determination

In the IOM, a weight is given to each input map according to the hypothesis considered. Each map is multiplied by its respective weight, summed, and finally normalized by the sum of weights. The final result is represented by values between 0 and 1 (Bonham-Carter, 1994), which are appropriate for mapping. The equation for the IOM is $S = (\sum_{i}^{n} W_i \, \text{class} \, (MAP_i))/(\sum_{i}^{n} W_i)$, where $Wi$ is the weight of the i-th map, class ($MAPi$) represents the input map of the i-th variable and n is the number of variables.

Four cases using the three main variables (eTh/K, eU/K, and relief) were proposed to clarify the application of the IOM and determine the best combination of weights. In all cases, the scores vary between 0 and 1 and indicate areas with the lowest (0) and highest probabilities (1) of finding lateritic crust. The final choice of the best combination of weights was the one that separated the set of variables into favorable or unfavorable classes according to score, enabling the best visual differentiation of each score. The procedures performed in the Boolean logic included several stages and produced a final predictability map (see Fig. 1).

## 2.2. Fuzzy logic

Fuzzy logic provides the base for the generation of powerful techniques for modeling spatial data and digital maps. It allows conclusions to be obtained and responses to be generated from information that can be ambiguous or inaccurate (Torres, 2014). In this work, fuzzy logic was applied to the same variables as Boolean logic. The raw data were rasterized and then simplified using fuzzification, which allowed for staggering in the degrees of variability or pertinence between "0" (absent pertinence) and "1" (total pertinence). The use of the large and linear fuzzy membership functions allowed for the reorganization of the rasterized digital maps according to the type of input. The linear function was applied to the relief map, which keeps the original data, only rescaling between 0 and 1, whereas the large function (favoring high values) was applied to the eTh/K and eU/K maps.

The gamma spectrometric data exhibit high values of eTh/K and eU/K on the inferior and superior surfaces. These high values can be explained by the strong association with oxisols and lateritic crusts. The large membership function was applied to these images to highlight the high values and consequently the areas with a higher probability of crust occurrence.

The linear function was applied to the relief, as applying any of the other functions (e.g., large, small, pi-shaped) potentializes (overvalues) or minimizes (underestimates) areas considered undesirable or desirable, respectively, for the model. Using a small membership function on the relief overvalues the areas on the inferior surface (<300 m) and underestimates areas on the superior surface (>500 m), whereas a large membership function overvalues areas on the superior surface (>500 m) and underestimates areas on the inferior surface (<300 m). The inverse pi-shaped membership function overvalues both low and high altitude areas, and as a result, it highlights the same areas of the small and large functions simultaneously. Thus, when these membership functions are applied to the relief and integrated with gamma spectrometry images, the areas highlighted as favorable are overly extensive and do not represent the best option for the construction of the model.

The following step was performed to combine the fuzzified maps and reorganize them using fuzzy operators, such as algebraic product — Fuzzy Algebraic Product Operator — FAPO (minimizes the results), algebraic sum — Fuzzy Algebraic Sum Operator — FASO (maximizes the results), and fuzzy gamma operator — FGO (balances the results). Details regarding these operators are provided in Zimmermann (1985); An et al. (1991); Bonham-Carter (1994); Eddy et al. (2006); Nykänen et al. (2008) and Carrino et al. (2011).

Regarding the operator "fuzzy gamma", which was used to create the final predictability maps, Bonham-Carter (1994) showed that γ values between 0 and 0.35 are "decreasive", i.e., always lower or equal to the lowest input fuzzy member, whereas values between 0.8 and 1 are "increasive" (i.e., the output value is larger or equal to the largest input fuzzy member) and values between 0.35 and 0.8 are neither
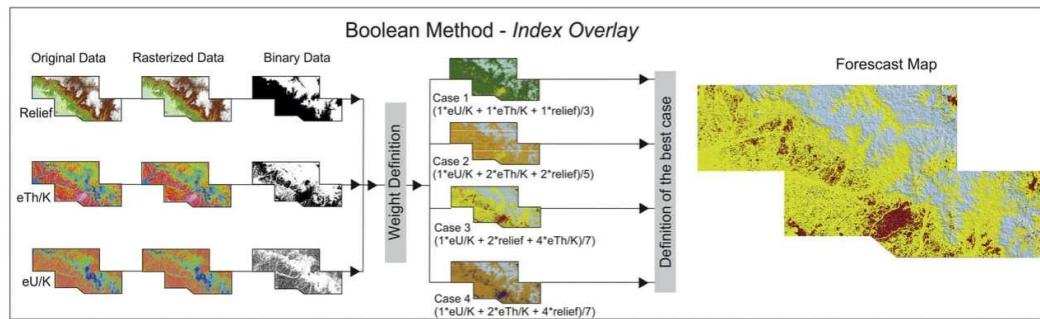


**Fig. 1.** Flowchart of procedures performed for the Boolean logic.

"increasive" nor "decreasive". In this last case, the values always lie within the range of input values.

In practice, the larger "fuzzy gamma" operators tend to restrict less the interest areas, whereas the smaller "fuzzy gamma" operators tend to restrict more. The fuzzy result obtained in this work considered the data equal to the average plus one and a half times the standard deviation as significant, and the fuzzy result was compared with the soil map and the Boolean model.

Different values for gamma between 0.1 and 0.9 were evaluated to clarify the application of the fuzzy method and determine the best gamma operator. The final choice of the best value was based on a comparison with the field data and Boolean results. The set of procedures performed to create the predictability map in the fuzzy technique used the gamma operators γ = 0.7 and γ = 0.3 (Fig. 2).

### 2.3. Regional geologic and geomorphologic context

The research area is located on the western portion of the Amazon craton and comprises the geochronological provinces of Sunsás and Rondônia-Juruena (Fig. 3). Within this context, there is the Alto Guaporé Belt, established during the evolution of the Rondoniano-San Ignácio Orogene (1.47–1.32 Ga) (Rizzotto, 2010). Regarding evolution, the geology is diverse, with ages from Mesoproterozoic up to the current period.

The Mesoproterozoic is represented by para-derived, granitoids, and mafic and ultramafic rocks (Rizzotto, 2010).The Paleozoic to Mesozoic units are represented by sandstones, conglomerates, and siltites of the Parecis Basin. The units associated with the Cenozoic are fluvial and swampy clayey–sandy as well as gravel deposits and lateritic crusts. The lateritic crusts are mainly composed of ferruginous crusts and colluviums originating from its dismantling process, covered by up to 1 m of soil (Quadros and Rizzotto, 2007).

The study area has altitudes ranging between 149 and 627 m. There are three major relief units: i) the Guaporé Depression, generally associated with a pediplained surface with elevations lower than 300 m (Cenozoic); ii) the desiccated unit in the Parecis plateau, related to the Parecis Basin (Mesozoic), with altitudes between 500 and 627 m; and iii) the intermediate zone with altitudes between 301 and 499 m, where there are sporadic Mesoproterozoic inselbergs and tors (Fig. 3). These domains are correlated to the inferior planation, topo II planation, and intermediate planation, surfaces of Kux et al. (1979), respectively. The lateritic crusts support the majority of the Guaporé Depression and the Parecis plateau.

#### 2.3.1. Lateritization on the study area
Three types of profiles were identified in the study area (Fig. 4):

i) The tabular surfaces developed over the quartz and arkose sandstones of the Utiariti formation of the Parecis Basin (at altitudes above 500 m, in the east-central portion of the study area). The profile has brown to yellow cellular lateritic crust with a thickness of up to 2 m that is mainly composed of goethite, grains, and gravels of quartz covered by red oxisol. There is occasionally superficial colluvium with lateritic fragments and spherulites embedded in red sandy to sandy–silty kaolinite matrix or a dismantled lateritic crust between the lateritic crust and oxisol (Fig. 4A, B, and G).

ii) The desiccated surfaces developed over the para-derived rocks and granitoids and, to a lesser extent, mafic–ultramafic rocks (at altitudes between 301 and 499 m, in the northwestern to southwestern portion of the study area). The profiles are truncated and are formed by soft mottled or saprolite horizons covered by colluvium and, to a lesser extent, red oxisol. They are composed of kaolinite, quartz grains, and low content of ferruginous concretions. At three sites, there are blocks of ferruginous pisoliths, nodular and vermiform lateritic crusts with diameters of 20–40 cm embedded in red sandy to sandy–silty kaolinite matrix.

iii) The surfaces developed over the para-derivades, granitoids, and subordinate mafic–ultramafic rocks (at altitudes below 300 m, on plain and low relief with some flooded areas and sporadic inselbergs and tors). The profiles have ochre to red soft vermiform lateritic crusts with thicknesses of 1–2 m. They are mainly composed of goethite, kaolinite, and quartz, with lower contents of hematite and rare gibbsite, and are covered by red oxisols. As in profile type i, there is occasionally superficial colluvium with lateritic fragments and spherulites embedded in red sandy to sandy–silty kaolinite matrix or a dismantled lateritic crust between the lateritic crust and oxisol (Fig. 4E, F, and G).

## 3. Results

### 3.1. Integration of airborne gamma-ray spectrometry and altimetry images

The ternary composition (K, eTh, and eU) shows several areas with gamma spectrometric signatures related to high values of eTh, low values of K and low to intermediate values of eU that could be credited to the presence of lateritic crusts and weathering materials according to Dickson and Scott (1997); Dauth (1997); Carrino et al. (2011); Minty (2011) and Wilford (2012). However, the airborne geophysical products alone were not sufficient to make a complete discrimination, as some areas mapped as lateritic crusts present inconclusive responses in the three channels (eU, eTh, and K). In the northeast, southwest and northwest, there are several sectors that highlight the predominance of eTh. The spectrometric response patterns (eTh, eU and K) are observed in profile A′ (Fig. 5), as is the outcrop location of the points described previously (Fig. 4). There is a relative decrease in K and increase in eU and eTh in areas where lateritic crusts are mapped. Table 1 shows a statistical summary of the eTh/K eU/K, and relief images.
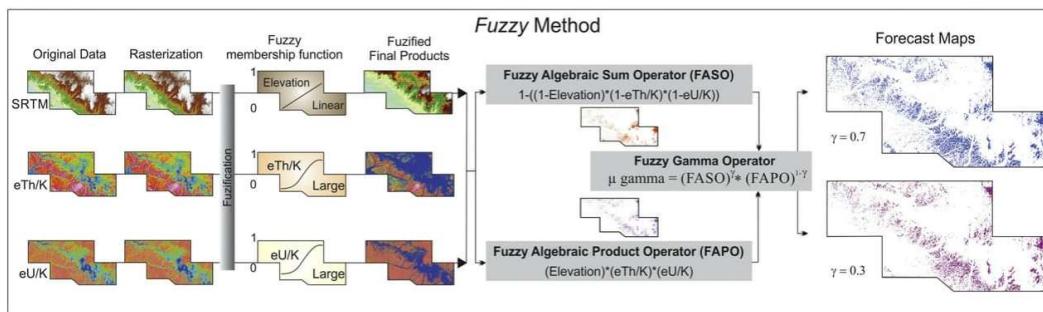


Fig. 2. Flowchart of the procedures performed for the fuzzy logic.
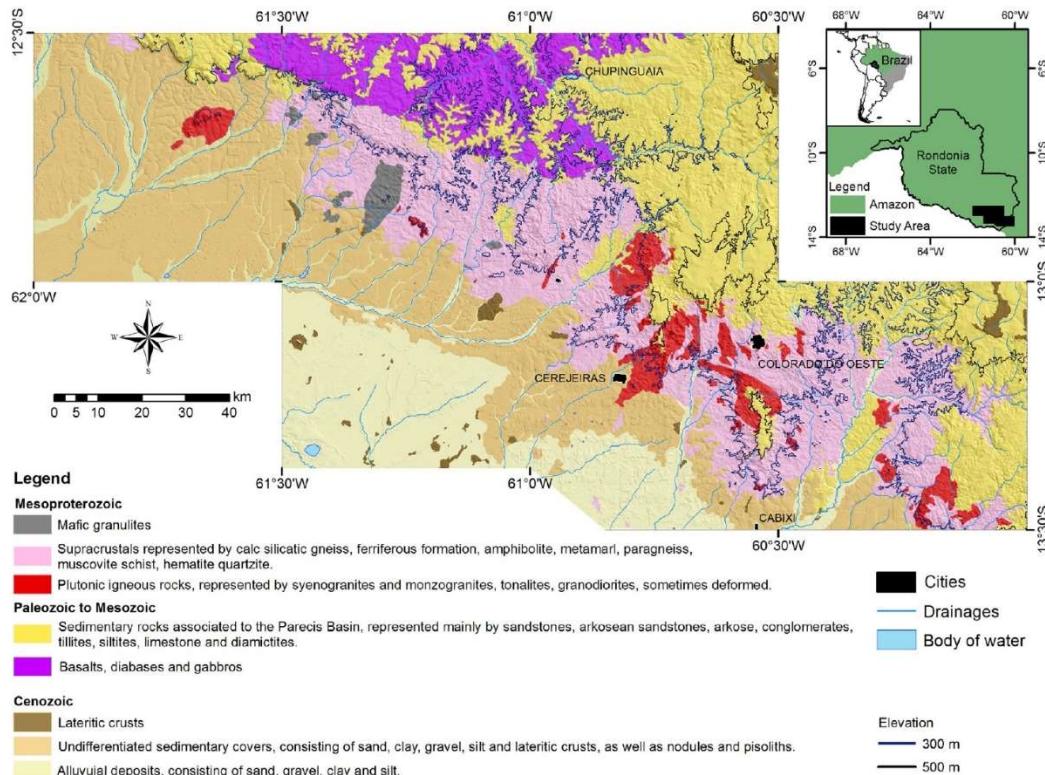
**Fig. 3.** Simplified geologic map, modified from Quadros and Rizzotto (2007); Rizzotto (2010), (2012a, b).

A previous evaluation of the SRTM image (relief) and the ratios eTh/K and eU/K using field data was performed to integrate the products and understand the response pattern associated with lateritic crusts. The ternary composition of eTh/K, SRTM (relief), and eU/K in the RGB channels showed a higher efficiency in the previous identification of lateritic crusts and indicated several areas with high and low elevations (often explained by tectonics and/or geomorphology; Taylor and Eggleton, 2001; Taylor, 2008), simultaneously associated with high values of eTh/K and eU/K (Fig. 6).

### 3.2. Spatial modeling and correlation with lateritization

#### 3.2.1. Boolean logic

The four cases presented above were analyzed to choose the optimal weight combination and obtain the best discrimination of areas with lateritic crusts and dismantling products.

In case 1, in which all of the variables have the same importance level (all weights equal to 1), some combinations that are likely to represent lateritic crust (eTh/K + relief) are mixed with combinations that are unlikely to represent lateritic crusts (eU/K + relief), which hinders the discrimination of potential areas. The combination of all variables, with a score of 1, represents areas with the highest probability of lateritic crust occurrence, covering 1.30% of the area.

In case 2, in which the ratio eU/K has a weight of 1 due to the higher mobility of U compared with Th and the other variables have weights of 2, there is an increase in the percentage of the potential areas considered favorable (7.84%). However, there is still a mixture of likely and unlikely combinations, as in case 1. This condition is undesirable for the evaluation of the model, as it does not completely discriminate the

potential areas and does not allow for a thorough interpretation and correlation with geologic, pedologic, and geomorphologic aspects.

In case 3, all variables have different weights arranged in a geometric progression of common ratio 2 ($A_n = 2^{n-1}$):($1 * eU/K + 2 * relief + 4 * eTh/K)/7$, which allows for the visual discrimination of all possible combinations of variables. In this case, the ratio eTh/K was considered the most significant variable because it represents the enrichment of Th in relation to K, which is an important condition in a weathering context. The final map highlights 8 scores (Fig. 7). The combinations are redistributed, as each score contains a single combination instead of a mixture of combinations, as observed in the previous cases. This enables a better understanding of the variables involved. The results considered as favorable or extremely favorable represent 7.84% of the area and yield a kappa value of 0.87.

Case 4 presents the same results as case 3 in terms of potential areas (7.84%) and the kappa value (0.87); however, the combination of variables is rearranged. All of the results regarding the Boolean cases are shown in Table 2, which provides the formulae, reasons for the weights assigned, the different combinations, the favorability level, and the confusion matrix elements and respective kappa values for each case.

#### 3.2.2. Fuzzy logic

In the fuzzy technique, the algebraic sum and product as well as the fuzzy gamma operator were used. The algebraic sum and product present different responses in relation to the delimitation of potential areas. In the case of the algebraic sum (FASO), the areas with altitudes above 500 m are overestimated, whereas those located below 300 m are observed less frequently. In the algebraic product (FAPO), the areas predicted by the algebraic sum, especially those above 500 m, are redistributed. The areas highlighted as the most favorable by FASO
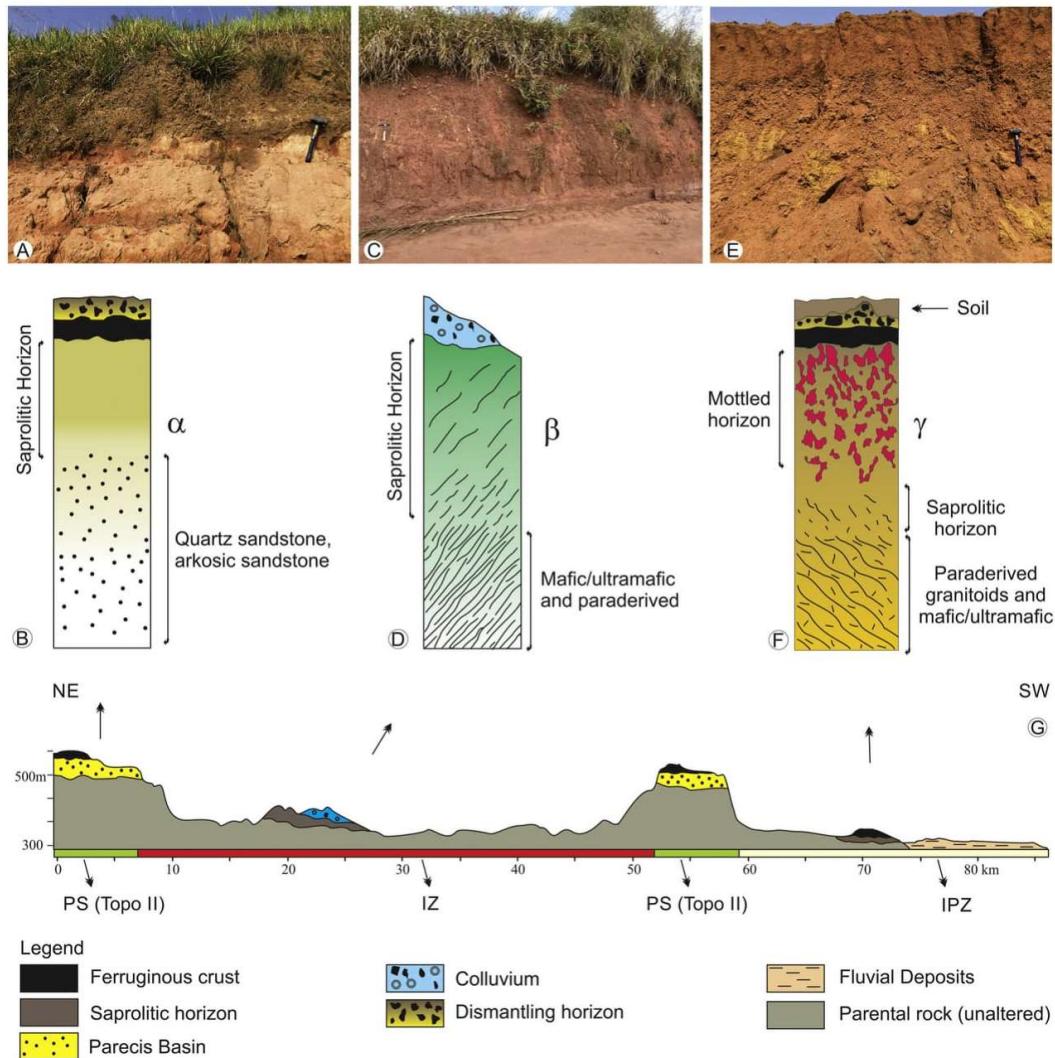
**Fig. 4.** Main forms of regolith and their respective profiles. A and B) Lateritic crust and dismantled horizon and the respective schematic profile (profile (α*)). C and D) Saprolitic horizon partially covered by colluvium (β*). E and F) Mottled horizon covered by crust and dismantling horizon (γ*). G) Simplified topographic profile shown in Figs. 5 and 6 PS = Planation Surface; IPZ = Inferior Planation Zone; IZ = Intermediate Zone. *The Greek letters refer to profiles related to actual lateritic crust sites in the field (Figs. 5 and 6).

and FAPO represent 6.07% and 4.37% of the area, respectively. The information related to the fuzzy intervals, the areas and the respective favorability levels, as well as information regarding the confusion matrix elements and kappa value associated for each operation, are provided in Table 3.

The fuzzy gamma operator (FGO) was used to balance the results obtained in FASO and FAPO. The results for fuzzy gamma values of 0.3 and 0.7, which illustrate the most pessimistic and optimistic results, respectively (Table 3, Figs. 8 and 9), approximated the largest proportion of the areas mapped as undifferentiated sedimentary covers and lateritic crusts, as well as oxisols. The similarity between the maps is evident; however, gamma values higher than 0.7 or lower than 0.3 increase and restrict the areas causing a decrease in kappa, respectively. The final maps (FGO 0.7 and FGO 0.3, Figs. 8 and 9) show new areas not represented by the FASO or FAPO. These new areas are due to the transformation suffered by the input data when the fuzzy gamma operator is applied, i.e., there is a restaggering of the original data matrix. The

final areas obtained in both cases (0.3 and 0.7) refer to values higher than the average plus one and a half times the standard deviation and represent the products with the highest reliability.

## 4. Discussion and model validation

The results obtained considered the gamma spectrometric responses for depths of up to 45 cm and highlighted the potential areas for the occurrence of lateritic crust or dismantling products on the surface.

Minty (1997) considered that the intensity of the gamma rays can increase or decrease according to the humidity conditions on the surface. A 20% increase in the humidity of the ground results in a 20% reduction in the amount of rays emitted on the ground surface. Vegetal tissues contain insignificant traces of Th and U and thus have an insignificant effect on the gamma-ray response; however, they can cause attenuation of the signal and should be considered in the gamma spectrometric
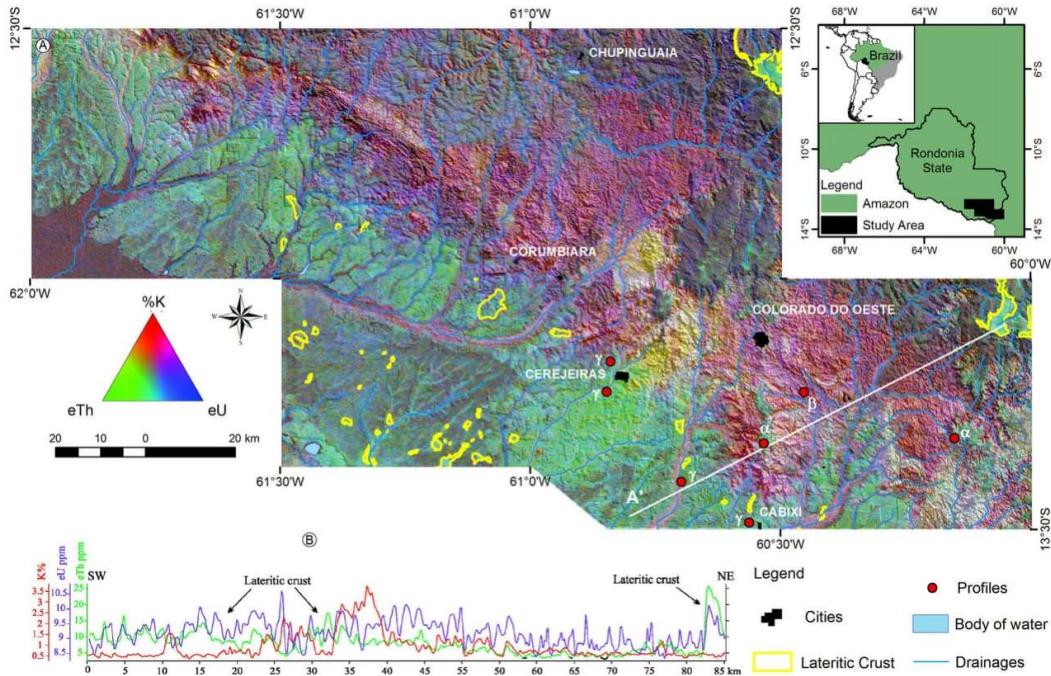
**Fig. 5.** Ternary map of K, eTh and eU on the RGB channels and relief image.

interpretation (Wilford et al., 1997). Furthermore, Kogan et al. (1969) showed that the absorption of K by plants can constitute up to 15% of the signal that reaches the aircraft. Although the study region is located within the official limits of the Amazon, it has a low vegetal cover compared with the remainder of the Amazon due to deforestation.

The airborne geophysical data were acquired during the drier season, providing the best possible conditions for data collection. Minty (2011) stated that when gamma spectrometric ratios are used, there is a tendency to remove environmental artifacts in the data due to soil moisture, vegetation, or the effect of non-radioactive overburden. In any case, the final results showed good correlation between the proposed models and field data.

Regarding the cases for weight determination for the IOM (Boolean method), cases 1 and 2 are not ideal combinations of weights, as they exhibit classes (scores) in which there is a mixture of variables considered favorable and not favorable, which prevents a complete evaluation of the models. Cases 3 and 4 are equivalent, only showing a rearrangement in the order of classes. They can be considered the best representation for the identification of lateritic crusts, as they allow the individualization of all possible variable combinations, which favors the evaluation and full judgment of the model.

The integration of the images in the Boolean logic exhibits a strong correlation between relief and the values of eTh/K in several sites, especially those over 500 m that were classified as extremely favorable. This identification was enabled using weights of 1, 2, and 4 on the eU/K, relief, and eTh/K images, respectively. The areas with elevations lower

than 300 m also have high values of eTh/K and thus a direct correlation with lateritic crusts or dismantling products. In general, these areas strongly overlap with the geologic units called undifferentiated sedimentary covers and also indicate new potential areas for the occurrence of lateritic crusts.

In areas classified as not favorable, the crusts were either not found or registered as restrict occurrences. The sites considered favorable or extremely favorable (i.e., influenced by relief, eTh/K, and eU/K) represent approximately 7.84% of the area and tend to show lateritic crusts in accordance with field data ($\kappa = 0.87$). Therefore, there is a good correlation between the favorability predicted and the presence of crusts in the study area, which confirms the efficiency of the Boolean model proposed.

This model is considered simple, and when combined with weights (IOM), it allows for the separation of the results in terms of scores that vary from 0 to 1. In this sense, the application of weights arranged in a geometric progression allows for not only the discrimination of the classes but also the visualization of the areas related to the influence of each variable or its possible combinations individually in logical order on the final map.

The other combinations of weights showed similar results as those observed in cases 1 and 2 (class overlapping) or cases 3 and 4 (total discrimination of classes). Therefore, it is important to guarantee that all combinations are represented visually through the choice of weights that result in distinct classes and representative of all possible combinations.

The fuzzy method FASO tends to overestimate the potential areas with altitudes over 500 m, whereas FAPO tends to overestimate areas below 300 m, although it shows potential sectors in the intermediate zone (altitudes of 301 to 499 m). Therefore, none of these methods represent the real data satisfactorily. The fuzzy gamma operator result is sufficiently correlated with the occurrence of lateritic crusts. A fuzzy gamma operator of 0.7 highlights areas not identified on the Boolean map, especially on the southeast and north central portions of the area, with excellent correlation, and it represents the most optimistic option for the occurrence of lateritic crusts and dismantling products.

**Table 1**
Statistical summary of the eTh/K, eU/K, and relief airborne geophysical products.

| Product | Min | Max | Sum | Mean | Standard deviation |
|---------|-----|-----|-----|------|--------------------|
| eTh/K | 0.38 | 107.73 | 12,463,240.24 | 11.36 | 7.06 |
| eU/K | 1.3 | 48.7 | 15,217,718.95 | 13.87 | 4.54 |
| Relief | 149 | 627 | 582,263,520 | 283.51 | 98.25 |
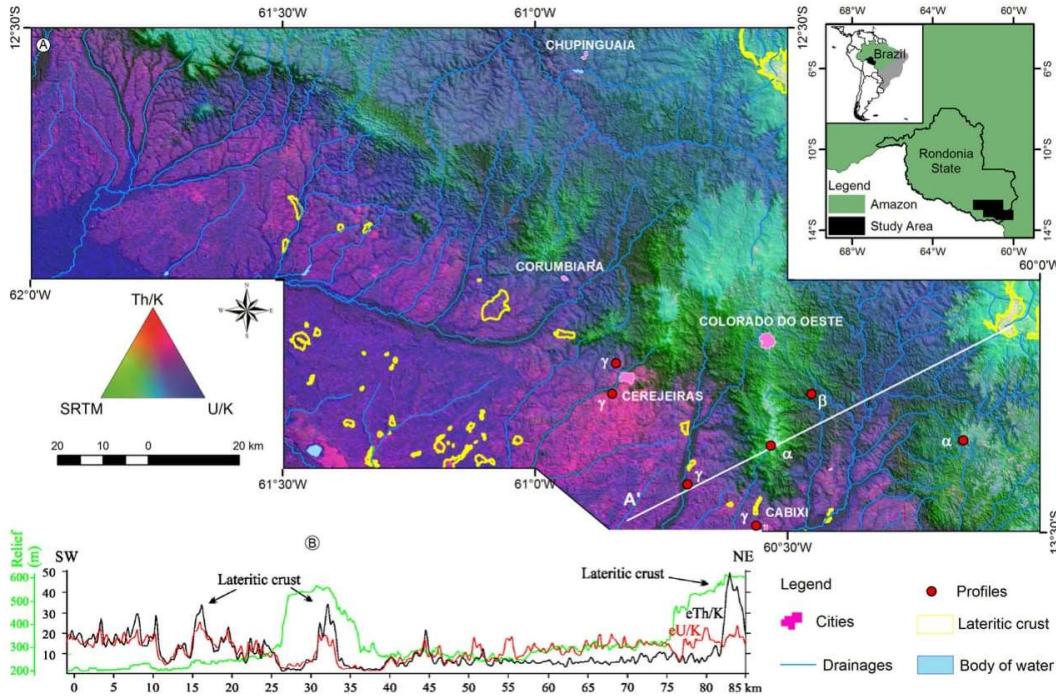
**Fig. 6.** A) Map of the integration of multi-source images: eTh/K, SRTM (relief) and eU/K on RGB channels, with the topographic profile (A′) (Fig. 4) and the areas of lateritic crust mapped by Rizzotto (2010), (2012a). B) Profiles of eTh/K and eU/K highlighting high values associated with lateritic crusts. The locations of some profiles described are highlighted in red: α) profiles associated with the superior surface (>500 m); β) profile associated with the intermediate zone (between 301 and 499 m); γ) profiles associated with the inferior surface (<300 m).
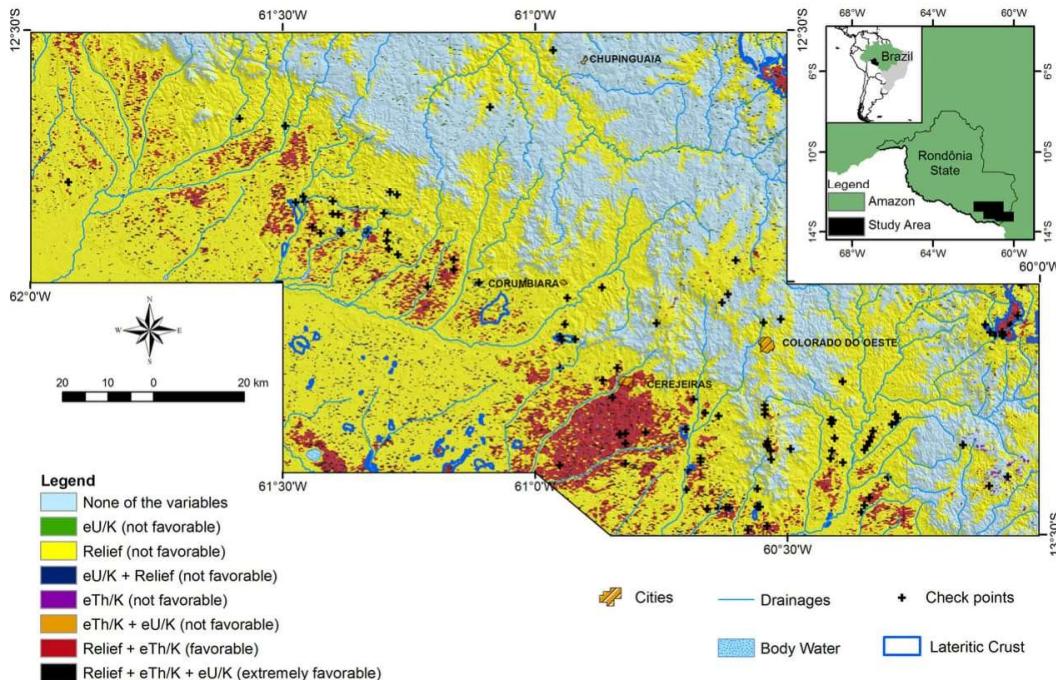


**Fig. 7.** Predictability map of lateritic crust occurrence based on Boolean logic — IOM Case 3.

**Table 2**
Results of the Boolean logic.

| Case | Formulae | Reasons | Products within each score | Scores | Area % | Favorability | Confusion matrix[*] | κ |
|---|---|---|---|---|---|---|---|---|
| 1 | $(1*eU/K + 1*eTh/K + 1*relief)/3$ | All variables have the same importance | NONE | 0 | 26.93 | Extremely not favorable | 19-86-730-40 | 0.84 |
| | | | eU/K, Relief OR eTh/K | 0.33 | 63.90 | Not favorable | | |
| | | | Relief + eU/K, eTh/K + eU/K OR | 0.67 | 7.86 | Not favorable | | |
| | | | Relief + eTh/K | 1 | 1.30 | Extremely favorable | | |
| | | | eU/K + Relief + eTh/K | | | | | |
| 2 | $(1*eU/K + 2*eTh/K + 2*relief)/5$ | The ratio eTh/K and relief are more relevant than the ratio eU/K due to the higher mobility of uranium compared with thorium | NONE | 0 | 26.93 | Extremely not favorable | 52-53-715-55 | 0.87 |
| | | | eU/K | 0.2 | 0.33 | Not favorable | | |
| | | | Relief OR eTh/K | 0.4 | 63.57 | Not favorable | | |
| | | | Relief + eU/K OR eTh/K + eU/K | 0.6 | 1.32 | Not favorable | | |
| | | | eTh/K + Relief | 0.8 | 6.54 | Favorable | | |
| | | | eTh/K + Relief + eU/K | 1 | 1.30 | Extremely favorable | | |
| 3 | $(1*eU/K + 2*relief + 4*eTh/K)/7$ | The ratio eTh/K is more relevant because it emphasizes areas with higher enrichment of thorium related to potassium, which is an important condition in a weathering context | NONE | 0 | 26.93 | Extremely not favorable | 64-41-710-60 | 0.87 |
| | | | eU/K | 0.14 | 0.33 | Not favorable | | |
| | | | Relief | 0.29 | 63.49 | Not favorable | | |
| | | | eU/K + Relief | 0.43 | 1.30 | Not favorable | | |
| | | | eTh/K | 0.57 | 0.08 | Not favorable | | |
| | | | eTh/K + eU/K | 0.71 | 0.02 | Not favorable | | |
| | | | eTh/K + Relief | 0.86 | 6.54 | Favorable | | |
| | | | eTh/K + Relief + eU/K | 1 | 1.30 | Extremely favorable | | |
| 4 | $(1*eU/K + 2*eTh/K + 4*relief)/7$ | The relief has more influence because it has a close relation with the genesis and development of lateritic crusts, and it also presents a wide continuity and forms vast regional planation surfaces | NONE | 0 | 26.93 | Extremely not favorable | 64-41-710-60 | 0.87 |
| | | | eU/K | 0.14 | 0.33 | Not favorable | | |
| | | | eTh/K | 0.29 | 63.49 | Not favorable | | |
| | | | eU/K + eTh/K | 0.43 | 1.30 | Not favorable | | |
| | | | Relief | 0.57 | 0.08 | Not favorable | | |
| | | | Relief + eU/K | 0.71 | 0.02 | Not favorable | | |
| | | | eTh/K + Relief | 0.86 | 6.54 | Favorable | | |
| | | | eTh/K + Relief + eU/K | 1 | 1.30 | Extremely favorable | | |

  [*] Respective values for laterites predicted as laterites, laterites predicted as non-laterites, non-laterites predicted as non-laterites and non-laterites predicted as laterites.

A gamma operator of 0.3, although highly similar to 0.7, is slightly more restrictive in some areas. However, it also delimits some favorable sectors on the southeast portion of the area that were not highlighted in the Boolean method. This value represents the most pessimistic option for the prediction of crust occurrence. Thereby, the "fuzzy gamma" method tends to balance the influences of the FASO and FAPO and consequently the input variables. In particular, the areas with intermediate altitudes (between 301 and 499 m) were not highlighted in the Boolean model, as they were not considered in the relief input binary map. This fact may be the reason for the slightly lower values of kappa observed in the Boolean cases compared with the FGO with a gamma value of 0.7,

which considers intermediate input values in all of the products, including altimetric data.

In general, the fuzzy method allows for the generation of images with favorable areas and high correlation, but it is not able to discriminate the influence of the input products individually (relief, eTh/K and eU/K), i.e., it is not possible to visually identify the influence of each variable. In contrast, the Boolean model generates favorable areas with only good correlation, but it enables the individualization of the influence of the input images (eTh/K, relief, eU/K), consequently allowing for an analysis of each variable involved in the construction of the model.

**Table 3**
Results of the fuzzy logic and the respective favorability classes.

| Case | Formulae | Fuzzy intervals | Areas % | Favorability | Confusion matrix[*] | κ |
|---|---|---|---|---|---|---|
| FASO | $1-((1-Elevation)*(1-eTh/K)*(1-eU/K))$ | 0.012–0.256 | 15.39 | Not favorable | 48-57-715-55 | 0.86 |
| | | 0.256–0.43 | 22.21 | Not favorable | | |
| | | 0.43–0.597 | 21.88 | Not favorable | | |
| | | 0.597–0.87 | 34.46 | Not favorable | | |
| | | 0.87–1 | 6.07 | Extremely favorable | | |
| FAPO | $(Elevation)*(eTh/K)*(eU/K)$ | 0–0.013 | 78.59 | Not favorable | 88-17-680-90 | 0.86 |
| | | 0.013–0.55 | 17.04 | Not favorable | | |
| | | 0.55–0.13 | 3.28 | Extremely favorable | | |
| | | 0.13–0.27 | 0.81 | Extremely favorable | | |
| | | 0.27–0.69 | 0.29 | Extremely favorable | | |
| $\gamma = 0.7$ | $\mu\,Gamma = (\mu\,FASO)^{0.7}*(\mu\,FAPO)^{1-0.7}$ | 0–0.073 | 65.99 | Not favorable | 89-16-718-52 | 0.91 |
| | | 0.073–0.20 | 11.12 | Not favorable | | |
| | | 0.20–0.3 | 12.18 | Not favorable | | |
| | | 0.3–0.48 | 9.31 | Extremely favorable | | |
| | | 0.48–0.89 | 1.40 | Extremely favorable | | |
| $\gamma = 0.3$ | $\mu\,Gamma = (\mu\,FASO)^{0.3}*(\mu\,FAPO)^{1-0.3}$ | 0–0.024 | 71.42 | Not favorable | 83-22-719-51 | 0.90 |
| | | 0.024–0.079 | 17.35 | Not favorable | | |
| | | 0.079–0.1 | 3.90 | Not favorable | | |
| | | 0.1–0.325 | 6.78 | Extremely favorable | | |
| | | 0.325–0.77 | 0.55 | Extremely favorable | | |

  [*] Respective values for laterites predicted as laterites, laterites predicted as non-laterites, non-laterites predicted as non-laterites and non-laterites predicted as laterites.
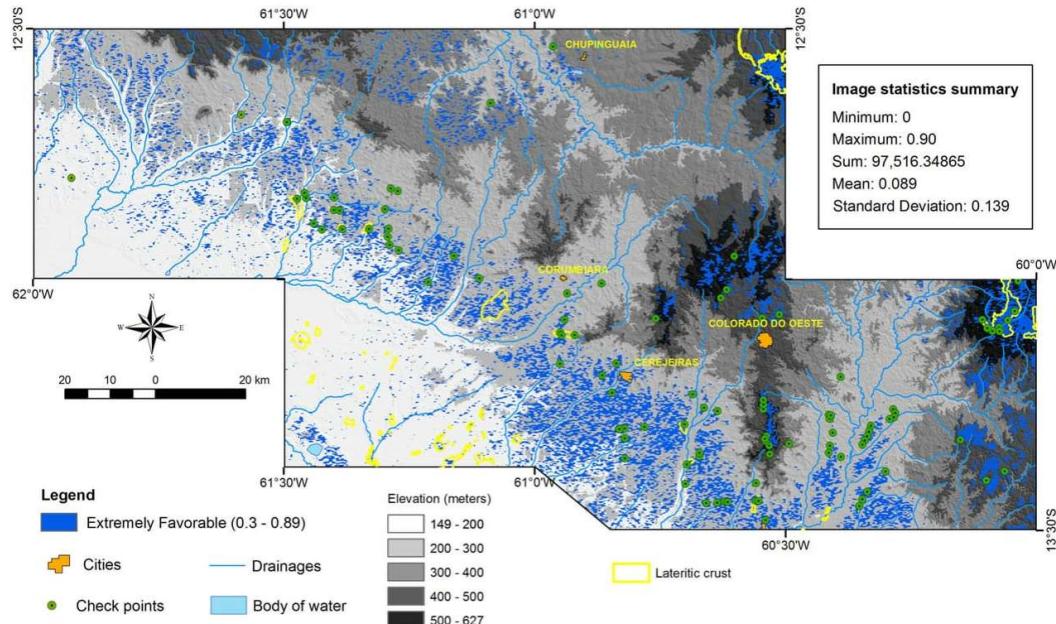
**Fig. 8.** Predictability map of the occurrence of lateritic crust based on the fuzzy gamma operator ($\gamma = 0.7$).

The correlation between the FGO 0.7 model and the map of soils is significant (Fig. 10) and even stronger when considering areas mapped as lateritic crusts and checkpoints. The overlap is substantial when compared with the geologic map, especially with the units referred to as undifferentiated sedimentary covers and with crusts mapped by previous works.

An aspect to be considered is the spatial resolution of the images and the expectation of the results. The images have pixels with 125 m

(airborne geophysics) and 30 m (SRTM), which limits the study to scales lower than 1:100,000. Therefore, the extension and the mode of occurrence of the crusts (e.g., blocks, boulders, pisoliths) must be considered.

The model developed highlights not only areas with lateritic crust (blocks and boulders) but also dismantling products (crust fragments, ferruginous concretions), with oxisols occasionally covering these ferruginous products. Although there is an excellent correlation with the field data, the models used were not able to discriminate or
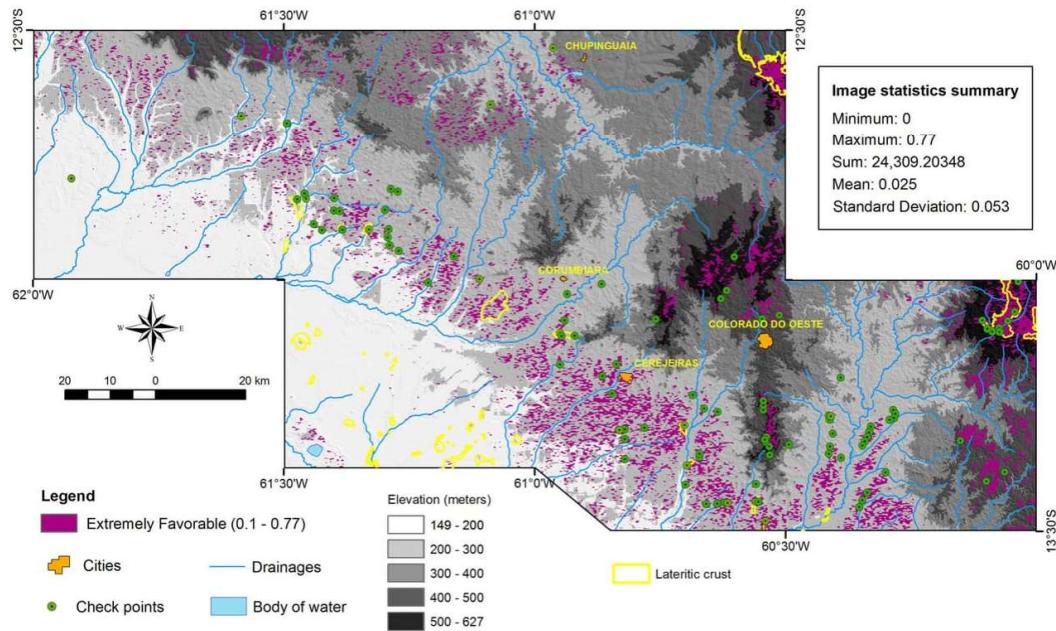


**Fig. 9.** Predictability map of the occurrence of lateritic crust based on the fuzzy gamma operator ($\gamma = 0.3$).
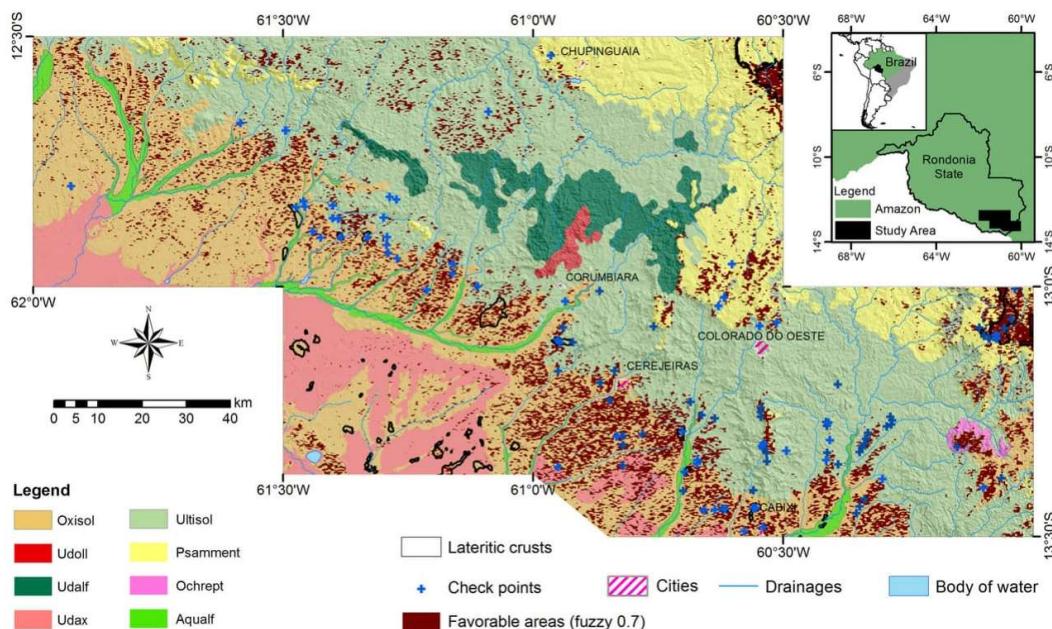
**Fig. 10.** Predictability map using the fuzzy gamma operator ($\gamma = 0.7$) overlapping the soil map* (IBGE) and respective check points. *Soil classification adapted to American nomenclature.

individualize the type of product (e.g., crusts, mottled horizon, oxisol) or response patterns of each individually.

## 5. Conclusions

The identification of lateritic crusts based on mathematic models applied to altimetric and airborne gamma-ray spectrometric data showed good reliability and good overlap with preexistent maps. From both methods applied, the fuzzy method was slightly more reliable than the Boolean method. Nevertheless, both methods can be used to identify potential areas for the occurrence of lateritic crusts and dismantling products, which will contribute significantly to geological mapping.

However, widespread and integrated support of the geological characteristics, regolith formation, and the relationship with relief are required to improve the interpretation. Areas that have high lithological variability with lateritic crusts or have gamma spectrometric responses that vary significantly must be evaluated carefully, as in some cases, high relief and the association with high values of eTh/K and eU/K could be associated with materials other rather than lateritic crust. This work highlighted that areas with low elevations and high values of eTh/K and eU/K show positive responses to the occurrence of lateritic crusts; however, field work is mandatory. The application of these mathematic models integrated with geomorphology, topography and remote sensing in other areas will enable the refinement of the application and increase its reliability, thus improving the model proposed in this work.

## Acknowledgments

## References

Aleva, G.J.J., 1993. The CORLAT Handbook: Guidelines and Background Information for the Description of Laterite Profiles for Interdisciplinary Use, Issue 1. International Soil Reference and Information Centre, Brussels.

An, P., Moon, W.M., Rencz, A., 1991. Application of fuzzy set theory to integrated mineral exploration. Can. J. Expl. 27 (1), 1–11.

Anand, R.R., Paine, M., 2002. Regolith geology of the Yilgarn Craton, Western Australia: implications for exploration. Aust. J. Earth Sci. 49 (1), 3–162. http://dx.doi.org/10.1046/j.1440-0952.2002.00912.x.

Bardossy, G., Aleva, G.J.J., 1989. The Amazon Basin: a discussion review. Travaux ICSOBA 19, 455–458.

Beauvais, A., 1999. Geochemical balance of lateritization processes and climatic signatures in weathering profiles overlain by ferricretes in Central Africa. Geochim. Cosmochim. Acta 63 (23–24), 3939–3957. http://dx.doi.org/10.1016/S0016-7037(99)00173-8.

Bonham-Carter, G.F., 1994. Geographic Information Systems for Geoscientists: Modelling with GIS. Computer Methods in the Geosciences. 13. Pergamon Publications, Oxford.

Boulangé, B., Carvalho, A., 1997. The Bauxite of Porto Trombetas. In: Carvalho, A., Boulange, B., Melfi, A.J., Lucas, Y. (Eds.), Brazilian Bauxites. USP/FAPESP/ORSTOM, São Paulo, pp. 55–73.

Büdel, J., 1982. Climatic Geomorphology. Princeton University Press, New Jersey http://dx.doi.org/10.1002/esp.3290080216.

Burrough, P.A., Macmillan, R.A., Van Deursen, W., 1992. Fuzzy classification methods for determining land suitability from soil profile observations and topography. J. Soil Sci. 43 (2), 193–210. http://dx.doi.org/10.1111/j.1365-2389.1992.tb00129.x.

Butt, C.R.M., Zeegers, H., 1992. Regolith Exploration Geochemistry in Tropical and Subtropical Terrains. Handb. Explor. Geochem. vol. 4. Elsevier Science Publishers, Amsterdam.

Carranza, E.J.M., 2008. Geochemical Anomaly and Mineral Prospectivity Mapping in GIS. In Handb. Explor. Environ. Geochem. 11 pp. 189–246. http://dx.doi.org/10.1016/S1874-2734(09)70001-4.

Carrino, T.A., Silva, A.M., Botelho, N.F., da Silva, A.A.C., 2011. Discriminação de áreas de espesso regolito do leste do Estado do Amazonas usando estatística multivariada, algoritmo hiperespectral e modelagem de dados espaciais. Rev. Bras. Geofís. 29 (1), 155–172.

Cohen, J., 1960. A coefficient of agreement of nominal scales. Educ. Psychol. Meas. 20 (1), 37–46. http://dx.doi.org/10.1177/001316446002000104.

Costa, M.L., 1997. Lateritization as a major process of ore deposit formation in the Amazon region. Explor. Min. Geol. 6 (1), 79–104.

CPRM — Serviço Geológico Do Brasil, 2006. Projeto Aerogeofísico Sudeste de Rondônia: relatório final de levantamento e processamento dos dados magnetométricos e gamaespectrométricos. vol. 1. Lasa Engenharia e Prospecções; Prospectors Aerolevantamentos e Sistemas, 27v, Rio de Janeiro.

da Silva, A.F., Barbosa, A.P., Zimback, C.R.L., Landim, P.M.B., Soares, A., 2015. Estimation of croplands using indicator kriging and fuzzy classification. Comput. Electron. Agric. 111, 1–11. http://dx.doi.org/10.1016/j.compag.2014.11.020.

Darnley, A.G., Grasty, R.L., 1971. Mapping from the air by gamma-ray spectrometry. Can. Inst. Min. Metall. 11, 485–500.

Dauth, C., 1997. Airborne magnetic radiometric and sat imagery for regolith mapping in the Yilgarn Craton of Western Australia. Explor. Geophys. 28 (2), 199–203. http://dx.doi.org/10.1071/EG997199.

Dent, D.L., MacMillan, R.A., Mayr, T.L., Chapman, W.K., Berch, S.M., 2013. Use of airborne gamma radiometrics to infer soil properties for a forested area in British Columbia, Canada. J. Ecosyst. Manag. 14 (1), 1–12.

Dickson, B.L., Scott, K.M., 1997. Interpretation of aerial gamma-ray surveys — adding the geochemical factors. AGSO J. Aust. Geol. Geophys. 17 (2), 187–200.

Duval, J.S., 1990. Modern aerial gamma-ray spectrometry and regional potassium map of the conterminous United States. J. Geochem. Explor. 39, 249–253. http://dx.doi.org/10.1016/0375-6742(90)90076-M.

Eddy, B.G., Graham, D.F., Bonham-Carter, G.F., Jefferson, C.W., 2006. Mineral Potential Analyzed and Mapped at Multiple scales—A Modified Fuzzy Logic Method Using Digital Geology. In: Harris, J.R. (Ed.), GIS for the Earth Sciences. Geological Associatino of Canada, Canada, pp. 143–162.

Graham, D.F., Bonham-Carter, G.F., 1993. Airborne radiometric data — a tool for reconnaissance geological mapping using a gis. Photogramm. Eng. Remote. Sens. 59 (8), 1243–1249.

Gregory, A.F., Horwood, J.L., 1961. A Laboratory Study of Gamma-Ray Spectra at the Surface of Rocks, Issue 85. Department of Mines and Technical Surveys, Ottawa.

Horbe, A.M.C., Da Costa, M.L., 1999. Geochemical evolution of a lateritic Sn–Zr–Th–Nb–Y–REE-bearing ore body derived from apogranite: the case of Pitinga, Amazonas — Brazil. J. Geochem. Explor. 66 (1–2), 339–351. http://dx.doi.org/10.1016/S0375-6742(99)00002-3.

Horbe, A.M.C., Da Costa, M.L., 2005. Lateritic crusts and related soils in eastern Brazilian Amazonia. Geoderma 126 (3–4), 225–239. http://dx.doi.org/10.1016/j.geoderma.2004.09.011.

Kogan, R.M., Nazarov, I.M., Fridman, S.D., 1969. Gamma-Ray Spectrometry of Natural Environments and Formation: Theory of the Method Application to Geology Dan Geophysics. Keter Press, Jerusalem.

Kotschoubey, B., Calaf, J.M.C., Lobato, a C.C., Leite, a S., Azevedo, C.H.D., 2005. Caracterização e gênese dos depósitos de bauxita da Província Bauxitífera de Paragominas, noroeste da Bacia do Grajú, nordeste do Pará/oeste do Maranhão. In: Marini, O.J., Queiroz, E.T. de, Ramos, B.W. (Eds.), Caracterização de depósitos minerais em distritos mineiros da Amazônia. DNPM; CT/Mineral; ADIMB, Brasília, pp. 687–782.

Kux, H.J.H., Brasil, A.E., Franco, M.S.M., 1979. Geomorfologia. Folha SD. 20 Guaporé: geologia, geomorfologia, pedologia, vegetação e uso potencial da terra. Brasil, Departamento Nacional de Produção Mineral. Projeto RADAMBRASIL, Rio de Janeiro, pp. 125–164.

Lagacherie, P., 2005. An algorithm for fuzzy pattern matching to allocate soil individuals to pre-existing soil classes. Geoderma 128 (3–4), 274–288. http://dx.doi.org/10.1016/j.geoderma.2005.04.009.

Landis, J.R., Koch, G.G., 1977. The measurement of observer agreement for categorical data. Biometrics 33 (1), 159–174. http://dx.doi.org/10.2307/2529310.

Lucas, Y., Kobilsek, B., Chauvel, A., 1989. Structure, genesis, and present evolution of Amazonian bauxites developed on sediments. Travaux ICSOBA 19, 81–94.

McBratney, A., Mendonça Santos, M., Minasny, B., 2003. On digital soil mapping. Geoderma 117, 3–52. http://dx.doi.org/10.1016/S0016-7061(03)00223-4.

McFarlane, M.J., 1976. Laterite and Landscape. Academic Press, London.

McKenzie, N.J., Ryan, P.J., 1999. Spatial prediction of soil properties using environmental correlation. Geoderma 89, 67–94.

Minty, B.R.S., 1997. Fundamental of airborne gamma-ray spectrometry. AGSO J. Aust. Geol. Geophys. 17, 39–50.

Minty, B., 2011. Short note: on the use of radioelement ratios to enhance gamma-ray spectrometric data. Explor. Geophys. 42 (1), 116–120. http://dx.doi.org/10.1071/EG10011.

Moreira, F.R.S., Almeida-Filho, R., Câmara, G., 2003. Spatial analysis techniques applied to mineral prospecting: an evaluation in the Poços de Caldas Plateau. Rev. Bras. Geosci. 33 (2), 183–190.

Nahon, D., Melfi, A., Conte, C.N., 1989. Presence d'un vieux système de cuirasses ferrugineuses latéritiques en Amazonie du Sud. As transformation in situ en latosols sous la forêt équatoriale actuelle. Comptes rendus de l'Académie des sciences. Série 2, mec. phys. chim. sci. univers, sci. Terre 308, 755–760.

Nykänen, V., Groves, D.I., Ojala, V.J., Eilu, P., Gardoll, S.J., 2008. Reconnaissance-scale conceptual fuzzy-logic prospectivity modelling for iron oxide copper–gold deposits in the northern Fennoscandian Shield, Finland. Aust. J. Earth Sci. 55 (1), 25–38. http://dx.doi.org/10.1080/08120090701581372.

Pomerol, C., Lagabrielle, Y., Renard, M., Guillot, S., 2013. Princípios de geologia: técnicas, modelos e teorias. 14th ed. Bookman, Porto Alegre.

Quadros, M.L.E.S.; Rizzotto, G.J., 2007. Geologia e recursos minerais do Estado de Rondônia: texto explicativo do mapa geológico e de recursos minerais do Estado de Rondônia. Escala 1:1.000.000. CPRM, Porto Velho.

Rizzotto, G.J., 2010. Geologia e recursos minerais da folha Pimenteiras SD.20-X-D: texto explicativo do mapa geológico e de recursos minerais da folha Pimenteiras. CPRM, Porto Velho.

Rizzotto, G.J., 2012a. Geologia e recursos minerais da Folha Vilhena (SD.20-X-B): Sistema de Informações Geográficas-SIG: texto explicativo do mapa geológico e de recursos minerais da folha Vilhena, escala 1:250.000. CPRM, Porto Velho.

Rizzotto, G.J., 2012b. Petrologia e geocronologia do complexo máfico-ultramáfico Trincheira, sudoeste do Craton Amazônico: implicações tectônicas do mesoproterozoico 193 p. Thesis (PhD in Science) Instituto de Geociências, Universidade Federal do Rio Grande do Sul, Porto Alegre.

Tardy, Y., Roquin, C., 1998. Derive dês continents, paléoclimats et altérations tropicales. Éditions BRGM, Orléans.

Taylor, G., 2008. Landscape and regolith. In: Scott, K.M., Pain, C.F. (Eds.), Regolith Science. Springer, Dordrecht, pp. 31–43.

Taylor, G., Eggleton, R.A., 2001. Regolith Geology and Geomorphology. first ed. John Wiley & Sons, Chichester.

Thomas, M.F., 1974. Tropical Geomorphology: A Study of Weathering and Landform Development in Warm Climates. John Wiley & Sons, New York.

Torres, J., 2014. Lógica fuzzy: teoria da complexidade. Available at: http://www.teoriadacomplexidade.com.br/ Accessed on: 10 nov. 2014.

Tucker, C.J., Holben, B.N., Goff, T.E., 1984. Intensive forest clearing in Rondonia, Brazil, as detected by satellite remote sensing. Remote Sens. Environ. 15, 255–261. http://dx.doi.org/10.1016/0034-4257(84)90035-X.

Wilford, J., 2012. A weathering intensity index for the Australian continent using airborne gamma-ray spectrometry and digital terrain analysis. Geoderma 183–184, 124–142. http://dx.doi.org/10.1016/j.geoderma.2010.12.022.

Wilford, J.R., Bierwirth, P.N., Craig, M.A., 1997. Application of airborne gamma-ray spectrometry in soil/regolith mapping and applied geomorphology. J. Aust. Geol. Geophys. 17 (2), 201–216.

Zhu, A.X., Yang, L., Li, B., Qin, C., Pei, T., Liu, B., 2010. Construction of membership functions for predictive soil mapping under fuzzy logic. Geoderma 155 (3–4), 164–174. http://dx.doi.org/10.1016/j.geoderma.2009.05.024.

Zimmermann, H.J., 1985. Fuzzy Set Theory and Its Applications. Kluwer Academic, Dordrecht.

# CAPÍTULO 3

## ARTIGO CIENTÍFICO 2

# INTEGRATION OF GEOCHEMICAL AND GEOPHYSICAL DATA TO CHARACTERIZE AND MAP LATERITIC REGOLITH: AN EXAMPLE IN THE BRAZILIAN AMAZON.

Corresponding Author: Mr. Edgar Romeo Herrera de Figueiredo Iza, M.D

Corresponding Author's Institution: Serviço Geológico do Brasil

First Author: Edgar Romeo Herrera de Figueiredo Iza, M.D

Order of Authors: Edgar Romeo Herrera de Figueiredo Iza, M.D; Adriana M Coimbra Horbe, Doctorate; Cassiano Castro e Costa, Doctorate; Isabel L Iza Echeverria Herrera, M.S.

# Integration of geochemical and geophysical data to characterize and map lateritic regolith: an example in the Brazilian Amazon.

[a,b]Edgar Romeo Herrera de Figueiredo Iza; [b]Adriana Maria Coimbra Horbe; [a]Cassiano Costa e Castro
[c]Isabel Leonor Iza Echeverria Herrera
[a]Serviço Geológico do Brasil-CPRM, Av. Lauro Sodré, 2561, São Sebastião, Porto Velho, 76801-581, Brazil,
edgar.iza@cprm.gov.br; cassiano.castro@cprm.gov.br
[b]Instituto de Geociências, Universidade de Brasília, *Campus* Universitário Darcy Ribeiro, Brasília, 70910-900
Brazil, ahorbe@unb.br.
[c]Universidade Federal de Rondônia, *Programa de Pós-Graduação em Geografia*, PPGG Porto Velho, 76801-
059 Brazil, isaiza@gmail.com

## Abstract

In tropical regions like the Amazon, there are extensive lateritic covers not properly mapped, despite the economic bearing mineral and the importance related to the denudation and regolith landscape studies. To consolidate tools for regolith cartography, geochemical and geophysical data (airborne gamma ray spectrometry and magnetometry) were integrated. Regional indexes (weathering intensity index – WII, lateritic index - LI and mafic index - MI) were generated and applied, which allowed the identification of regolith properties. The WII highlighted areas with high weathering level located between 149 and 300 m and between 500 and 627 m of altitude that are related to the lower planation surface (LPS) and upper planation surfaces (UPS), respectively. The LI ratified the WII and highlighted areas with high Th/K and U/K ratios associated to lateritic duricrusts. The correlation between LI and MI showed lateritic duricrusts related to mafic and felsic substrates, especially on altitudes below 300 m, confirming the geochemical data. All these products leaded to the reinterpretation of areas previously considered sedimentary as residual associated to oxisols and lateritic duricrusts, and allowed the proposal of regolith mapping techniques and models generation (weathering intensity and lateritic indexes) with good level of reliability. The consolidated techniques are extremely useful in regions similar to the Amazon (tropical areas), where there are significant areas with difficult or restricted access (indigenous lands, areas of environmental preservation, etc.).

Keywords: Th/K; U/K; weathering intensity index; lateritic duricrust; lateritic index.

32 **1 Introduction**

33    The application of gamma-ray spectrometric data using mathematical techniques

34 integrated with geology and altimetry, has increasingly contributed to the development of

35 mapping techniques in order to interpret geomorphological and weathering processes (Wilford

36 *et al.* 1997; Moreira *et al.,* 2003; McBratney *et al.,* 2003; Carranza, 2009; Wilford, 2012; Arhin

37 *et al.,* 2015). Wilford (2012), for example, developed the weathering intensity index (WII) for

38 Australia using gamma-ray spectrometric and altimetric data, and obtained excellent results in

39 a regional scale defining areas with different levels of weathering. Other authors confirm that

40 high values of eU and eTh, often above the earth crust average, together with low values of K,

41 identify lateritic products (lateritic duricrust, gossan, bauxites, etc.) and their respective parent

42 rocks (Dickson and Scott, 1997; Dauth, 1997; Isles and Rankin, 2000; Carrier *et al.,* 2006;

43 Carrino *et al.,* 2011; Barbosa, 2013; Iza *et al.*, 2016). On the other hand, Minty (2011) states

44 that the radiometric ratios tend to remove environmental artefacts related to humidity and

45 vegetation. The previously mentioned results make the gamma-ray spectrometry a useful and

46 reliable tool in the study of the regolith.

47    Brazil, with about 65% of its land with lateritic regolith, has important supergene

48 mineral deposits, especially in the Amazon (e.g. Costa, 1997; Boulangé and Carvalho, 1997;

49 Kotschoubey *et al.,* 2005; Oliveira *et al.*, 2016, Albuquerque *et al*., 2017). However,

50 multisource techniques for mapping the regolith, have not yet been developed or applied widely

51 and systematically. In this sense, the objective of this research was to compare and evaluate

52 geophysical and geochemical data in order to characterize the regolith, and to develop and

53 consolidate tools for its cartography, applicable in other tropical regions. To achieve it, the

54 lateritic index (LI) and the weathering intensity index (WII) were developed, and the mafic

55 index (MI) of Pires and Moraes (2006) was applied.

56

## 2 Location, geological and geomorphological aspects

The study area is located in the southwest of the Brazilian Amazon, border with Bolivia, and has about 17,000 km$^2$ (Figure 1). The climate is type Aw – Tropical rainy with precipitations between 1400 and 2600 mm/year. The area consists of three major geomorphologic domains according to Iza *et al.* (2016): i) Upper Planation Surface (UPS), with altitudes between 500 and 627 m, and associated with Mesozoic sedimentary (Parecis basin) and Paleozoic mafic rocks covered by lateritic duricrusts; ii) Lower Planation Surface (LPS), with altitudes below 300 m, locally limited by abrupt scarps and related to undifferentiated sedimentary covers, lateritic duricrusts and recent deposits of clay, silt, sand and gravel. On altitudes below 250 m the flooded areas are frequent, especially near rivers and lakes; and iii) Intermediate Zone (IZ), with altitudes between 301 and 499 m, with convex to sharp tops, related to Mesoproterozoic mafic rocks, gneisses, schists and granitoids (Figure 1).
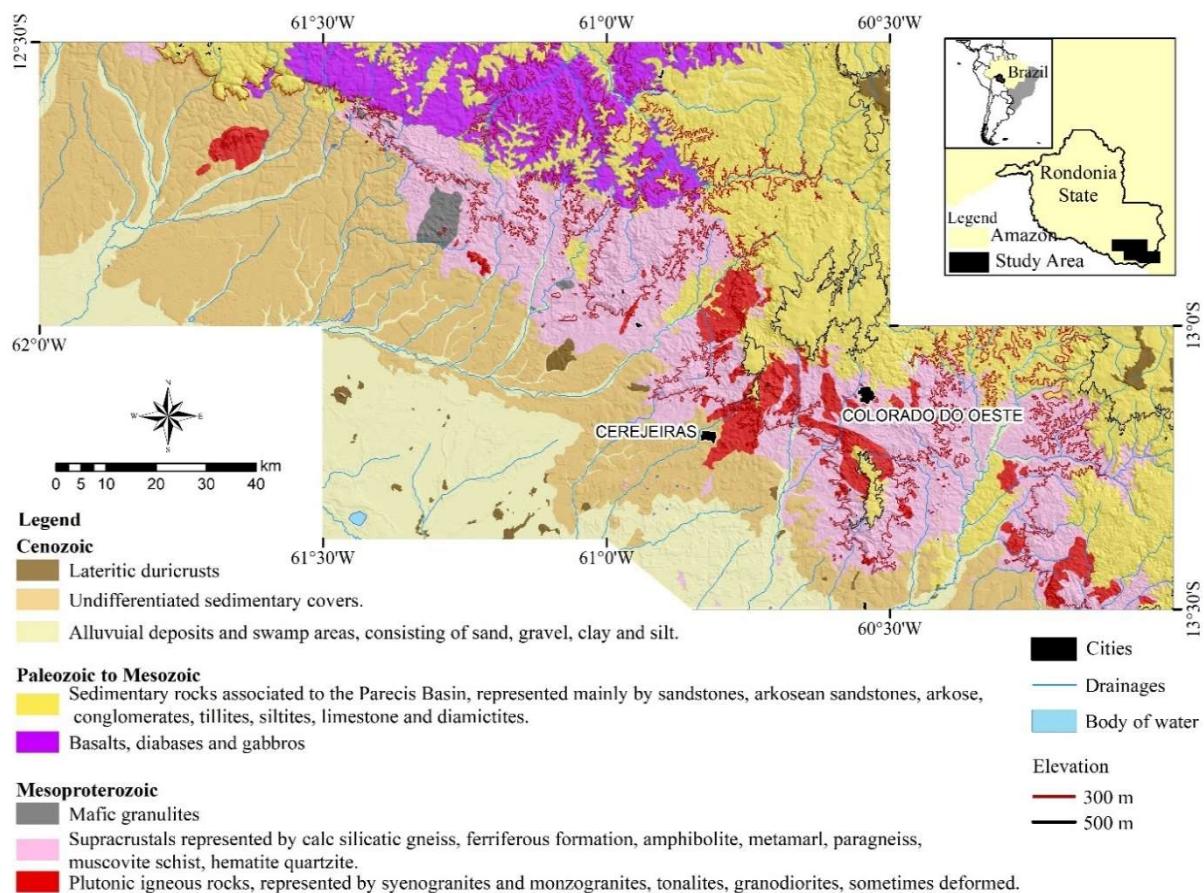


Figure 1 – Simplified geologic map of the area, modified from Quadros and Rizzotto (2007).

72 **3 Materials and methods**

73 **3.1 Regolith geochemistry**

74       The regolith geochemistry was performed in 586 samples of stream sediments collected

75 in the main drainage channel with a nylon sieve (1mm), 428 soil samples collected prioritizing

76 horizon B and 35 samples of lateritic duricrusts. The stream sediments geochemical survey

77 covered 11,550 $km^2$, resulting in approximately one sample/19 $km^2$, while soil samples were

78 collected in a regular grid with spacing of 4 km. The stream sediments and soil samples were

79 sieved at 80 mesh (1mm), pulverized and digested with aqua regia to analyze 54 elements by

80 ICP-OES and ICP-MS (Ag, Al, As, Au, B, Ba, Be, Bi, Ca, Cd, Ce, Co, Cu, Cr, Cs, Fe, Ga, Ge,

81 Hf, Hg, In, K, La, Li, Lu, Mg, Mn, Mo, Na, Nb, Ni, P, Pb, Rb, Re, S, Sb, Sc, Se, Sn, Sr, Ta, Tb,

82 Te, Th, Ti, Tl, U, V, W, Y, Yb, Zn, Zr). The lateritic duricrusts samples were crushed and

83 pulverized in a puck mill and the same trace elements of the stream sediments and soil

84 geochemistry (except for Hg, B and Re), besides REEs were analyzed. The major oxides in the

85 lateritic duricrust ($Al_2O_3$, $Fe_2O_3$, $SiO_2$, CaO, $K_2O$, $Na_2O$, MgO, $TiO_2$ and $P_2O_5$) were analyzed

86 by x-ray fluorescence. The preparation of the samples was performed in the Mineral Analysis

87 Laboratory of the Brazilian Geological Survey and the chemical analysis in the SGS Geosol

88 Laboratory LTDA, Brazil.

89       The data were analyzed through univariate statistic (summary of estimators, histograms

90 and plots of normal probability), multivariate statistic (correlation matrix and principal

91 component analysis) and interpreted with the support of the geological base. The samples with

92 more than 30% of the chemical analysis below the detection limit were discarded and those

93 with sporadic results below the detection limit were multiplied by 0.5, according to Reimann *et*

94 *al.* (2008). In the correlation matrix, the intervals considered were: weak (0 to ±0.29); regular

95 (±0.3 to ±0.79); strong (±0.8 to ±0.89); very strong (±0.9 to ±0.99) and perfect (±1). In the

96 principal component analysis (PCA) the elements with correlations above 0.60 were used. In

97   the selection of the factors, the eigenvalues higher than 1 were used, and, to maximize the

98   variance, the varimax rotation was used (Kaiser, 1958). The scores of the samples, defined for

99   each factor, were interpolated by the inverse of the distance (ISW deterministic weighted

100  univariate interpolation) and used in the preparation of the geochemical maps (anomalous

101  zones) of stream sediments and soil.

102

103  **3.2 Airborne γ-ray spectrometry and magnetometry**

104  The gamma-ray spectrometric and magnetometric data used in this paper were acquired

105  by FUGRO AIRBORNE SURVEYS for the Brazilian Geological Survey (CPRM) between

106  2005 and 2006 (Projeto Sudeste de Rondônia – Southeastern Rondônia Project). The main

107  products used were the dose, K, Th, U and the Th/K and U/K ratios. The softwares used were

108  Oasis Montaj 8.5 and ArcGis 10.3 with the Geosoft extension, which permitted the processing

109  of the aerogeophysical images and management of all data, including altimetry (SRTM –

110  Shuttle Radar Topography Mission).

111  To determine the weathering intensity index (WII), the procedure from Wilford (2012)

112  was used (Australian context), with some adaptions to fit the study area (Amazon context). The

113  WII was calculated in three stages: a) classification of the regolith in 5 weathering classes (WC)

114  using data from 174 sites (Table 1). The weathering classes were divided according to the

115  presence or absence of outcrops, preservation of the fabrics of the rock, proportion of clay

116  minerals and degree of mottling and ferruginization. The areas considered unweathered were

117  those where rocky outcrops are predominant (>70%) with rare signals of decomposition and no

118  soil cover. The areas considered more intensely weathered and less eroded were those where

119  lateritic duricrusts and soil covers are predominant (presence of clay minerals); b) statistical

120  parameters (average, maximum, minimum, standard deviation, asymmetry, etc.) and correlation

121  analysis, considering altimetry, Th, U, K, Th/K, U/K and dose with the weathering classes (WC)

122 (Table2). The correlation (r) intervals used (weak to perfect) were the same mentioned above

123 (item 3.3) and the results are shown on Table 3; and c) generation of the regression equation

124 and final WII map.

125 Table 1 – Classification of regolith level of weathering for the study area (modified from Wilford, 2012).

| Level (WC) | Weathering Intensity | Descriptions |
|---|---|---|
| 1 | Unweathered | Unaltered rock with no signs of decomposition or discoloring. Rock outcrops are very common (>70%). |
| 2 | Slightly weathered | Rock slightly discolored with eventual staining. The overall fabric of the rock is well preserved and the outcrops are common (20-70%). Soils are typically lithosols. Primary minerals are largely preserved, however feldspars can be slightly weathered. |
| 3 | Moderately weathered | Residual sands and clays are common in the upper part of the weathering profile. Rock partially weathered but still cohesive. Most of the feldspars are weathered. Primary minerals still present, as well as smectite, kaolinite and iron oxi-hydroxides. Outcrops are rare or absent <20%. |
| 4 | Highly weathered | Residual sands and clays are common in the upper part of the weathering profile. The fabric of the rock is weakly preserved. Saprolite commonly mottled and ferruginous. The material can be broken with the hands. The mineral content is dominated by clays, quartz and oxi-hydroxides and the main primary minerals like feldspars, are weathered. Minor outcrops frequently highly weathered. |
| 5 | Intensely weathered | Residual sands and clays are common in the upper part of the profile; mottling and leaching are intense and frequent. Lateritic duricrust and lateritic gravels are common. Saprolite is soft with primary minerals completely weathered forming clays or oxi-hydroxides. Quartz is the only remaining primary mineral and quartz veins can still appear. The few outcrops are typically weathered and indurated by oxi-hydroxides. |

126

127 Table 2 –Basic statistics

| | N | Average | Minimum | Maximum | St. Dev. | Asymmetry |
|---|---|---|---|---|---|---|
| Altimetry | 174 | 346.5 | 187.0 | 611.7 | 104.4 | 0.34 |
| Dose | 174 | 4.3 | 1.6 | 11.7 | 1.9 | 1.37 |
| K | 174 | 1.3 | 0.4 | 4.6 | 0.9 | 1.62 |
| Th | 174 | 6.8 | 1.0 | 22.0 | 4.3 | 1.48 |
| U | 174 | 1.2 | 0.0 | 2.8 | 0.5 | 0.41 |
| ThK | 174 | 10.8 | 1.9 | 51.1 | 8.6 | 1.59 |
| U/K | 174 | 10.1 | 1.7 | 21.7 | 5.1 | 0.33 |

128

129 Table 3 – Pearson correlation coefficient. WC = Weathering classes described on table 1.

| | WC | Altimetry* | Dose | K | Th | U | Th/K | U/K |
|---|---|---|---|---|---|---|---|---|
| **WC** | 1.00 | **-0.51** | -0.29 | **-0.70** | 0.32 | 0.08 | **0.71** | **0.82** |
| **Altimetry*** | | 1.00 | 0.25 | 0.35 | -0.01 | -0.02 | -0.26 | -0.38 |
| **Dose** | | | 1.00 | 0.67 | 0.59 | 0.28 | 0.09 | -0.40 |
| **K** | | | | 1.00 | -0.06 | -0.08 | -0.58 | -0.82 |
| **Th** | | | | | 1.00 | 0.13 | 0.72 | 0.25 |
| **U** | | | | | | 1.00 | 0.15 | 0.16 |
| **Th/K** | | | | | | | 1.00 | 0.77 |
| **U/K** | | | | | | | | 1.00 |

130 *SRTM

131      In the correlation phase (WII), 7 variables (altimetry, Th, U, K, Th/K, U/K and dose)

132  were considered and correlated with field data (WC). Those with correlations between -0.5 and

133  0.5 were discarded. Thus, only the variables altimetry (SRTM), the K channel, and the Th/K

134  and U/K ratios were used in the multiple regression procedure. The method of regression used

135  was the backward stepwise regression, which begins with all highly correlated variables and,

136  according to the significance factor p (p<0.05), the variables are kept or removed, one by one,

137  in order to obtain the best fit of the model.

138      After the first regression, it was observed that, even though there was an acceptable

139  inverse correlation of K with WC (-0.70), the significance factor for such variable was too high

140  (p>0.05), which carried its removal from the regression process. After the second regression

141  was performed with the remaining variables (SRTM, Th/K and U/K), there were values of "p"

142  within the limits, indicating that the multiple regression equation has an overall good

143  significance and that it is statistically appropriate for weathering predictions. The statistic F

144  ratifies the significance of the regression showing values above the critical limit calculated for

145  the sample set (3.1161). Such value was obtained based on the degrees of freedom (3 to 170)

146  acquired on the calculation of the regression (Table 4). The result is the linear regression line

147  with equation 1:

148      Eq. 1: $WII = 2.2688 - 0.003*SRTM + 0.411*Th/K + 0.167*U/K$

149      Where: WII is the weathering intensity index of the area.

150

151      On the next stage, altimetric (SRTM) and gamma-ray spectrometric images (Th/K and

152  U/K) were used in the equation of weathering (WII), in ArcGis software, through map algebra,

153  to obtain the final WII map. The WII was later correlated with geochemistry, in order to

154  understand the weathering patterns and other associations (geomorphology, landscape

155  evolution, etc.).

156

| | Variables included | Multiple R | Multiple R squared | F Statistic | P-level |
|---|---|---|---|---|---|
| **Altimetry*** | 1 | 0.5035 | 0.2535 | 58.3975 | 0.0000 |
| **Th/K** | 2 | 0.7856 | 0.6172 | 137.8591 | 0.0003 |
| **U/K** | 3 | 0.8566 | 0.7337 | 156.1413 | 0.0000 |

Table 4 - Summary of stepwise regression.

157 *SRTM

158 The lateritic index (LI), developed in this paper and used to highlight the favorable areas

159 for the occurrence of lateritic duricrusts, was determined based on the direct relationship

160 between the WC and the Th/K and U/K ratios (Table 3), according to Eq. 2:

161 $$\text{Eq. 2:} \quad LI = (eTh/K) \times (eU/K) = (eTh \times eU)/K^2$$

162

163 The mafic index (MI = ASA / (K*U*Th); Pires and Moraes, 2006) was applied in order

164 to differentiate the parent rocks of lateritic duricrusts (basic rocks vs acidic rocks). The ASA

165 (Analytic Signal Amplitude) is calculated through the combination of the horizontal (Dx and

166 Dy) and vertical (Dz) first-order derivatives of the magnetic anomaly (Eq. 3) and is independent

167 from the magnetization direction or the earth magnetic field direction (Roest *et al.*, 1992). The

168 horizontal derivatives highlight the eventual sources of anomalies, while the vertical derivative

169 amplifies the short wavelength in detriment of the long wavelength. The MI contributes with

170 the delimitation of domains with higher or lower magnetism without the influence of the most

171 superficial portions represented by soils and/or overlying duricrusts rich in iron.

172 $$\text{Eq. 3:} \quad ASA = \sqrt{dx^2 + dy^2 + dz^2}$$

173 Where: ASA is the amplitude, dx and dy are the horizontal derivatives and dz is the vertical derivative.
174

175 The final products of the LI and the MI are presented in maps where the favorable areas

176 for the occurrence of lateritic duricrusts are highlighted (LI) with the different magnetic

177 domains (MI).

**178**   **3.3 Regolith mapping**

**179**        The procedure to map the regolith considered descriptions of 875 sites, including those

**180**   studied for this paper and other from the CPRM database (Geosgb), WII, LI, MI, altimetry

**181**   (SRTM) and the geomorphological and geological bases of the area. These data were associated

**182**   with the genetic model of Anand *et al.* (1993) that subdivides the regolith in three main regime

**183**   classes: residual, erosional and depositional. In the regolith map, the units were divided into: *in*

**184**   *situ* regolith and transported regolith. *In situ* regolith was subdivided in pedolith, in which soils

**185**   and lateritic duricrusts are predominant (residual) and saprolith, in which saprolite and saprock

**186**   are predominant (erosional). Alluvial deposits were included in transported regolith

**187**   (depositional); while rocky outcrops were described as bedrock in the referred map. The

**188**   geophysical products of this study (WII, LI, MI) supported the construction of the regolith map

**189**   and contributed with the final interpretations. The flowchart on figure 2 shows the products

**190**   used in the preparation of the WII (black arrow), LI (red arrow), MI (blue arrow) and the

**191**   regolith map, as well as the integration with the geochemistry and geophysics, which led to the

**192**   final interpretations and discussions (yellow arrow).
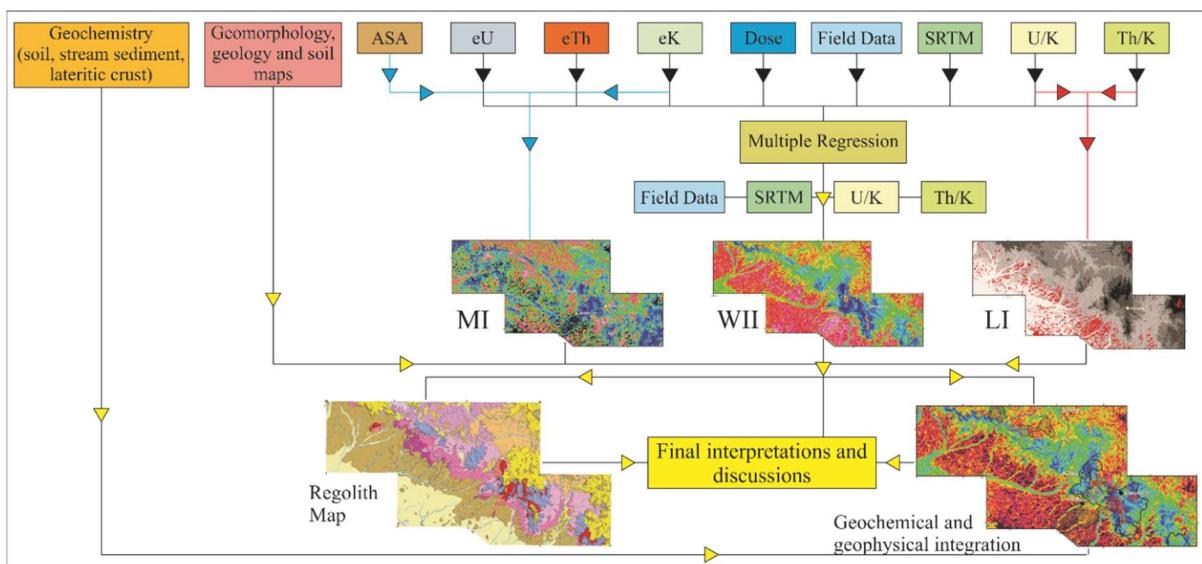


**193**
**194**        Figure 2 – Summary of procedures for mapping the regolith and lateritic duricrusts, and geochemical and
**195**        geophysical integration. ASA = Analytic Signal Amplitude, WII (Weathering Intensity Index), MI (Mafic
**196**                                            Index), and LI (Lateritic Index).
**197**

198    **4    Results**

199    **4.1 Geochemistry**

200        **4.1.1    Stream sediments**

201        In the stream sediments analysis Ag, As, Au, B, Ge, Hg, S, Sb, Re, Se, Ta, Te and W

202    have 30% or more of the samples below the detection limit and, therefore, were not used in the

203    statistical calculations. All the other elements mentioned on item 3.3 were included.

204        The univariate statistic identified 41 anomalous elements when compared to the regional

205    background (Al, Ba, Be, Bi, Ca, Cd, Ce, Co, Cr, Cs, Cu, Fe, Ga, Hf, In, K, La, Li, Lu, Mg, Mn,

206    Mo, Na, Nb, Ni, P, Pb, Rb, Sc, Sn, Sr, Tb, Th, Ti, Tl, U, V, Y, Yb, Zn and Zr) and 149

207    anomalous sites that delimited three anomalous zones (I, II and III) represented by two or more

208    contiguous watersheds (Figure 3). The anomalous zone I, defined by the association of Cu-Fe-

209    Ni-V, covers 135 km$^2$ on the northeast side of the area and consists of watersheds draining

210    basalts, diabases, gabbros, conglomerates, sandstones, siltstones and claystones. The

211    anomalous zone II, defined by the association of Al-Co-Cu-Cr-Fe-Ga-Ni-Sc-V, covers 158 km$^2$

212    on the central-north region of the area and corresponds to watersheds draining basalts, diabases

213    and gabbros. The anomalous zone III, defined by the association Ce-Hf-La-Nb-P-Tb-Th-U-Y-

214    Yb-Zr covers 628 km$^2$ on the central-southwest region of the area and corresponds to

215    watersheds draining granitoids, supracrustals, sandstones and associated lateritic duricrusts. On

216    other parts of the area, there were isolated anomalies, highlighting Cd-Zn; Ca-Mg-Na; Bi-Tl;

217    Be-Cs-K-Li-Rb-Tl; Al-Ga, Bi-Cd-Tl, or single anomalies of Bi, Ca, Cd, Co, Cr, Cs, Cu, Hf, In,

218    La, Ni, Pb, Sr, Ti, Tl, U and V.

219        The principal component analysis (PCA) determined three main factors that account for

220    74.13% of the variance. Factor 1 (Al-Co-Cr-Cu-Fe-Ga-In-Lu-Mn-Ni-Sc-Sn-V-Zn) corresponds

221    to 44.69% of the variance and is associated to basalts, diabases, gabbros and subordinately

222    schists and paragneisses. Factor 2 (Ce-La-Tb-Th-U-Y-Zr), accounts for 17.18% of the variance

223  and is related to granitoids and associated lateritic duricrusts, supracrustals and sandstones.

224  Factor 3 (Ba-Be-Ca-Cs-K-Li-Mg-Na-Rb-Sr), corresponds to 12.26% of the variance and is

225  related to supracrustals and its saprolites, located in the intermediate zone and LPS (figure 3).

226  The other factors have low variance (<5%) and have no geological meaning.
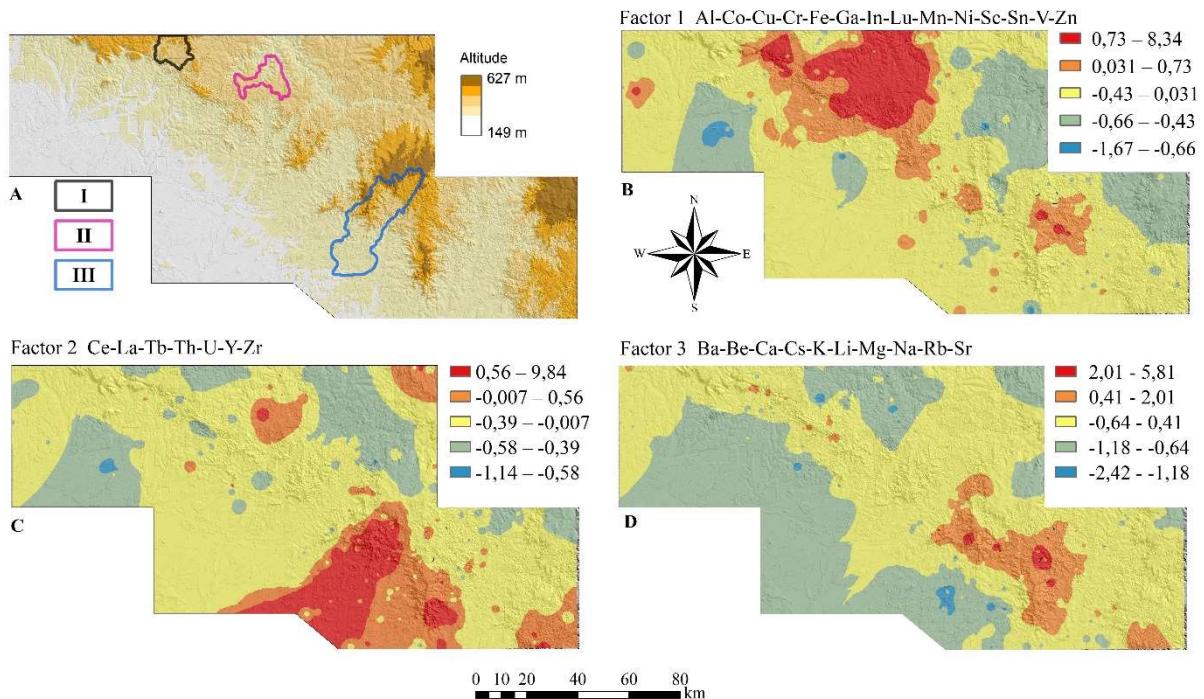


227
228  Figure 3 – A) Anomalous zones (I, II and III) represented by two or more contiguous watersheds. B, C e D)
229  Maps of stream sediments geochemical zones (interpolated scores) (high scores regions above the regional
230  background in red and orange).
231

232  **4.1.2 Soil**

233  Among the elements analyzed for the soil samples, V (689 ppm), Cr (717 ppm), Cu (516

234  ppm), Ni (312ppm), Ce (280 ppm), La (111 ppm) and Y (125 ppm) showed the highest

235  concentrations, but still within the averages found on the earth crust, rocks and/or weathered

236  products (Wedepohl, 1969). Silver, Au, As, B, Ge, Hf, Hg, Na, Re, Se, Ta, Te and W are below

237  the detection limit in at least 30% of the samples and were discarded. The PCA highlighted four

238  factors that account for 69.71% of the variance. Factor 1 was defined by the association of Cd-

239  Lu-Mn-Tb-Y-Yb-Zn, corresponding to 34.53% of the total variance and is related mainly to the

240  paragneisses and schists located in the intermediate zone and, locally, to the sandstones of the

241     UPS. The association of Al-Cu-Fe-Ga-In-Sc-Ti-V-Zr defined factor 2, and it accounts for

242     18.83% of the variance; it is associated to great part of the intermediate zone and UPS, in the

243     northwest and central part of the area, where there are basalts, diabases and gabbros, besides

244     sandstones and siltstones. Factor 3 was defined by the association of Ce-La-Th-U,

245     corresponding to 10.51% of the variance and is related to granitoids and lateritic duricrusts

246     associated, distributed over the LPS and, subordinately, to the sandstones in the intermediate

247     zone and UPS. Factor 4 was defined by the association of Be-Cs-K-Li-Mg-Rb-Tl, accounting

248     for 5.84% of the variance and it is related to the granites, gneisses, para-derived rocks and their

249     saprolites located on the intermediate zone, UPS and subordinately on the LPS (Figure 4).
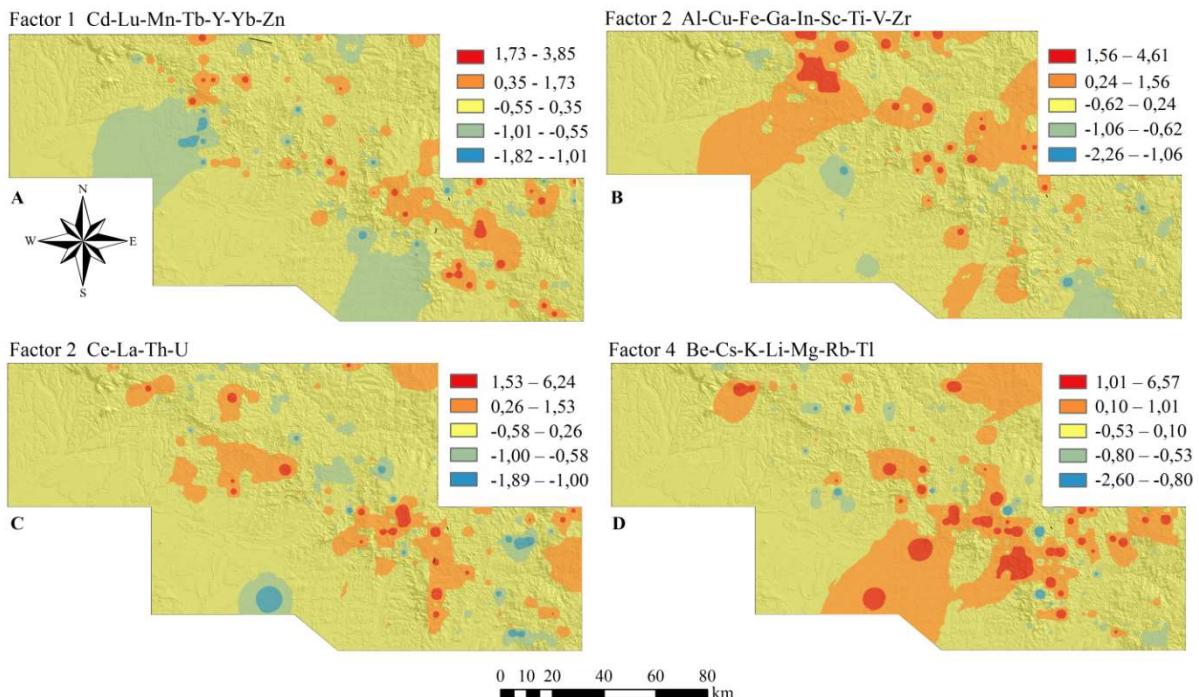


250
251     Figure 4 – Maps of anomalous soil geochemical zones (interpolated scores) (high scores regions above the
252                        regional background in red and orange), integrated with the relief.
253

254     **4.1.3 Lateritic duricrust**

255       The samples of the LPS have an inverse relationship between $Fe_2O_3$ and $SiO_2$

256     ($Fe_2O_3/SiO_2$ average of 1.36), while $Al_2O_3$ shows no relationship with $SiO_2$ (dispersion),

257     presenting an $Al_2O_3/SiO_2$ average of 0.53 (Figure 5). $TiO_2$, $K_2O$, $P_2O_5$, $CaO$, $MgO$ and $Na_2O$

have contents below 2% (Appendix) and the correlation with major oxides showed dispersion. Among the trace elements, Ba, Cd, Cr, Cs, K, Ni, P, Pb, Rb, Sr, Ta and V are above the regional background in 17 sites. From those, only Ta (10.47 ppm) and V (2723 ppm) are three to five times above the average concentration of lateritic duricrusts (Wedepohl, 1969; Tardy, 1993; Hill *et al.,* 2001; Kotschoubey *et al.,* 2005) indicating relevant anomalies. REEs have an average of 72.9 ppm, there is an enrichment of LREEs in detriment of HREEs ($La_N/Yb_N = 3.22$) and the average of the Eu/Eu* and Ce/Ce* anomalies are 0.64 and 2.75 respectively (figure 6, Appendix). The plot $Al_2O_3$ - $Fe_2O_3$ - ($CaO+K_2O+MgO+Na_2O+P_2O_5$) highlights samples with higher values of alkali and less content of iron when compared to the samples of the UPS and intermediate zone (Figure 7B). These samples are classified as laterite and subordinately ferruginous and fersiallitic laterites, and related to moderate lateritization (Schellmann, 1981 and 1983; Dury, 1969) (Figures 7A and 7C).

Similar to the LPS, the samples of the UPS have an inverse relationship between $Fe_2O_3$ and $SiO_2$ (figure 5), however, the average ratio is higher, 3.01. $Al_2O_3$ and $SiO_2$ are directly proportional (Figure 5) and have an average ratio higher than the LPS (average of 0.7). $TiO_2$, $K_2O$, $P_2O_5$ e CaO, MgO and $Na_2O$ have concentrations lower than those found on the LPS, except for $P_2O_5$, and show a dispersion pattern when correlated individually to major oxides. Among the trace elements, only Ta and V have concentrations (11.29 and 1,849 ppm, respectively) above lateritic duricrusts and bauxite average (Wedepohl, 1969; Tardy, 1993; Hill *et al.,* 2001; Kotschoubey *et al.,* 2005). REEs have average concentration of 52.4 ppm, strong enrichment of the LREEs ($La_N/Yb_N = 6.61$) and ratios Eu/Eu* and Ce/Ce* of 0.64 each, which is generally lower than those found on the LPS (Figure 6), while the ratio $La_N/Yb_N$ is approximately two times higher. In general, there is a lower concentration of Co+Cr+Ni and higher Th/K ratio when compared to the LPS (Figures 7D and E). The plot $Al_2O_3$ - $Fe_2O_3$ - ($CaO+K_2O+MgO+Na_2O+P_2O_5$) highlights high content of $Fe_2O_3$ and simultaneously low

283    content of alkali on the UPS (Figure 7B). These samples are classified as ferruginous and

284    fersiallitic laterites and are related to intense lateritization (Dury, 1969; Schellmann, 1981 and

285    1983), (Figures 7A and C).

286         The samples of the intermediate zone have $Fe_2O_3$ and alkali concentrations similar to

287    those observed on the UPS, i.e., high values of $Fe_2O_3$ and simultaneously low values of alkali

288    (Figure 7B). The average $Fe_2O_3/SiO_2$ ratio is 1.74, while the average $Al_2O_3/SiO_2$ ratio is 0.54.

289    $TiO_2$, $K_2O$, $P_2O_5$, CaO, MgO and $Na_2O$ have lower contents than those found on the LPS. None

290    of the trace elements are above the regional background. REEs have average concentration of

291    43 ppm, average Eu/Eu* of 0.56, $La_N/Yb_N$ ratio of 4.3, and Ce/Ce* of 0.90. The REEs

292    concentrations and the Eu/Eu* and Ce/Ce* ratios are lower than those found on the other

293    surfaces, but the $La_N/Yb_N$ ratio is higher than that found on the LPS. The Th/K-U/K-$SiO_2$/$Fe_2O_3$

294    and REE-CoCrNi-ScYZr plots are similar to the UPS, as well as high Th and low K and U

295    concentrations (Figure 7B and E). These samples are categorized as moderate lateritization, and

296    are classified as laterite/ferruginous and fersiallitic laterite (figures 7A and C).

297         The PCA identified 6 factors that account for 81.6% of the variance and define the

298    following geochemical associations: REE-(La+Ce) (factor 1); In -La-Mo-Sn-Ta-Te-W (factor

299    2); Cs-Ge-K-Ni-Rb-Sr-Y (factor3), Hf-Th-Zr (factor 4), Cu-Sc-U (factor 5) and Ba-Ce-Nb-Pb

300    (factor 6), mostly associated to residual minerals (zircon, monazite, muscovite, etc.).
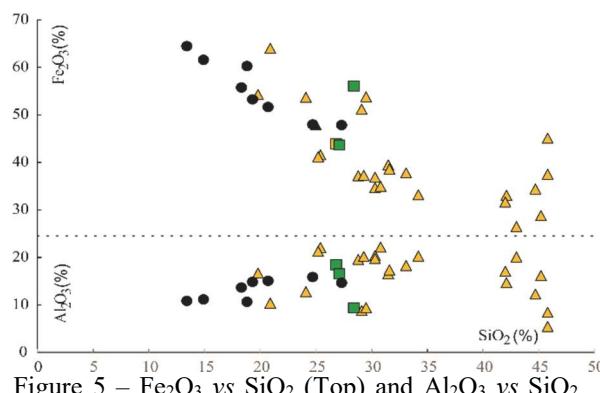


Figure 5 – $Fe_2O_3$ vs $SiO_2$ (Top) and $Al_2O_3$ vs $SiO_2$ (Bottom) ● UPS; ■ IZ; ▲ LPS.
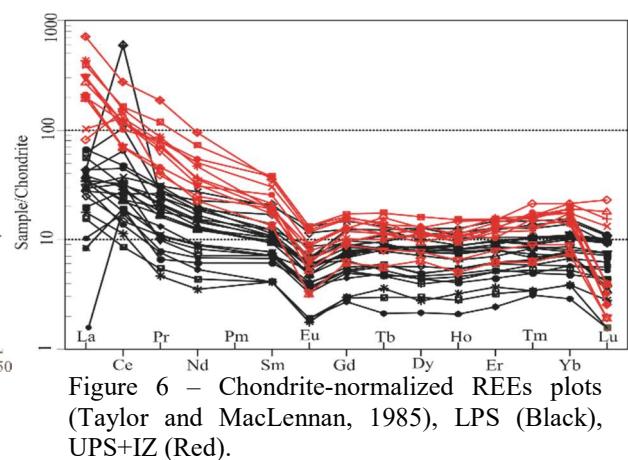


Figure 6 – Chondrite-normalized REEs plots (Taylor and MacLennan, 1985), LPS (Black), UPS+IZ (Red).
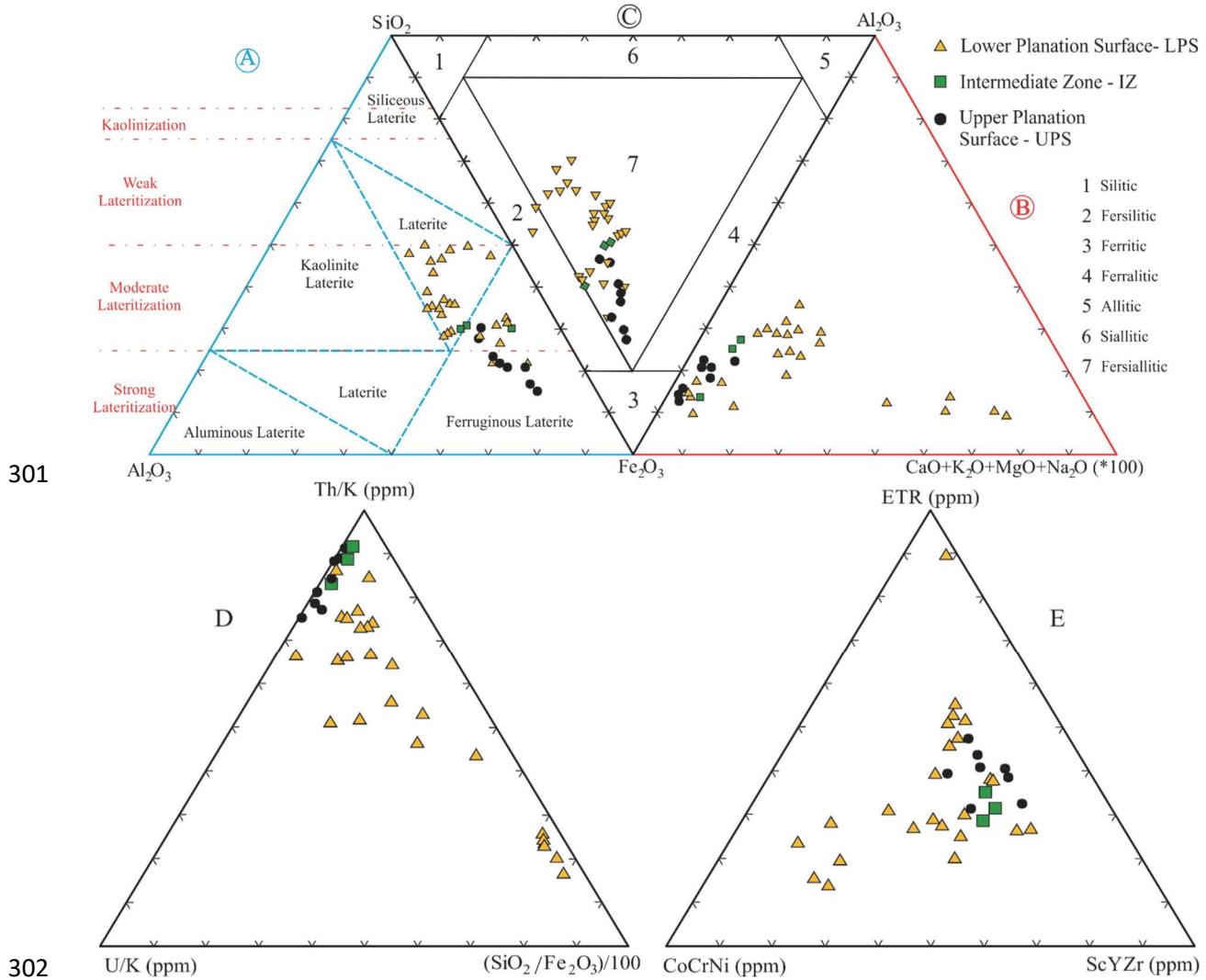
Figure 7 – A) Ternary plot $SiO_2$ –$Al_2O_3$ –$Fe_2O_3$ (Schellmann, 1983), and degree of lateritization. B) Ternary plot $Al2O3$ – $Fe2O3$ – alkali evidencing the decrease of alkali on the UPS. C) Ternary plot $SiO_2$ – $Fe_2O_3$ - $Al_2O_3$ (Dury 1969) highlighting the fersiallitic classification of most of the samples. D) Ternary plot Th/K-U/K-$SiO_2$-$Al_2O_3$/100 emphasizing higher values of Th and $Fe_2O_3$ and lower values of K on the samples of the UPS. E) Ternary plot REE-CoCrNi-ScYZr remarking the samples of the LPS with high values of CoCrNi and low values of REE, and lower values of CoCrNi and high values of REE on lateritic duricrusts derived from sandstones.

The weathering indexes CIA and WIP (Nesbit and Young, 1982 and Parker, 1970, respectively), indicate weathering rates similar to those found on lateritic duricrusts from Africa, Guyana and India (Harrison, 1934; Giorgis *et al.,* 2014, Wimpenny *et al.*, 2007) (Figure 8), and predominantly higher than those from Iran, Ireland, China and Australia (Asghar Calagari *et al.,* 2015; Hill *et al.,* 2000; Xiao *et al.,* 2014; Cornelius *et al.*, 2007).
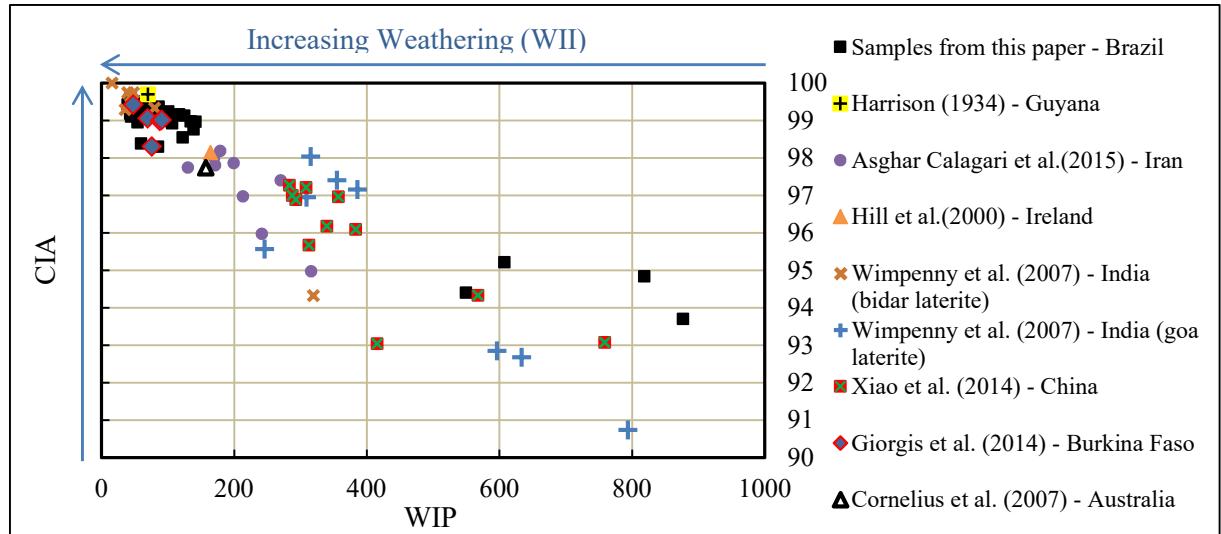
Figure 8– Plot of WIP vs CIA of lateritic duricrusts of the study area and other parts of the world.

## 4.2 Weathering intensity index (WII)

The classification of the weathering level allowed the distinction of areas with similar weathering characteristics (Table 1). The WII highlighted four major domains: i) south-southwest-west side of the area (altitudes below 300 m) and mainly marked by high weathering intensity (WC = 4 and 5; red on figure 9) that corresponds to alluvial deposits, lateritic duricrusts, dismantling products and oxisols; ii) southeast-central-northwest region of the area (altitudes between 300 and 500 m) and marked by intermediate weathering intensity (WC = 3; green and yellow on figure 9) that correspond to the sites with weathered rocky outcrops (saprolite); iii) southeast-central-northwest areas (altitudes between 300 and 500 m), low weathering intensity (WC = 1 and 2, blue on figure 9) with mafic rock outcrops, schists and granites with weak or no weathering at all; and iv) north and northeast parts of the area (high weathering intensity; WC = 4 and 5; red and pink on figure 9) with the presence of lateritic duricrusts and oxisols. Both domains "i" and "iv" are partially coincident with the areas predicted as favorable for the occurrence of lateritic duricrusts and oxisols proposed by Iza *et al.* (2016).
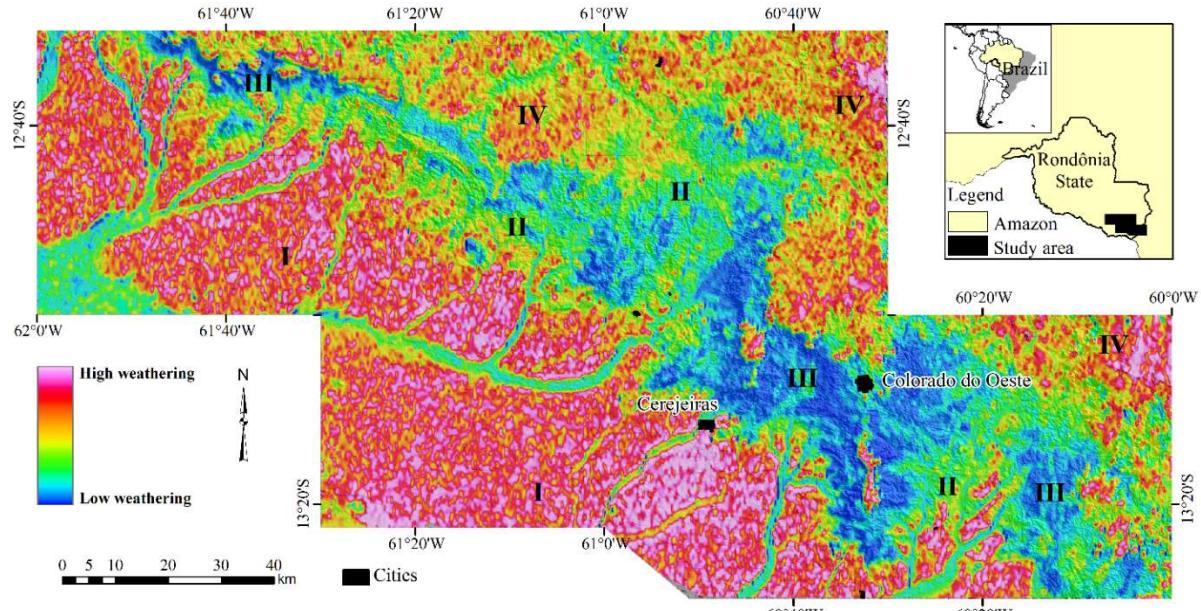
Figure 9 – Weathering Intensity Index (WII) overlying the shaded altimetry highlighting main domains of weathering.

## 4.3 Lateritic index (LI)

The calculation of the LI highlighted 4 major domains: i) South-southwest-west regions of the area (altitudes below 300 m) mainly marked by high lateritic index (red to pink on figure 10); ii) southeast-central-northwest portions of the area with altitudes between 300 and 500 m, marked by intermediate lateritic index (green and yellow on figure 10); iii) southeast-central-northwest regions of the area associated with altitudes between 300 and 500 m and marked by low lateritic index (blue on figure 10); and iv) north and northeast side of the area with high lateritic index (red to pink on figure 10). In a general view, the domains previously described cover the same geological domains as the WII. The main differences between the WII and the LI, are on the "i" and "iii" domains where there are areas slightly more weathered (more continuous) on the WII than on the LI.
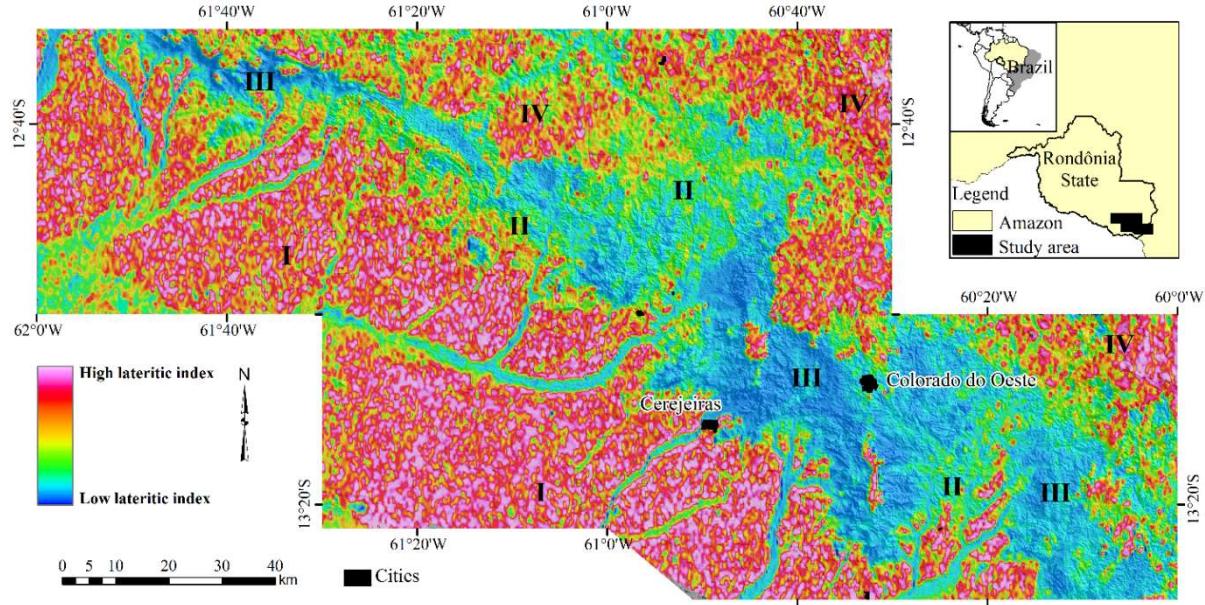
Figure 10 – Lateritic Index (LI) overlying the shaded altimetry of the altimetry highlighting the main domains.

353        The predicted areas for the occurrence of lateritic duricrusts defined by the LI and

354  WII represent about 7.5% and 8% of the area, respectively. These values are lower than those

355  found by Iza *et al.* (2016) using the fuzzy gamma operator 0.7, which determined about 11%

356  of the area with potential for the occurrence of lateritic duricrusts. These areas have a strong

357  relationship with flat areas (slopes <5%) and with altimetry below 300 m and above 500 m.

358  This disparity is probably associated to the methods and mathematical techniques used on the

359  corresponding models. In any case, these areas are considered to have higher probability of

360  occurrence of lateritic duricrusts and therefore related to the predominance of residual

361  processes.

362

## 363  4.4 Mafic index (MI)

364        The mafic index (MI) defined 4 major domains of substrates according to the magnetic

365  degree: i) north side with a predominant magnetic substrate, associated mainly with mafic rocks

366  (red to pink on figure 11); ii) central-southeast and southeast side of the area of predominantly

367  less magnetic materials, associated with granitoid rocks (blue on figure 11); iii) northwest-

368    central-south portion where there is an alternation of magnetic materials with less magnetic

369    materials, related to para-derived rocks, gneisses, granitoids, etc. (blue and pink on figure 11);

370    and iv) northeast-central portion where there is an alternation of magnetic materials with less

371    magnetic materials, related to the Parecis Basin that consists of sandstones and siltstones, (blue

372    and pink on figure 11). The areas with high LI (more intensely lateritized, represented by the

373    areas with the average plus 1.5 times the standard deviation) present an overlap on the northeast

374    side with domains that are less magnetic (sandstones), and an overlap on the northwest and

375    south region with domains that present high and low MI (mafic and felsic rocks, respectively)

376    (Figure 11). These results are important to clarify the origin of the lateritic duricrusts (parental

377    rocks), especially those on the LPS (iii-northwest-south) where the area is mainly covered by

378    soils and sediments.
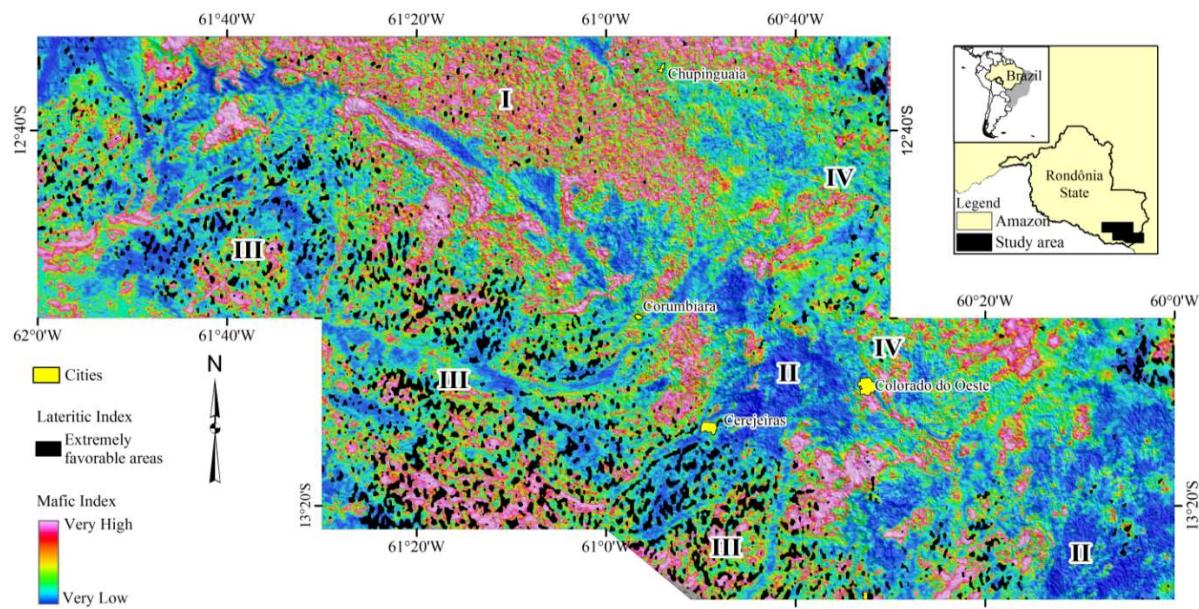


379
380    Figure 11 – Lateritic Index (black) overlying the mafic index (MI) highlighting the 4 main domains.
381
382

**4.5 Regolith map**

384         The regolith map, which is pioneer in the Amazon, was developed based on field work

385    and supported by the WII, LI and the results of Iza *et al.* (2016). This integration showed an

386    expansion of the areas more intensely weathered and strongly related to residual materials

387  (Figures 1 and 12). It was confirmed that the highly weathered domains (figures 9 and 10) are

388  associated with lateritic duricrusts and oxisols on the UPS and on the LPS, as indicated by Iza

389  *et al.* (2016). The area mapped as undifferentiated sedimentary covers (Quadros and Rizzotto,

390  2007) was interpreted and mapped as consisting only of residual materials since it represents

391  oxisols, lateritic duricrusts and dismantling products.



**TRANSPORTED REGOLITH**
**Depositional Landforms**

Alluvial deposits consisting mostly of sand, gravel, clay and silt, mainly associated with the flood plain of the Guaporé river tributaries and subject to periodic floods. The relief is plain and related to fluvial plains and terraces with altitudes below 300 m. On altitudes below 250 m swampy terrains consisting of clay and silt may occur.

**IN SITU REGOLITH**
**Pedolith**

Lateritic crusts and dismantling products besides oxisols, associated with plain relief occurring mainly in altitudes below 300 m and above 500 m.

Quartzipsamment and coarse saprolite derived from sandstones, arcosean sandstones and siltstones. The landforms have flat tops and altitudes between 300 and 500 m.

Red to yellow dystrophic ultisols with rare occurrence of coarse and fine saprolite, basalts, diabases and gabbros located on altitudes below 400 m. The relief has tabular and convex tops.

Red-yellow eutrophic ultisol with frequent occurrence of coarse and fine saprolite derived from granitic rocks, located on altitudes of up to 400 m. The landforms have convex tops and sometimes evidence structural control.

Red-yellow eutrophic ultisol with eventual occurrences of fine saprolite derived from granitic rocks, located on altitudes of up to 300 m.

Red-yellow dystrophic ultisol with medium to fine texture mainly associated to paraderived rocks. Outcrops of fine saprolite are rares and altitudes reach 300 m.

**Saprolith**

Fine saprolite, clayey horizon and colluvium derived from paraderived rocks. The relief is plain with eventual convex tops, with maximum altitudes of 350 m.

Sandstones, arcosean sandstones and siltstones commonly associated with coarse saprolite to quartzipsamment. The landforms have flat tops and altitudes are below 500 m.

Coarse and fine saprolite, consisting of basalts, diabases and gabbros located on altitudes below 400 m. The ocurrence of red-yellow dystrophic ultisols is common. The relief has tabular and convex tops.

Coarse saprolite, and colluvium locally derived from paraderived rocks. The landforms have convex tops and, in general, evidence structural control. The altitudes vary between 350 and 500 m. The soils are mainly ultisols and subordinately alfisols.

**Bedrock**

Sandstones, arcosean sandstones and siltstones with eventual coarse saprolite. The landforms have flat tops and are rarely convex. The altitudes are above 500 m.

Granitic rocks sometimes with little signs of decomposition and eventual occurrence of coarse saprolite, located on altituted of up to 400 m. The landforms have convex tops and sometimes evidence structural control.

Paraderived rocks with very rare presence of coarse saprolite. The landforms have convex tops and, in general, evidence structural control. Altitudes vary between 350 and 500 m.

Figure 12 – Regolith map.

**5 Integration of geochemical and geophysical data**

The regolith study using gamma-ray spectrometric data is discussed by several authors (Dauth, 1997; Carrino, 2011; Barbosa, 2013; Wilford, 2012; Iza *et al.,* 2016). They remark that high Th/K and U/K ratios (in this paper between 254 and 1148 and between 29 and 111 respectively) have excellent correlation with lateritic duricrusts.

The WII and LI contributed to the regolith mapping and the identification of lateritic domains (residual) previously considered sedimentary by other authors. This statement can be extrapolated to all the western portion of the Brazilian Amazon, expanding, thereby, the areas with mineral potential related to supergene enrichment. The correlation between WIP and CIA reflects the high weathering indexes registered in the Amazon when compared to those in China, India, Iran, Ireland and Australia (Figure 8). Additionally, the WII, as well as the LI, have excellent spatial correlation with geochemical data from soil and stream sediments. In any case, the WII shows to be more robust because it considers the altimetry and delimits weathering areas (high and low) and not only the domains with higher probability of occurrence of lateritic duricrusts.

The MI, ratified by the geochemical results (stream sediments and soil), discriminated lateritic duricrusts developed on substrates with different magnetic signatures responses (mafic and felsic). The respective averages of the LPS and UPS lateritic duricrusts samples of Ba (134 and 15 ppm,), Co (10 and 2.5 ppm), Cr (335 and 138 ppm), Ni (21 and 8 ppm), Rb (12 and 2 ppm), Th (23 and 41 ppm) (Apendix) ratify the influence of the mafic bedrock on the LPS. On the other hand, the lower concentration of Co+Cr+Ni and simultaneous higher concentration of Sc+Y+Zr (Figure 7E) of a set of samples reflect the felsic parent rock of those lateritic duricrusts. The stream sediments zones I and II and PCA factor 1, together with soil PCA factor 2 show a good spatial overlap and delimit the weathering area of mafic rocks, confirming part of the MI results and high WII response.

421      The high concentrations of Al, Ce, Co, Cr, Cu, Fe, Ga, Hf, Ni, Th, U, V and Zr, and

422      simultaneous lower concentrations of alkali is another geochemical criteria for the

423      determination of highly weathered areas and identification of lateritic domains. These results

424      are particularly true when compared with areas showing high WII and/or LI (Figures 9, 10 and

425      13).

426      The integration of geophysics and geochemistry, through gamma-ray spectrometry and

427      analysis of stream sediments, soil and lithochemistry of lateritic duricrusts, allowed the

428      subdivision of the study area in two major weathering domains: i) central-southeast portion of

429      the area: with lower WII (WC = 1 and 2, table 1) and geochemical association of Ba-Be-Ca-

430      Cs-K-Li-Mg-Na-Rb-Sr. This domain is between 300 and 500 m high, has undulated relief and

431      slopes between 10º and 65º corresponding to the intermediate zone of Iza *et al.* (2016), where

432      the erosive process, which exposes rocks and saprolite, is dominant over the weathering

433      process; ii) south-southwest-west and northeast portions of the area, with higher WII (WC = 4

434      and 5, table 1) related to lateritic duricrusts and geochemical association of Al-Ce-Ga-Hf-La-

435      Tb-Th-U-Y-Zr. In this domain, between 149 and 300 m and between 500 and 627 m high,

436      which corresponds mostly to the LPS and UPS of Iza *et al*. (2016), respectively, the weathering

437      process is dominant over the erosive process.

438      The lateritic duricrusts of the UPS, where the sedimentary parent rocks are predominant,

439      show higher content of $Fe_2O_3$ and Th, and lower of $SiO_2$ and $CaO+K_2O+MgO+Na_2O+P_2O_5$.

440      These results allowed the differentiation of these lateritic duricrust from those on the LPS. The

441      LI, WII and the data from Iza *et al.* (2016), ratify these findings, as they highlight high

442      weathering level on the UPS, high eTh/K ratio and intense lateritization. Table 5 shows the

443      main characteristics of the lateritic duricrusts in the respective geomorphological domains.
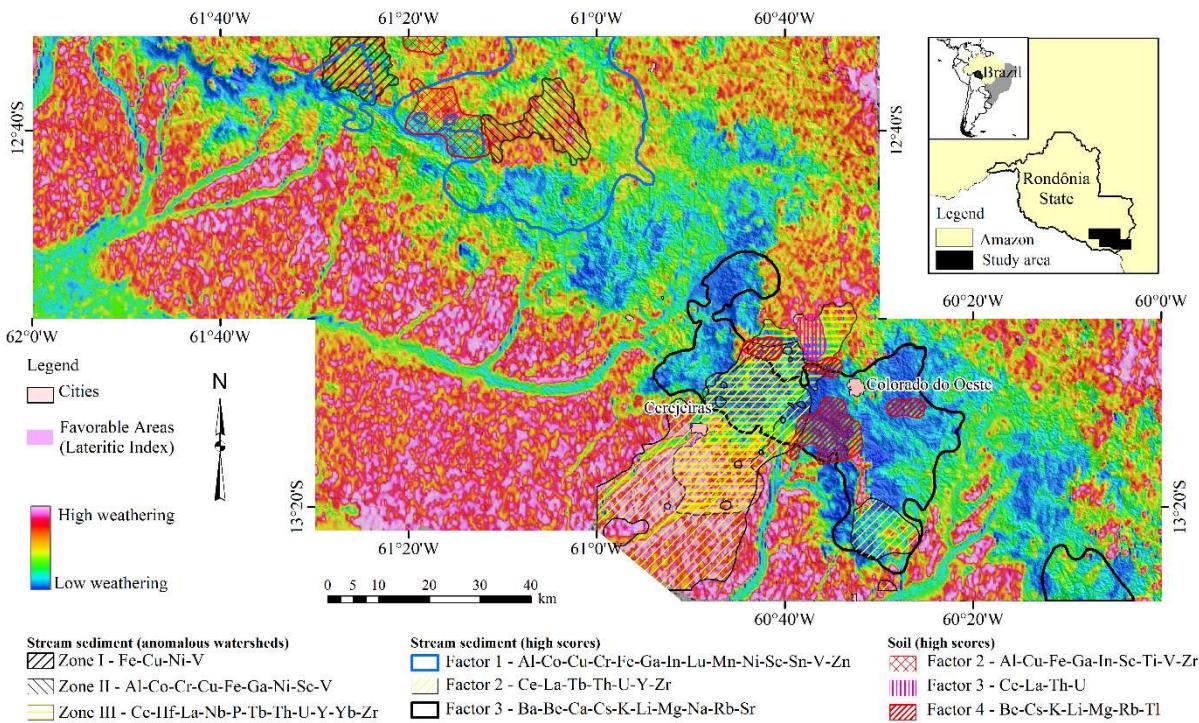
449         Table 5 – Main characteristics of lateritic crusts and respective geomorphological domains.

| | Upper Planation Surface (UPS) | Lower Planation Surface (LPS) Intermediate Zone (IZ) |
|---|---|---|
| Texture/Structure | Cellular; Pisolithic; Nodular | Pisolithic; Nodular; vermiform/columnar |
| Macro-mineralogy | +Hem; +Gt; -Kln; +Qz + Gbs | +Hem; + Gt; Kln; -Qz; -Gbs |
| Type of occurrence | Blocks and large outcrops | Blocks < 3 m (mainly) and restrict outcrops |
| Altimetry | Plateaus above 500m | Floodplains below 300 m/ >300 and <500m |
| Preserved fabrics (parent rock) | Not observed | Present, very rarely (schist) |
| Lithology | Sandstones (Parecis Basin), mainly. | Varied (bedrock) and recent deposits (absence of sedimentary rocks). |
| Geochemistry (SS) Intersection with PM* | Zone III (restrict) | Zone III / Zone I and II; Factor 1 |
| Geochemistry (Soil) Intersection with PM* | Factor 3 | Not observed |
| Lithochemical anomaly | V-Ta | V-Ta |
| Major elements (Crust) | $Fe_2O_3 > SiO_2$ (trend) | $Fe_2O_3 < SiO_2$ (trend) |
| REE | LREE>HREE | LREE>HREE (Ce anomaly) |
| Th/K | Th>>K | Th>K |
| Alkali (CaO, MgO, $K_2O$, $Na_2O$) | Lower concentration | Higher concentration |
| Lateritization (Schellmann, 1983) | Intense (trend) | Moderate (trend) |
| Classification (Dury 1969) | Fersiallitic | Fersiallitic |
| WII | High index | High/low index |
| LI | High Index | High/low index |
| IM | Low (predominantly) | High and low (variable) |

450     *PM = Predictability Model

451

## 6 Final remarks

452

453 The integration of geophysical indexes WII, LI and MI with geochemical data, altimetry,

454 as well as the relationship between the geochemical weathering indexes (WIP vs CIA), are

455 efficient tools for regolith characterization and mapping and should be considered tools of wide

456 spectrum. This multisource integration provided, besides the generation of the regolith map, the

457 reinterpretation of geological units.

458 The WII highlighted areas with different weathering levels, including those propitious to

459 the occurrence of lateritic duricrusts (high WII and LI) and those with rocks weakly weathered

460 or unaltered. The LI and MI, as well as integration techniques of multisource data (Iza *et al.*,

461 2016), are complementary tools and contribute directly to the identification of lateritic

462 duricrusts and respective parent rock. The geochemistry confirms the efficiency of these tools,

463 as they support the identification of areas with different weathering levels. Thus, the

464 combination of these techniques can be used to refine geologic maps in scales of 1:100.000 or

465 of less detail and consequently open new prospective frontiers related to supergene deposits.

466 This approach can be confidently applied in areas with difficult access (Amazon rainforest),

467 with restrict access (indigenous and environmental preservation lands) and/or areas with a lack

468 of mapping works in detail and semi-detail scale, like the Brazilian Amazon.

469

470

477
478
479
Appendix – Lateritic duricrusts samples analyzed at GEOSOL Laboratories (Belo Horizonte, Brazil); Eu/Eu* ¼[EuN/(SmN + GdN)/2]; LOI ¼ loss on ignition; major elements in wt,% and trace elements in ppm.

| Sample | TB-191 | TB-74 | TB-70 | TB-197 | TB-187 | TB-68 | TB-165 | TB-211 | EI-7 | EI-39 | TB-134 | TB-124A |
|---|---|---|---|---|---|---|---|---|---|---|---|---|
| Surface | LPS | LPS | LPS | LPS | LPS | LPS | LPS | LPS | LPS | LPS | LPS | LPS |
| Altitude m | 199 | 204 | 214 | 214 | 219 | 222 | 228 | 232 | 234 | 255 | 258 | 258 |
| SiO$_2$ | 45.2 | 28.8 | 29.3 | 29.1 | 31.5 | 30.3 | 30.8 | 34.2 | 42.1 | 45.8 | 45.8 | 33.1 |
| TiO2 | 0.78 | 1.07 | 1.15 | 0.58 | 0.65 | 1.16 | 0.9 | 0.78 | 0.56 | 0.24 | 0.37 | 0.65 |
| Al$_2$O$_3$ | 16.2 | 19.6 | 20.2 | 8.83 | 16.6 | 20.4 | 22.2 | 20.3 | 14.7 | 5.47 | 8.47 | 18.3 |
| Fe$_2$O$_3$ | 28.8 | 37.2 | 37.3 | 51.2 | 39.5 | 34.7 | 35 | 33.2 | 33.1 | 45.1 | 37.5 | 37.8 |
| CaO | 0.02 | 0.02 | 0.02 | 0.02 | 0.04 | 0.03 | 0.08 | 0.06 | 0.005 | 0.01 | 0.01 | 0.02 |
| K$_2$O | 0.13 | 0.08 | 0.1 | 0.01 | 0.08 | 0.1 | 0.1 | 0.04 | 0.13 | 0.03 | 0.01 | 0.05 |
| P$_2$O$_5$ | 0.07 | 0.112 | 0.096 | 0.145 | 0.135 | 0.107 | 0.109 | 0.066 | 0.169 | 0.078 | 0.168 | 0.06 |
| MgO | <0.1 | <0.1 | <0.1 | <0.1 | <0.1 | 0.11 | 0.13 | 0.11 | <0.1 | <0.1 | <0.1 | 0.11 |
| Na$_2$O | <0.1 | <0.1 | <0.1 | <0.1 | <0.1 | <0.1 | <0.1 | <0.1 | <0.1 | <0.1 | <0.1 | <0.1 |
| LOI | 9.3 | 12.24 | 11.56 | 10.23 | 11.29 | 12.03 | 11.1 | 10.78 | 9.21 | 3.96 | 6.8 | 10.04 |
| Total | 100.6 | 99.5 | 100.0 | 100.1 | 99.8 | 99.1 | 100.4 | 99.5 | 100.0 | 100.7 | 99.2 | 100.1 |
| Fe$_2$O$_3$/Al$_2$O$_3$ | 1.78 | 1.90 | 1.85 | 5.80 | 2.38 | 1.70 | 1.58 | 1.64 | 2.25 | 8.24 | 4.43 | 2.07 |
| Fe$_2$O$_3$/ SiO$_2$ | 0.6 | 1.29 | 1.76 | 1.273 | 1.25 | 1.15 | 1.14 | 0.97 | 0.78 | 0.98 | 1.14 | 0.81 |
| Al$_2$O$_3$/SiO$_2$ | 0.36 | 0.68 | 0.30 | 0.69 | 0.53 | 0.67 | 0.72 | 0.59 | 0.35 | 0.12 | 0.55 | 0.18 |
| Ag | <0.01 | <0.02 | <0.02 | <0.02 | <0.02 | <0.02 | <0.02 | <0.02 | <0.02 | <0.02 | 1.54 | 3.08 |
| As | 186.0 | 227.0 | 235.0 | 77.0 | 32.0 | 237.0 | 188.0 | 130.0 | 29.0 | 141.0 | 168.0 | 147.0 |
| Ba | 28.0 | 20.0 | 26.0 | 14.0 | 27.0 | 27.0 | 38.0 | 11.0 | 1525.0 | 17.0 | 22.0 | 20.0 |
| Be | 1.10 | 0.80 | 0.80 | 1.10 | 2.00 | 0.90 | 1.20 | 0.80 | 0.90 | 0.30 | 0.40 | 0.70 |
| Bi | 0.40 | 0.59 | 0.57 | 0.12 | 0.17 | 0.65 | 0.28 | 0.26 | 0.13 | 0.02 | 0.29 | 0.22 |
| Co | 11.80 | 3.10 | 3.60 | 11.10 | 10.80 | 4.00 | 5.90 | 7.40 | 24.30 | 2.90 | 2.20 | 10.20 |
| Cd | 0.03 | 0.04 | 0.02 | 0.01 | 0.01 | 0.07 | 0.01 | 0.03 | 0.05 | 0.02 | 0.09 | 0.06 |
| Cr | 505.0 | 1221.0 | 1138.0 | 102.0 | 113.0 | 1052.0 | 304.0 | 170.0 | 28.0 | 64.0 | 196.0 | 215.0 |
| Cs | 0.88 | 0.72 | 0.84 | 0.10 | 1.01 | 0.83 | 0.78 | 0.98 | 0.76 | 0.17 | 0.12 | 0.54 |
| Cu | 45.80 | 48.30 | 41.60 | 75.20 | 184.10 | 58.40 | 24.50 | 31.70 | 83.10 | 10.00 | 28.50 | 55.50 |
| Ga | 31.70 | 51.20 | 47.10 | 12.90 | 24.70 | 56.40 | 48.00 | 33.10 | 29.20 | 11.00 | 18.90 | 34.30 |
| Ge | 0.90 | 0.90 | 0.50 | 0.50 | 0.70 | 0.60 | 0.40 | 0.90 | 0.50 | 1.00 | 0.60 | 1.50 |
| Hf | 8.79 | 11.04 | 11.89 | 5.32 | 4.56 | 11.45 | 12.62 | 6.20 | 9.50 | 4.42 | 6.99 | 5.21 |
| In | 0.24 | 0.35 | 0.34 | 0.09 | 0.14 | 0.39 | 0.31 | 0.16 | 0.14 | 0.10 | 0.45 | 0.18 |
| Mo | 5.85 | 9.75 | 9.27 | 2.75 | 5.02 | 9.22 | 7.62 | 5.74 | 6.27 | 1.16 | 4.58 | 6.40 |
| Na | 0.06 | 0.01 | 0.01 | 0.03 | 0.06 | 0.01 | 0.01 | 0.19 | 0.01 | 0.01 | 0.01 | 0.15 |
| Nb | 8.89 | 12.65 | 13.27 | 6.26 | 6.94 | 13.41 | 13.84 | 7.01 | 26.24 | 5.49 | 7.70 | 4.76 |
| Ni | 17.10 | 17.20 | 17.90 | 17.20 | 17.90 | 19.40 | 15.80 | 19.40 | 8.70 | 4.20 | 6.80 | 19.90 |
| P | 420.0 | 412.0 | 421.0 | 708.0 | 630.0 | 548.0 | 497.0 | 333.0 | 588.0 | 328.0 | 685.0 | 279.0 |
| Pb | 88.30 | 25.10 | 29.70 | 13.80 | 28.60 | 28.20 | 19.10 | 17.10 | 121.20 | 34.70 | 70.70 | 27.00 |
| Rb | 7.30 | 5.00 | 6.10 | 0.70 | 4.30 | 6.30 | 9.70 | 4.00 | 6.80 | 3.10 | 1.00 | 3.60 |
| Sn | 2.20 | 2.00 | 2.50 | 0.90 | 3.30 | 2.40 | 2.10 | 1.70 | 3.80 | 1.80 | 2.10 | 1.50 |
| Sr | 9.70 | 6.90 | 10.00 | 8.50 | 8.30 | 11.10 | 11.00 | 7.80 | 7.30 | 9.40 | 13.30 | 7.20 |
| Sb | 1.68 | 1.98 | 2.62 | 0.50 | 0.57 | 1.94 | 0.91 | 1.66 | 0.45 | 0.80 | 1.85 | 1.32 |
| Sc | 30.30 | 14.90 | 45.00 | 26.10 | 50.50 | 42.00 | 26.40 | 37.40 | 32.90 | 7.00 | 44.50 | 51.70 |
| Th | 24.10 | 32.40 | 35.40 | 10.10 | 15.50 | 35.10 | 32.30 | 16.00 | 32.10 | 20.00 | 30.40 | 17.00 |
| Ta | 0.61 | 0.13 | 0.02 | 0.39 | 0.73 | 0.07 | 0.07 | 0.85 | 3.35 | 0.31 | 0.14 | 0.44 |
| Te | 0.25 | 0.26 | 0.53 | 0.02 | 0.02 | 0.31 | 0.02 | 0.29 | 0.13 | 0.39 | 1.08 | 0.19 |
| U | 5.69 | 6.83 | 5.93 | 4.55 | 9.34 | 6.97 | 5.74 | 5.34 | 6.36 | 1.61 | 4.33 | 5.17 |
| V | 365.0 | 721.0 | 572.0 | 196.0 | 404.0 | 608.0 | 389.0 | 538.0 | 253.0 | 649.0 | 2723.0 | 645.0 |
| W | 0.90 | 0.80 | 1.80 | 0.30 | 0.50 | 0.80 | 0.30 | 0.60 | 0.60 | 0.30 | 0.80 | 0.40 |
| Y | 12.54 | 14.85 | 14.92 | 16.39 | 12.64 | 14.97 | 15.00 | 5.16 | 14.72 | 4.20 | 6.62 | 7.66 |
| Zn | 78.00 | 58.00 | 66.00 | 51.00 | 98.00 | 77.00 | 43.00 | 22.00 | 66.00 | 10.00 | 16.00 | 39.00 |
| Zr | 288.70 | 356.50 | 379.60 | 189.50 | 148.00 | 366.30 | 428.60 | 201.50 | 188.40 | 143.50 | 180.10 | 145.50 |
| La | 15.2 | 4.9 | 9.4 | 10.5 | 7.9 | 10.3 | 12.4 | 2 | 12.1 | 6.1 | 3.2 | 3.4 |
| Ce | 35.9 | 26.2 | 18.5 | 30 | 21 | 30 | 25.4 | 9.1 | 483.3 | 11.1 | 38.5 | 19.7 |
| Pr | 3.51 | 2.6 | 2.41 | 3.77 | 3.24 | 3.77 | 2.97 | 0.57 | 3 | 0.92 | 3.74 | 1.24 |
| Nd | 12 | 9.1 | 7.9 | 16.4 | 13.6 | 16.4 | 10 | 2.1 | 11.2 | 3.2 | 11.8 | 4.9 |
| Sm | 2.7 | 2 | 1.8 | 3.9 | 4.1 | 2.1 | 2.1 | 0.8 | 3.3 | 0.8 | 2.2 | 1.4 |
| Eu | 0.52 | 0.45 | 0.35 | 0.97 | 0.84 | 0.41 | 0.35 | 0.13 | 0.49 | 0.14 | 0.44 | 0.26 |
| Gd | 2.51 | 1.79 | 1.77 | 3.8 | 3.24 | 1.89 | 2.06 | 0.77 | 3.18 | 0.7 | 1.66 | 1.34 |
| Tb | 0.44 | 0.42 | 0.38 | 0.63 | 0.58 | 0.4 | 0.38 | 0.17 | 0.58 | 0.1 | 0.25 | 0.22 |
| Dy | 2.46 | 2.69 | 2.53 | 3.59 | 3.24 | 2.77 | 2.61 | 0.89 | 4.14 | 0.69 | 1.41 | 1.26 |
| Ho | 0.54 | 0.63 | 0.59 | 0.74 | 0.64 | 0.64 | 0.63 | 0.23 | 0.78 | 0.15 | 0.29 | 0.31 |
| Er | 1.75 | 2.07 | 1.88 | 2.2 | 2.02 | 2.01 | 2.05 | 0.77 | 2.57 | 0.51 | 0.93 | 1.07 |
| Tm | 0.28 | 0.33 | 0.34 | 0.34 | 0.29 | 0.34 | 0.3 | 0.11 | 0.44 | 0.1 | 0.16 | 0.17 |
| Yb | 1.7 | 2.3 | 2.1 | 2.2 | 2.1 | 2.3 | 2.2 | 0.8 | 3.1 | 0.6 | 1 | 1.1 |
| Lu | 0.24 | 0.33 | 0.31 | 0.32 | 0.3 | 0.32 | 0.3 | 0.09 | 0.35 | 0.05 | 0.14 | 0.14 |
| REE | 79.75 | 55.81 | 50.26 | 79.36 | 63.09 | 73.65 | 63.75 | 18.53 | 528.53 | 25.16 | 36.31 | 33.94 |
| LREE | 69.83 | 45.25 | 40.36 | 65.54 | 50.68 | 62.98 | 53.22 | 14.70 | 513.39 | 22.26 | 30.70 | 27.31 |
| HREE | 9.92 | 10.6 | 9.9 | 13.8 | 12.4 | 10.7 | 10.53 | 3.83 | 15.1 | 2.9 | 5.61 | 6.63 |
| LREE/HREE | 7.04 | 4.29 | 4.08 | 4.74 | 4.084 | 5.9 | 5.05 | 3.84 | 33.9 | 7.68 | 5.472 | 4.119 |
| Eu/Eu* | 0.61 | 0.58 | 0.73 | 0.77 | 0.7 | 0.60 | 0.51 | 0.51 | 0.46 | 0.57 | 0.67 | 0.58 |
| Ce/Ce* | 1.15 | 2.32 | 1.72 | 1.12 | 0.97 | 0.91 | 0.98 | 2.00 | 18.8 | 1.10 | 1.24 | 1.69 |
| La$_N$/Yb$_N$ | 6.04 | 1.97 | 1.44 | 3.23 | 2.54 | 3.02 | 3.81 | 1.69 | 2.64 | 6.87 | 2.65 | 1.64 |

480
481
482
Appendix - Lateritic duricrusts samples analyzed at GEOSOL Laboratories (Belo Horizonte, Brazil); Eu/Eu* ¼[EuN/(SmN + GdN)/2]; LOI ¼ loss on ignition; major elements in wt,% and trace elements in ppm.

| Sample | TB-124C | EI-4 | CC-152 | CC-151 | RO-23 | CC-51 | CC-1 | TB-205 | EI-29 | EI-28 | RO-10 | GS-10 |
|---|---|---|---|---|---|---|---|---|---|---|---|---|
| Surface | LPS | LPS | LPS | LPS | LPS | LPS | LPS | LPS | LPS | LPS | LPS | LPS |
| Altitude m | 258 | 259 | 267 | 269 | 278 | 282 | 283 | 286 | 292 | 300 | 300 | 300 |
| $SiO_2$ | 43 | 25.4 | 25.2 | 19.8 | 44.7 | 31.6 | 24.1 | 25 | 30.3 | 42 | 29.5 | 20.9 |
| $TiO_2$ | 0.89 | 0.56 | 1.2 | 1.08 | 0.7 | 1.53 | 0.59 | 0.62 | 0.67 | 0.76 | 0.55 | 0.42 |
| $Al_2O_3$ | 20.1 | 22.1 | 21.3 | 16.7 | 12.3 | 17.4 | 12.8 | 15.6 | 19.8 | 17.1 | 9.45 | 10.4 |
| $Fe_2O_3$ | 26.5 | 41.6 | 41.2 | 54.3 | 34.4 | 38.6 | 53.7 | 47.9 | 36.9 | 31.7 | 53.8 | 64 |
| CaO | 0.02 | 0.03 | 0.1 | 0.04 | 0.06 | 0.07 | 0.05 | 0.1 | 0.05 | 0.08 | 0.01 | 0.08 |
| K2O | 0.07 | 0.06 | 0.78 | 0.57 | 0.62 | 0.07 | 0.02 | 0.08 | 1.44 | 1.02 | 0.02 | 0.05 |
| P2O5 | 0.057 | 0.069 | 0.068 | 0.081 | 0.109 | 0.061 | 0.101 | 0.259 | 0.085 | 0.071 | 0.069 | 0.076 |
| MgO | 0.13 | <0.1 | 0.18 | 0.13 | 0.15 | 0.11 | 0.14 | 0.25 | 0.19 | <0.1 | <0.1 | <0.1 |
| $Na_2O$ | 0.12 | <0.1 | 0.28 | 0.23 | <0.1 | <0.1 | <0.1 | <0.1 | 0.14 | <0.1 | <0.1 | <0.1 |
| LOI | 10.05 | 11.48 | 10.52 | 7.75 | 7.57 | 10.35 | 9.16 | 10.09 | 9.36 | 7.77 | 7.92 | 5.54 |
| Total | 100.7 | 101.3 | 100.5 | 100.5 | 100.5 | 99.7 | 100.6 | 99.7 | 98.6 | 100.6 | 101.3 | 101.5 |
| $Fe_2O_3/Al_2O_3$ | 1.32 | 1.88 | 1.93 | 3.25 | 2.80 | 2.22 | 4.20 | 3.07 | 1.86 | 1.85 | 5.69 | 6.15 |
| $Fe_2O_3/SiO_2$ | 0.62 | 1.63 | 1.63 | 2.74 | 0.76 | 1.22 | 2.228 | 1.916 | 1.22 | 3.06 | 1.82 | 0.755 |
| $Al_2O_3/SiO_2$ | 0.47 | 0.87 | 0.85 | 0.84 | 0.28 | 0.55 | 0.53 | 0.62 | 0.65 | 0.50 | 0.32 | 0.41 |
| Ag | 1.62 | <0.02 | <0.02 | <0.02 | <0.02 | <0.02 | 1.28 | <0.02 | <0.02 | <0.02 | <0.02 | <0.02 |
| As | 82.0 | 93.0 | 222.0 | 263.0 | 74.0 | 123.0 | 131.0 | 28.0 | 142.0 | 55.0 | 141.0 | 189.0 |
| Ba | 15.0 | 14.0 | 213.0 | 160.0 | 248.0 | 11.0 | 94.0 | 58.0 | 217.0 | 268.0 | 13.0 | 17.0 |
| Be | 0.80 | 0.50 | 1.20 | 1.00 | 1.10 | 0.40 | 1.70 | 1.70 | 2.20 | 1.10 | 0.60 | 0.40 |
| Bi | 0.14 | 0.25 | 0.18 | 0.14 | 0.05 | 1.33 | 0.08 | 0.18 | 0.24 | 0.18 | 0.79 | 0.96 |
| Co | 9.80 | 5.20 | 12.20 | 11.00 | 19.40 | 1.50 | 23.30 | 15.60 | 8.30 | 20.40 | 9.90 | 3.00 |
| Cd | 0.08 | 0.03 | 0.02 | 0.04 | 0.34 | 0.02 | 0.13 | 0.14 | 0.01 | 0.03 | 0.06 | 0.08 |
| Cr | 142.0 | 104.0 | 457.0 | 642.0 | 100.0 | 106.0 | 98.0 | 148.0 | 122.0 | 155.0 | 93.0 | 120.0 |
| Cs | 0.48 | 0.50 | 1.34 | 1.03 | 3.51 | 0.15 | 0.74 | 1.05 | 3.45 | 3.55 | 0.09 | 0.16 |
| Cu | 60.40 | 36.90 | 76.10 | 61.30 | 51.60 | 34.30 | 58.50 | 31.30 | 62.70 | 30.50 | 22.20 | 17.40 |
| Ga | 30.90 | 37.20 | 29.30 | 23.00 | 16.80 | 29.60 | 28.00 | 21.80 | 31.70 | 27.90 | 31.90 | 37.60 |
| Ge | 0.90 | 1.80 | 1.10 | 1.40 | 1.00 | 1.20 | 1.30 | 0.80 | 2.30 | 2.30 | 1.10 | 1.00 |
| Hf | 5.98 | 5.01 | 4.60 | 4.23 | 4.69 | 9.51 | 5.56 | 4.73 | 7.21 | 9.90 | 9.07 | 6.61 |
| In | 0.16 | 0.14 | 0.13 | 0.13 | 0.06 | 0.49 | 0.17 | 0.09 | 0.09 | 0.08 | 0.28 | 0.32 |
| Mo | 3.79 | 6.51 | 4.11 | 4.33 | 1.36 | 8.72 | 6.94 | 4.23 | 4.02 | 2.71 | 5.35 | 6.32 |
| Na | 0.06 | 0.02 | 0.16 | 0.11 | 0.04 | 0.02 | 0.03 | 0.05 | 0.19 | 0.05 | 0.02 | 0.07 |
| Nb | 6.63 | 5.47 | 7.59 | 5.94 | 6.49 | 13.38 | 4.96 | 6.53 | 17.80 | 14.65 | 10.95 | 8.20 |
| Ni | 20.60 | 13.80 | 57.90 | 48.60 | 28.40 | 5.50 | 24.80 | 17.20 | 37.70 | 39.60 | 9.50 | 6.30 |
| P | 310.0 | 265.0 | 286.0 | 404.0 | 452.0 | 382.0 | 197.0 | 1183.0 | 347.0 | 307.0 | 301.0 | 346.0 |
| Pb | 19.50 | 22.90 | 15.90 | 21.00 | 22.80 | 50.60 | 26.10 | 22.00 | 39.80 | 28.00 | 29.80 | 33.70 |
| Rb | 3.80 | 4.20 | 22.10 | 17.50 | 41.50 | 1.40 | 6.10 | 6.60 | 81.70 | 56.90 | 2.00 | 3.90 |
| Sn | 1.70 | 3.20 | 1.40 | 1.70 | 1.90 | 3.50 | 1.80 | 1.20 | 2.50 | 2.90 | 3.00 | 3.30 |
| Sr | 4.50 | 6.10 | 54.00 | 35.60 | 28.40 | 7.70 | 5.40 | 8.70 | 28.00 | 34.60 | 6.80 | 14.90 |
| Sb | 0.47 | 1.46 | 0.96 | 2.69 | 0.37 | 2.43 | 0.59 | 0.79 | 0.48 | 0.46 | 2.29 | 2.18 |
| Sc | 41.50 | 42.30 | 26.00 | 28.70 | 13.10 | 29.60 | 13.50 | 21.80 | 16.90 | 15.30 | 34.60 | 28.70 |
| Th | 12.30 | 22.80 | 11.10 | 12.40 | 10.80 | 57.10 | 12.70 | 6.90 | 31.50 | 27.10 | 43.10 | 48.10 |
| Ta | 0.22 | 10.47 | 0.11 | 0.25 | 1.24 | 0.75 | 0.42 | 0.42 | 9.96 | 5.47 | 2.42 | 3.14 |
| Te | 0.02 | 0.49 | 0.02 | 0.18 | 0.02 | 0.86 | 0.02 | 0.02 | 0.02 | 0.19 | 0.69 | 0.67 |
| U | 4.50 | 5.00 | 2.16 | 2.00 | 2.77 | 4.54 | 2.12 | 3.34 | 5.10 | 3.69 | 5.37 | 4.47 |
| V | 431.0 | 605.0 | 655.0 | 801.0 | 256.0 | 485.0 | 834.0 | 407.0 | 225.0 | 262.0 | 448.0 | 581.0 |
| W | 0.30 | 1.20 | 2.00 | 2.10 | 0.30 | 1.70 | 0.30 | 0.30 | 1.60 | 1.50 | 1.30 | 1.00 |
| Y | 9.58 | 5.23 | 15.58 | 13.10 | 14.47 | 7.41 | 7.97 | 7.76 | 26.07 | 21.39 | 9.09 | 9.81 |
| Zn | 41.00 | 33.00 | 51.00 | 44.00 | 119.00 | 22.00 | 52.00 | 51.00 | 99.00 | 66.00 | 12.00 | 16.00 |
| Zr | 176.50 | 121.20 | 122.80 | 102.60 | 161.20 | 254.90 | 135.10 | 155.90 | 199.20 | 289.40 | 315.30 | 241.80 |
| La | 18.2 | 2.2 | 2.5 | 4.7 | 7.5 | 1.1 | 4.7 | 2.1 | 10.4 | 5.8 | 7.7 | 18.3 |
| Ce | 15.4 | 6.9 | 25.9 | 22.3 | 24.1 | 15.5 | 14.5 | 13.9 | 52.4 | 84.2 | 11.9 | 17.9 |
| Pr | 1.34 | 0.66 | 1.21 | 2.2 | 1.98 | 0.81 | 1.61 | 0.97 | 2.06 | 3.33 | 1.32 | 2.06 |
| Nd | 5.4 | 2.6 | 4.3 | 9.3 | 7.3 | 3.7 | 5.3 | 4.1 | 7.6 | 11.1 | 5.3 | 7.6 |
| Sm | 1.5 | 0.8 | 1.4 | 2.4 | 1.9 | 1.2 | 1.4 | 1.3 | 1.8 | 2.4 | 1.4 | 2 |
| Eu | 0.27 | 0.14 | 0.39 | 0.64 | 0.43 | 0.29 | 0.28 | 0.24 | 0.47 | 0.51 | 0.3 | 0.41 |
| Gd | 1.35 | 0.76 | 1.99 | 2.36 | 2.2 | 1.45 | 1.15 | 1.27 | 2.47 | 2.31 | 1.32 | 1.93 |
| Tb | 0.28 | 0.14 | 0.39 | 0.39 | 0.38 | 0.28 | 0.23 | 0.22 | 0.51 | 0.45 | 0.27 | 0.37 |
| Dy | 1.56 | 0.96 | 2.76 | 2.53 | 2.55 | 1.59 | 1.4 | 1.49 | 4.05 | 3.59 | 1.83 | 2.29 |
| Ho | 0.39 | 0.2 | 0.58 | 0.53 | 0.56 | 0.38 | 0.33 | 0.35 | 0.91 | 0.83 | 0.39 | 0.47 |
| Er | 1.26 | 0.67 | 1.79 | 1.69 | 1.68 | 1.28 | 1.07 | 1.12 | 3.09 | 2.71 | 1.31 | 1.48 |
| Tm | 0.19 | 0.11 | 0.27 | 0.22 | 0.24 | 0.21 | 0.19 | 0.16 | 0.48 | 0.41 | 0.21 | 0.27 |
| Yb | 1.4 | 0.8 | 1.8 | 1.6 | 1.5 | 1.6 | 1.2 | 1.2 | 3.2 | 2.9 | 1.5 | 1.6 |
| Lu | 0.2 | 0.05 | 0.24 | 0.23 | 0.13 | 0.23 | 0.18 | 0.17 | 0.36 | 0.3 | 0.12 | 0.11 |
| REE | 80.72 | 16.99 | 45.52 | 51.09 | 52.45 | 29.62 | 33.54 | 28.59 | 89.8 | 120.8 | 34.87 | 56.79 |
| LREE | 74.88 | 13.30 | 35.70 | 41.54 | 47.61 | 22.6 | 27.79 | 22.61 | 74.73 | 107.34 | 27.92 | 48.27 |
| HREE | 5.84 | 3.69 | 9.82 | 9.55 | 9.24 | 7.02 | 5.75 | 5.98 | 15.07 | 13.5 | 6.95 | 8.52 |
| LREE/HREE | 12.82 | 3.60 | 3.63 | 4.35 | 4.68 | 3.22 | 4.83 | 3.78 | 4.96 | 7.95 | 4.02 | 5.67 |
| Eu/Eu* | 0.70 | 0.55 | 0.63 | 0.71 | 0.64 | 0.82 | 0.67 | 0.57 | 0.68 | 0.66 | 0.67 | 0.64 |
| Ce/Ce* | 1.09 | 1.34 | 1.13 | 3.49 | 1.47 | 1.62 | 3.85 | 2.28 | 2.65 | 4.49 | 0.87 | 0.68 |
| LaN/LuN | 12.30 | 1.86 | 3.03 | 0.94 | 3.38 | 1.99 | 0.46 | 1.18 | 2.20 | 1.35 | 3.47 | 7.73 |

483
484
485
Appendix - Lateritic duricrusts samples analyzed at GEOSOL Laboratories (Belo Horizonte. Brazil); Eu/Eu* ¼[EuN/(SmN + GdN)/2]; LOI ¼ loss on ignition; major elements in wt.% and trace elements in ppm.

| Sample | CM-16 | TB-88B | TB-266 | TB-215A | TB-215C | EI-55 | EI-56 | EI-52A | EI-52B | EI-54 | EI-53 |
|---|---|---|---|---|---|---|---|---|---|---|---|
| Surface | IZ | IZ | IZ | UPS | UPS | UPS | UPS | UPS | UPS | UPS | UPS |
| Altitude m | 318 | 323 | 488 | 500 | 500 | 530 | 546 | 556 | 556 | 564 | 572 |
| $SiO_2$ | 28.4 | 26.8 | 27.1 | 18.3 | 24.7 | 14.9 | 20.7 | 27.3 | 19.3 | 18.8 | 13.4 |
| $TiO_2$ | 0.36 | 0.89 | 0.5 | 0.47 | 0.33 | 0.49 | 0.67 | 0.76 | 0.61 | 0.47 | 0.38 |
| $Al_2O_3$ | 9.42 | 18.5 | 16.6 | 13.7 | 15.9 | 11.2 | 15.1 | 14.7 | 14.9 | 10.7 | 10.9 |
| $Fe_2O_3$ | 56.1 | 43.9 | 43.7 | 55.8 | 48 | 61.6 | 51.7 | 47.9 | 53.3 | 60.3 | 64.5 |
| CaO | 0.03 | 0.03 | 0.02 | 0.02 | 0.02 | 0.01 | 0.005 | 0.005 | 0.005 | 0.005 | 0.005 |
| K2O | 0.02 | 0.03 | 0.03 | 0.03 | 0.05 | 0.01 | 0.02 | 0.01 | 0.03 | 0.01 | 0.01 |
| P2O5 | 0.062 | 0.07 | 0.044 | 0.06 | 0.071 | 0.103 | 0.104 | 0.133 | 0.096 | 0.087 | 0.064 |
| MgO | <0.1 | <0.1 | <0.1 | <0.1 | <0.1 | <0.1 | <0.1 | <0.1 | <0.1 | <0.1 | 0.11 |
| $Na_2O$ | <0.1 | <0.1 | <0.1 | <0.1 | <0.1 | <0.1 | <0.1 | <0.1 | <0.1 | <0.1 | 0.05 |
| LOI | 7.13 | 10.41 | 11.82 | 11.95 | 12.06 | 11.33 | 11.27 | 10.14 | 12.14 | 10.95 | 12.49 |
| Total | 101.6 | 100.7 | 99.9 | 100.4 | 101.2 | 99.7 | 99.6 | 101.0 | 100.4 | 101.3 | 101.8 |
| $Fe_2O_3/Al_2O_3$ | 5.96 | 2.37 | 2.63 | 4.07 | 3.02 | 5.50 | 3.42 | 3.26 | 3.58 | 5.64 | 5.92 |
| $Fe_2O_3/ SiO_2$ | 1.98 | 1.64 | 1.613 | 3.05 | 1.94 | 4.13 | 2.49 | 2.76 | 1.75 | 3.20 | 4.81 |
| $Al_2O_3/SiO_2$ | 0.33 | 0.69 | 0.61 | 0.75 | 0.64 | 0.75 | 0.73 | 0.77 | 0.54 | 0.57 | 0.81 |
| Ag | <0.02 | <0.02 | <0.02 | <0.02 | <0.02 | <0.02 | <0.02 | <0.02 | <0.02 | <0.02 | <0.02 |
| As | 161.0 | 135.0 | 204.0 | 218.0 | 162.0 | 231.0 | 213.0 | 209.0 | 219.0 | 266.0 | 147.0 |
| Ba | 14.0 | 11.0 | 20.0 | 15.0 | 26.0 | 13.0 | 9.0 | 18.0 | 25.0 | 8.0 | 10.0 |
| Be | 0.50 | 0.30 | 0.60 | 0.90 | 1.40 | 0.50 | 0.30 | 0.30 | 0.40 | 0.50 | 0.40 |
| Bi | 0.74 | 1.91 | 1.15 | 1.00 | 0.43 | 0.87 | 0.85 | 0.96 | 1.00 | 0.84 | 0.51 |
| Co | 2.50 | 1.00 | 3.40 | 3.20 | 2.00 | 2.20 | 2.50 | 2.10 | 2.20 | 3.50 | 2.80 |
| Cd | 0.03 | 0.01 | 0.01 | 0.29 | 0.04 | 0.03 | 0.01 | 0.04 | 0.01 | 0.01 | 0.03 |
| Cr | 117.0 | 160.0 | 202.0 | 188.0 | 105.0 | 110.0 | 209.0 | 112.0 | 157.0 | 103.0 | 58.0 |
| Cs | 0.17 | 0.17 | 0.23 | 0.19 | 0.26 | 0.13 | 0.16 | 0.14 | 0.26 | 0.14 | 0.14 |
| Cu | 12.60 | 36.90 | 43.50 | 132.30 | 29.70 | 70.50 | 110.30 | 46.20 | 114.70 | 144.00 | 102.60 |
| Ga | 31.60 | 38.20 | 41.30 | 34.80 | 25.10 | 47.20 | 56.00 | 47.50 | 54.50 | 33.50 | 28.30 |
| Ge | 0.80 | 1.10 | 0.60 | 0.80 | 0.60 | 0.40 | 1.10 | 1.50 | 1.00 | 0.50 | 0.50 |
| Hf | 6.04 | 10.05 | 10.51 | 6.06 | 10.95 | 5.26 | 6.20 | 8.97 | 7.10 | 5.01 | 4.08 |
| In | 0.23 | 0.42 | 0.39 | 0.54 | 0.14 | 0.44 | 0.57 | 0.42 | 0.50 | 0.49 | 0.26 |
| Mo | 4.29 | 11.04 | 8.66 | 15.93 | 3.92 | 13.06 | 17.62 | 11.92 | 14.91 | 19.57 | 7.93 |
| Na | 0.01 | 0.01 | 0.05 | 0.03 | 0.17 | 0.03 | 0.01 | 0.07 | 0.04 | 0.01 | 0.03 |
| Nb | 6.79 | 17.01 | 10.31 | 8.20 | 9.71 | 8.55 | 13.37 | 15.39 | 12.17 | 8.39 | 7.00 |
| Ni | 5.60 | 9.80 | 6.60 | 8.20 | 4.70 | 6.80 | 8.70 | 7.30 | 10.90 | 7.90 | 7.70 |
| P | 271.0 | 292.0 | 248.0 | 241.0 | 360.0 | 374.0 | 451.0 | 498.0 | 417.0 | 342.0 | 301.0 |
| Pb | 49.60 | 43.70 | 27.30 | 62.80 | 30.00 | 27.10 | 45.80 | 34.60 | 29.90 | 69.70 | 21.30 |
| Rb | 3.10 | 1.80 | 2.10 | 1.80 | 3.40 | 1.80 | 2.00 | 1.80 | 2.90 | 1.70 | 1.80 |
| Sn | 2.50 | 4.00 | 2.20 | 2.30 | 1.40 | 3.90 | 4.40 | 4.80 | 6.30 | 3.30 | 3.20 |
| Sr | 6.50 | 12.40 | 14.20 | 11.00 | 10.50 | 13.00 | 15.60 | 15.40 | 22.50 | 8.80 | 10.00 |
| Sb | 1.92 | 2.82 | 5.35 | 8.25 | 4.55 | 3.83 | 3.91 | 2.77 | 4.08 | 6.17 | 2.59 |
| Sc | 32.10 | 24.20 | 34.40 | 67.60 | 22.50 | 43.10 | 45.00 | 32.10 | 44.60 | 40.00 | 55.50 |
| Th | 46.80 | 49.00 | 43.10 | 43.40 | 36.00 | 41.30 | 41.50 | 42.70 | 39.60 | 37.60 | 28.90 |
| Ta | 1.54 | 0.11 | 0.53 | 0.38 | 0.63 | 2.92 | 2.66 | 6.24 | 11.29 | 2.14 | 5.06 |
| Te | 0.54 | 0.66 | 0.89 | 1.07 | 0.91 | 1.14 | 0.98 | 0.81 | 2.18 | 1.33 | 0.80 |
| U | 4.88 | 3.79 | 7.80 | 11.29 | 9.11 | 5.21 | 4.86 | 3.83 | 6.66 | 8.51 | 9.32 |
| V | 531.0 | 451.0 | 636.0 | 1253.0 | 772.0 | 885.0 | 749.0 | 470.0 | 763.0 | 1849.0 | 560.0 |
| W | 0.80 | 1.40 | 1.50 | 1.40 | 0.80 | 1.40 | 1.90 | 2.00 | 4.20 | 1.30 | 1.40 |
| Y | 6.73 | 9.17 | 9.87 | 7.92 | 10.10 | 6.35 | 9.59 | 8.73 | 8.55 | 7.28 | 4.84 |
| Zn | 11.00 | 28.00 | 22.00 | 47.00 | 19.00 | 39.00 | 47.00 | 30.00 | 51.00 | 33.00 | 38.00 |
| Zr | 203.90 | 327.20 | 328.80 | 231.20 | 310.50 | 178.30 | 217.30 | 304.40 | 243.40 | 171.00 | 130.70 |
| La | 7.1 | 10.3 | 11.2 | 6.4 | 7.7 | 10.8 | 15.8 | 13.5 | 20.5 | 11.9 | 8.8 |
| Ce | 13.9 | 19.6 | 19.6 | 20.7 | 22.6 | 19.5 | 24.2 | 23.3 | 34.2 | 17.6 | 13.7 |
| Pr | 1.56 | 2.16 | 2.06 | 2.25 | 1.4 | 1.96 | 2.93 | 2.39 | 3.98 | 2.28 | 1.48 |
| Nd | 5.9 | 6.5 | 6.6 | 8.2 | 5.1 | 6 | 10.4 | 7.8 | 12.5 | 8.6 | 4.8 |
| Sm | 1.7 | 1.4 | 1.5 | 1.9 | 1.4 | 1.3 | 2.2 | 1.4 | 2.1 | 2.2 | 1.1 |
| Eu | 0.32 | 0.22 | 0.24 | 0.38 | 0.31 | 0.26 | 0.41 | 0.29 | 0.39 | 0.41 | 0.16 |
| Gd | 1.44 | 1.16 | 1.35 | 1.59 | 1.4 | 1.11 | 1.72 | 1.22 | 1.62 | 1.65 | 0.87 |
| Tb | 0.24 | 0.24 | 0.24 | 0.26 | 0.3 | 0.19 | 0.32 | 0.22 | 0.28 | 0.27 | 0.15 |
| Dy | 1.69 | 1.43 | 1.53 | 1.64 | 1.77 | 1.26 | 2.05 | 1.63 | 1.59 | 1.8 | 1.11 |
| Ho | 0.32 | 0.36 | 0.38 | 0.32 | 0.43 | 0.25 | 0.44 | 0.35 | 0.34 | 0.36 | 0.21 |
| Er | 1.13 | 1.23 | 1.32 | 1.08 | 1.28 | 0.84 | 1.3 | 1.15 | 1.15 | 1 | 0.71 |
| Tm | 0.22 | 0.21 | 0.21 | 0.17 | 0.25 | 0.14 | 0.2 | 0.21 | 0.18 | 0.2 | 0.11 |
| Yb | 1.4 | 1.5 | 1.6 | 1.4 | 1.6 | 0.9 | 1.5 | 1.4 | 1.3 | 1.2 | 0.8 |
| Lu | 0.06 | 0.22 | 0.2 | 0.18 | 0.26 | 0.05 | 0.08 | 0.08 | 0.06 | 0.07 | 0.05 |
| REE | 36.98 | 46.53 | 48.03 | 46.47 | 45.8 | 44.56 | 63.55 | 54.94 | 80.19 | 49.54 | 34.05 |
| LREE | 30.48 | 40.18 | 41.2 | 39.83 | 38.51 | 39.82 | 55.94 | 48.68 | 73.67 | 42.99 | 30.04 |
| HREE | 6.5 | 6.35 | 6.83 | 6.64 | 7.29 | 4.74 | 7.61 | 6.26 | 6.52 | 6.55 | 4.01 |
| LREE/HREE | 4.69 | 6.33 | 6.03 | 6.00 | 5.28 | 8.40 | 7.35 | 7.78 | 11.30 | 6.56 | 7.49 |
| Eu/Eu* | 0.63 | 0.53 | 0.52 | 0.67 | 0.68 | 0.66 | 0.64 | 0.68 | 0.65 | 0.66 | 0.5 |
| Ce/Ce* | 0.98 | 0.97 | 0.96 | 1.28 | 1.61 | 0.99 | 0.83 | 0.96 | 0.89 | 0.79 | 0.89 |
| LaN/LuN | 3.43 | 4.64 | 4.73 | 3.09 | 3.25 | 8.11 | 7.12 | 6.52 | 10.66 | 6.70 | 7.43 |

486

487 **References**
488

489 ANAND, R.R.; CHURCHWARD, H.M.; SMITH, R.E.; SMITH, K.; GOZZARD, J.R.; CRAIG, M.A.;
490     MUNDAY, T.J. (1993). Classification and atlas of regolith landform mapping units, Exploration perspectives
491     for the Yilgarn Craton, Australia. CSIRO *Division of Exploration and Mining*, Restricted Report 440R
492     (unpublished).
493 ALBUQUERQUE, M.F.D., HORBE, A.M.C., BOTELHO, N.F. (2017) Genesis of manganese deposits in
494     southwestern Amazonia: mineralogy, geochemistry and paleoenvironment, *Ore Geology Reviews (2017)*, doi:
495     http://dx.doi.org/10.1016/j.oregeorev.2017.06.012
496 ARHIN, E., JENKIN, G.R.T., CUNNINGHAM, D., NUDE, P. (2015). Regolith mapping of deeply weathered
497     terrain in savannah regions of the Birimian Lawra Greenstone Belt, Ghana. *Journal of Geochemical
498     Exploration, 159*, 194-207. doi: 10.106/j.gexplo.2015.09.008.
499 ASGHAR CALAGARI A., KANGARANI FARAHANI, F., ABEDINI, A. (2015). Geochemical characteristics
500     of a laterite: the Jurassic Zan Deposit, Iran. *Acta Geodynamica et Geomaterialia, 12*, (177), 67–77. doi:
501     10.13168/AGG.2015.0001
502 BARBOSA, I.O. PIRES. A.C.B. LACERDA, M.P.C. CARMELO, A.C. (2013). Geology, airborne geophysics,
503     geomorphology and soils in the individualization of the niquelândia mafic-ultramafic complex, goiás state,
504     Brazil. *Revista Brasileira de Geofísica, 31*(3), 463 - 481. doi: http://dx.doi.org/10.22564/rbgf.v31i3.316
505 BOULANGÉ, B.; CARVALHO A. (1997). The bauxite of Porto Trombetas. *In*: Carvalho A., Boulangé B., Melfi
506     A.J., Lucas Y. (eds.) *Brazilian Bauxites*. São Paulo, USP/FAPESP/ORSTOM, p. 55-73.
507 CARRANZA, E. J. M. (2009). Knowledge-driven modeling prospectivity. In: ____. *Geochemical anomaly and
508     mineral prospectivity mapping in GIS*, v 11. Amsterdam: Elsevier. Cap 7. p. 189-246.
509 CARRIER, F., BOURDON, B., PILI, É., TRUFFERT, C., WYNS, R. (2006) Airborne Gamma-Ray spectrometry
510     to quantify chemical erosion process. *Journal of Geochemical Exploration 88*, 266-270. doi:
511     10.1016/j.gexplo.2005.08.053.
512 CARRINO, T. A.; SILVA, A.M.; BOTELHO, N.F.; SILVA, A.A.C. (2011). Discriminação de áreas de espesso
513     regolito do leste do Estado do Amazonas usando estatística multivariada, algoritmo hiperespectral e
514     modelagem de dados espaciais. *Revista Brasileira de Geofísica, 29*, 155-172. doi: 10.1590/S0102-
515     261X2011000100011.
516 COLIN, F; NAHON, D; TRESCASES, J.J; MELFI, A.J. (1990). Lateritic Weathering of Pyroxenites at
517     Niquelandia, Goias, Brazil: The Supergene Behavior of Niekel. *Economic Geology, 85*, 1010-1023. doi:
518     10.2113/gsecongeo.85.5.1010.
519 CORNELIUS, M., ROBERTSON, I.D.M., CORNELIUS, A.J., MORRIS, P.A. (2007). *Laterite geochemical
520     database for the Western Yilgarn Craton, Western Australia*. Perth: Department of Industry and Resources.
521 COSTA, M.L. (1997). Lateritization as a major process of ore deposit formation in the Amazon region. *Exploration
522     and Mining Geology, 6*(1), 79-104.
523 CPRM - SERVIÇO GEOLÓGICO DO BRASIL. Banco de dados da CPRM – Geosgb. Disponível em:
524     www.geosgbcprm.gov.br
525 CPRM - SERVIÇO GEOLÓGICO DO BRASIL. (2006). Projeto Aerogeofísico Sudeste de Rondônia: relatório
526     final de levantamento e processamento dos dados magnetométricos e gamaespectrométricos. Rio de Janeiro:
527     Lasa Engenharia e Prospecções; Prospectors Aerolevantamentos e Sistemas, 27 v. 1.
528 DAUTH, C. (1997). Airbone magnetic, radiometric and satellite imagery for regolith mapping in the Yilgarn
529     Craton of Western Australia. *Exploration Geophysics 28*, 199-203. doi: 10.1071/EG997199.
530 DICKSON, B. L.; SCOTT, K. M. (1997). Interpretation of aerial gamma-ray surveys - adding the geochemical
531     factors. *Journal of Australian Geology & Geophysics, v. 17*(2), 187-200.
532 DURY, G.H. (1969). Rational descriptive classification of duricrust. *Earth Science Journal, 3*, 77-86.
533 GIORGIS, I., BONETTO, S., GIUSTETTO, R., LAWANE, A., PANTET, A., ROSSETTI, P., THOMASSIN, J.,
534     VINAI, R. (2014). The lateritic profile of Balkouin, Burkina Faso: Geochemistry, mineralogy and genesis.
535     *Journal of African Earth Sciences 90*, 31–48. doi: 10.1016/j.jafrearsci.2013.11.006.
536 HARRISON, J. B. (1934), The katamorphism of igneous rocks under humid tropical conditions: Harpenden,
537     England, *Imperial Bureau of Soil Science*, Rothamsted Experimental Station.
538 HILL, I.G, WORDEN, R.H, MEIGHAN, I.G. (2001). Formation of interbasaltic laterite, horizons in NE Ireland
539     by early Tertiary weathering process. *Proceedings of the Geologist Association, 112*. 339-348. doi:
540     10.1016/S0016-7878(01)80013-4
541 HILL, I.G., WORDEN, R.H., MEIGHAN, I.G. (2000). Geochemical evolution of a palaeolaterite: the Interbasaltic
542     Formation, Northern Ireland. *Chemical Geology, 166*(1-2): 65-84. doi: 10.1016/S0009-2541(99)00179-5.
543 ISLES, D.; RANKIN, L. (2000). *Geological interpretation and exploration targeting from aeromagnetic data.
544     Workshop*. Brasília, DF: ADIMB.

545 IZA, E.R.H.F; HORBE, A.M.C; SILVA, A.M. (2016). Boolean and fuzzy methods for identifying lateritic
546     regoliths in the Brazilian Amazon using gamma-ray spectrometric and topographic data. *Geoderma*, *269*, 27-
547     38. doi: 10.1016/j.geoderma.2016.01.037
548 KAISER, H.F. (1958). The varimax criterion for analytic rotation in factor analysis. *Psycometrika, 23*(3), 187-
549     200.
550 KOTSCHOUBEY, B., CALAF, M.J.C., LOBATO, A.C.C., LEITE, A.S., AZEVEDO, C.H. D. (2005).
551     Caracterização e gênese dos depósitos de bauxita da provincial bauxitífera de Paragominas, Noroeste da Baica
552     do Grajaú, Nordeste do Pará/Oeste do Maranhão. In: O. J. Marini, E. T. Queiroz & B. W. Ramos (eds.) –
553     *Caracterização de depósitos minerais em distritos mineiros da Amazônia*. Brasília-DF: ADIMB. 691-782.
554 MCBRATNEY, A. B.; MENDONÇA SANTOS, M.L.; MINASNY, B. (2003). On digital soil mapping.
555     *Geoderma, 117*(2)*, 3-52. doi: 10.1016/S0016-7061(03)00223-4
556 MELFI, A.J.; TRESCASES, J.J.; CARVALHO, A; OLIVEIRA, S.M.B.; RIBEIRO FILHO, E.; FORMOSO,
557     M.L.L. (1988). The lateritic ore deposits of Brazil. *Geological Science Bulletin, v. 41*, 5-36.
558 MINTY, B. (2011). Short note: on the use of radioelement ratios to enhance gamma-ray spectrometric data.
559     *Exploration Geophysics. 42*(1), 116–120. doi: 10.1071/EG10011
560 MOREIRA, F. R. S.; ALMEIDA-FILHO, R.; CAMARA, G. (2003). Spatial analysis techniques applied to mineral
561     prospecting: an evaluation in the Poços de Caldas Plateau. *Revista Brasileira de Geociências, 33*(2), 183-190.
562 NESBITT, H.W., YOUNG, G.M. (1982). Early Proterozoic climates and plate motions inferred from major
563     element chemistry of lutites. *Nature. 299*. 715-717.
564 OLIVEIRA, S.M.B., TRESCASES, J.-J., MELFI, A.J. (1992). Lateritic nickel deposits of Brazil. *Mineralium
565     Deposita*, *27*, 137-146.
566 OLIVEIRA, S.B., COSTA, M.L., FILHO, H.J.P. (2016). The Lateritic Bauxite Deposit of Rondon do Pará: A new
567     giant deposit in the Amazon Region, Northern Brazil. *Economic Geology, 111*, 1277-1290. doi:
568     10.2113/econgeo.111.5.1277
569 PARKER, A. (1970). An index of Weathering for Silicate Rocks. *Geological Magazine, 107*, 501-504.
570 PIRES, A.C.B., MORAES, R.A.V. (2006). New processing Technologies applied do airborne geophysical data:
571     impact on interpretation. *II Simpósio Brasileiro de Exploração Mineral – Simexmin*. Ouro Preto, Minas Gerais-
572     Brasil.
573 QUADROS, M.L. do E.S.; RIZZOTTO, G.J. (2007). *Geologia e recursos minerais do Estado de Rondônia: texto
574     explicativo do mapa geológico e de recursos minerais do Estado de Rondônia-escala 1:1.000.000*. Porto
575     Velho: CPRM. Programa Geologia do Brasil-PGB.
576 REIMANN, C., FILZMOSER, P., GARRET, R., DUTTER, R. (2008). *Statistical data analysis explained: applied
577     environmental statistics with R*. Chichester: John Wiley.
578 ROEST, W.R., VERHOEF, J., PILKINGTON, M. (1992). Magnetic interpretation using the 3-D analytic signal,
579     *Geophysics, 57*, 116-125.
580 SCHELLMAN, W. (1981). Considerations on the definition and classification of laterites. Proc. Int. *Seminar on
581     Lateritisation Processes.* Trivandrum, Proceedings, 1-10.
582 SCHELLMANN, W., (1983). A new definition of laterite. *Geological Survey of India, Memoirs, 120*, 1-7.
583 TARDY, Y. (1993). *Pétrologie des latérites et des sols tropicaux*. Paris: Masson.
584 WEDEPOHL, K. H. (1969). *Handbook of geochemistry*. Berlin: Springer-Verlag.
585 WILFORD, J. R.; BIERWIRTH, P.N.; CRAIG, M.A. (1997). Application of airborne gamma-ray spectrometry in
586     soil/regolith mapping and applied geomorphology. *Journal of Australian Geology & Geophysics, 17*(2), 201-
587     216.
588 WILFORD, J. (2012). A weathering intensive index for the Australian continent using airborne gamma-ray
589     spectrometry and digital terrain analysis. *Geoderma, 183-184*, 124-142. doi: 10.1016/j.geoderma.2010.12.022
590 WIMPENNY, J., GANNOUN, A., BURTON, K.W., WIDDOWSON, K., JAMES, R.H., GÍSLASON, S.R.
591     (2007). Rhenium and osmium isotope and elemental behavious accompanying laterite formation in the Deccan
592     Region of India. *Earth and Planetary Science Letters, 261,* 239–258. doi: 10.1016/j.epsl.2007.06.028.
593 XIAO, W., HONGBING, J., SHIJIE, W., HUASHUO, C., CHANGSHUN, S. (2014). The formation of
594     representative lateritic weathering covers in south-central Guangxi (Southern China). *Catena*, *118,* 55-72. doi:
595     10.1016/j.catena.2014.01.019.

# CAPÍTULO 4

# COMPARAÇÃO ENTRE OS RESULTADOS DOS MODELOS PREVISIONAIS PARA A PRESENÇA DE LATERITOS NO SUDOESTE DA AMAZÔNIA.

## 4.1 INTRODUÇÃO

Neste capítulo foram comparados os resultados do modelo de detecção de áreas potenciais para a presença de lateritos, aplicado em duas áreas distintas, localizadas no sudoeste da Amazônia brasileira, doravante denominadas de área norte (Herrera, 2016) e área sul (Iza *et al.* 2016a). A área norte foi escolhida devido à expressividade das ocorrências de lateritos, ao contexto geológico/geofísico similar e/ou relativamente próximo à área de estudo principal (área sul) e à possibilidade de integrar futuras interpretações regionais sobre a evolução do regolito e dos aspectos geomorfológicos.

O objetivo é enfatizar as discrepâncias e similaridades entre os resultados, discutir sobre as variáveis envolvidas e padrões de respostas radiométricas associados aos lateritos, enaltecendo a importância e eficiência da integração dos dados multifonte como ferramenta de apoio ao mapeamento de lateritos em áreas distintas.

## 4.2 LOCALIZAÇÃO DAS ÁREAS, GEOLOGIA E MODO DE OCORRÊNCIA DOS LATERITOS

As áreas estão localizadas na porção sudoeste da Amazônia brasileira (figura 4.1) e, em termos geológicos, inseridas no sudoeste do cráton amazônico. A área norte está localizada na província Rondonia-Juruena, constituída por tonalitos, quartzo-dioritos, granitos, anfibolitos e supracrustais subordinados, com idades Paleo a Mesoproterozoicas. O Cenozoico é representado por lateritos, terraços fluviais e coberturas sedimentares indiferenciadas (Quadros e Rizzotto, 2007). Os lateritos do leste da área norte (margem direita do rio Madeira) ocorrem nos topos dos platôs em dois principais intervalos altimétricos: i) entre 120 e 150 m e; ii) entre 180 e 204 m. Em ambos os casos as declividades são inferiores a 2% e a drenagem tem densidade muito baixa. As espessuras dos perfis lateríticos são de até 6 m, e são normalmente ferruginosos, compostos por goethita, hematita, caulinita, gibbsita e quartzo e exibem textura pisolítica/nodular e estrutura colunar. Os lateritos da margem esquerda não estão associados a platôs e ocorrem apenas entre 80 e 110 m de altitude, entretanto, têm características similares em termos mineralógicos, texturais, estruturais e gamma espectrométricos (Herrera, 2016) (figura 4.2).

O contexto geológico da área sul foi apresentado nos capítulos anteriores e não será abordado aqui. Entretanto, destaca-se que nesta área os lateritos não formam platôs isolados e ocorrem principalmente na superfície de aplanamento superior (planalto) e na superfície de aplanamento inferior (planície), (figura 4.3).
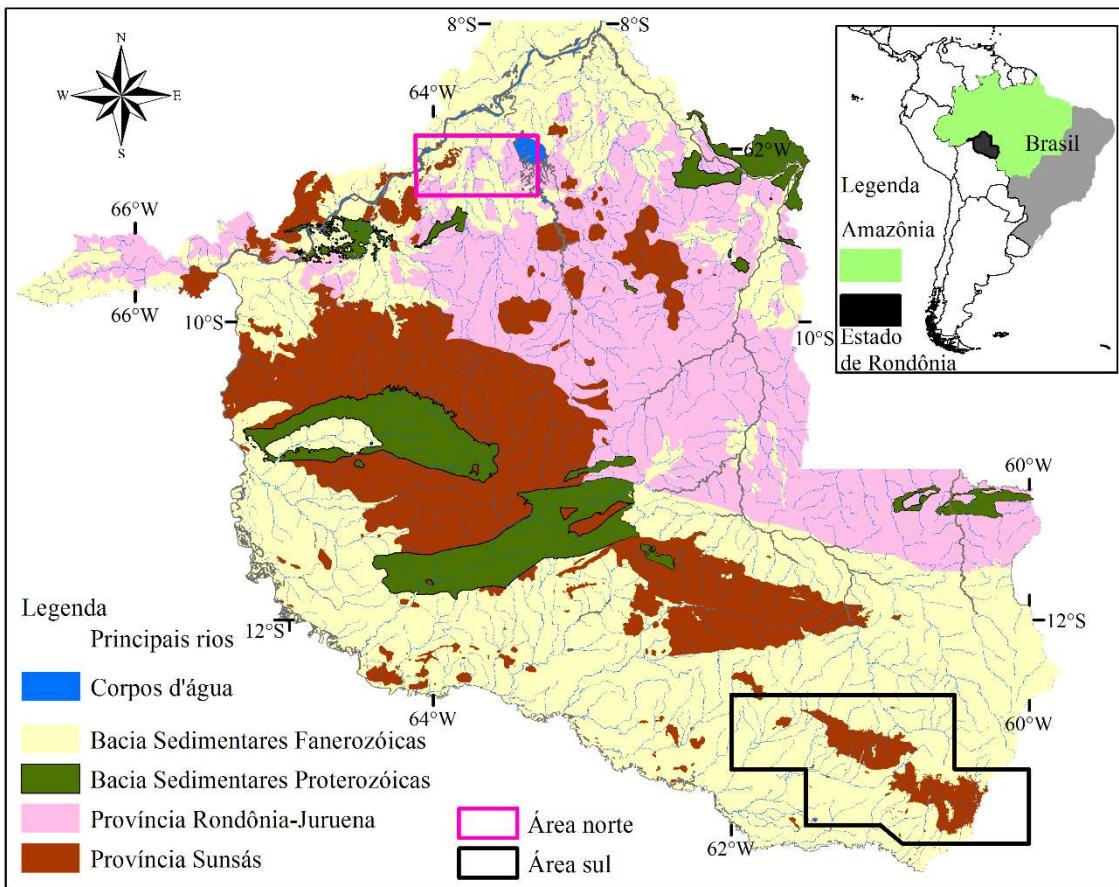
Figura 4.1 – Mapa tectônico simplificado e de localização das áreas (modificado de Quadros e Rizzotto 2007).



Figura 4.2 – A) Aspecto geral do afloramento com presença de lateritos (topo). B) Relevo plano (platô).

Figura4.3– A) Aspecto geral do afloramento tipo de lateritos (relevo plano), superfície de aplanamento inferior. B) Detalhe do afloramento com altura aproximada de 3 metros.

## 4.3 MATERIAIS E MÉTODOS DAS ÁREAS NORTE E SUL

Os trabalhos desenvolvidos na área norte e sul tiveram como objetivo a integração e interpretação altimétrica, geomorfológica, pedológica e geológica nas respectivas áreas além dos dados de aerogeofísica. A base de dados altimétricos utilizada em ambos os trabalhos foi a do SRTM.

A base geomorfológica é a do Projeto Planafloro (Rondônia, 2002), junto com as informações de hidrografia, cobertura vegetal, uso e ocupação de solos, entre outros, além da base geomorfológica do IBGE (2013). Os mapas geológicos utilizados foram aqueles publicados por Quadros e Rizzotto (2007), Rizzotto (2010 e 2012) e Oliveira e Filho (2013) que serviram como base para a determinação dos alvos a serem visitados nas etapas de campo.

A gamaespectrometria foi realizada pela FUGRO AIRBORNE SURVEYS para o Serviço Geológico do Brasil/CPRM por meio do projeto "Rondônia Central – RO" (CPRM, 2010), para a área norte, e "Sudeste de Rondônia" (CPRM, 2006) para a área sul.

O processamento das imagens foi realizado, em ambas as áreas, exatamente com o mesmo software e interpoladores, de acordo com o apresentado nos capítulos 2 e 3. Dentre os

produtos utilizados destacam-se: os canais do eTh, eU, e K e as razões eU/K, eTh/K, além das composições ternárias RGB: K, eTh e eU, e eTh/K, SRTM e eTh.

Os dados aerogamaespectrométricos e de elevação (SRTM) foram analisados com apoio do método booleano (*index overlay*) e *fuzzy*, este último por meio da soma e produto algébrico e o operador gamma *fuzzy*, com a finalidade de criar mapas de potencialidade para presença de lateritos. Em termos gerais, o embasamento teórico foi fundamentado pelos trabalhos de Zimmermann (1985); An *et al.* (1991), Bonham-Carter (1994); Moreira *et al.* (2003); McBratney *et al.* (2003); Lagacherie (2005); Carranza (2009); Carrino *et al.* (2011), entre outros. Para verificar e calibrar os modelos apresentados, foram usados como suporte atividades de campo, mapas geológicos, pedológicos e geomorfológicos disponíveis (Rondônia, 2002; IBGE, 2013; Quadros e Rizzotto, 2007). A figura 4.4 exibe as etapas desenvolvidas neste capítulo.
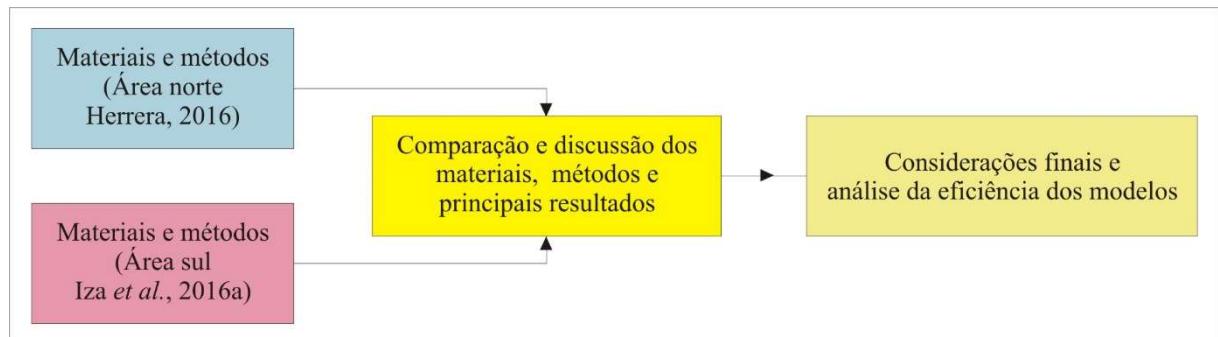


Figura 4.4 – Fluxograma dos principais procedimentos realizados neste capítulo.

### 4.3.1 Área Norte

*4.3.1.1 Lógica Booleana*

Na área norte, as imagens eU/K, eTh/K, e altimetria (SRTM) foram redefinidas para valores 0 e 1 (binários) com o objetivo de determinar áreas potenciais para a presença de lateritos. Os valores menores do que a média mais 1 vez o desvio padrão ($\bar{X} + 1\sigma$) de eTh/K e eU/K foram associados a menor probabilidade de ocorrência de lateritos e assim, transformados em "0" e os valores iguais ou mais altos foram transformados em "1", gerando novas imagens reclassificadas (0 e 1) para ambas as razões.

No procedimento com o modelo de elevação (SRTM), a área foi dividida em dois setores. O primeiro correspondeu à porção oeste (margem esquerda do rio Madeira) e o segundo ao centro-leste (margem direita). A distinção foi realizada devido aos diferentes modos de ocorrência dos lateritos e às diferentes características geomorfológicas associadas. Para a margem esquerda, o valor "0" foi atribuído a altitudes menores que 80 m, por sua vez o valor

"1" foi relacionado à altitudes entre 80 e 110 m. Por outro lado, na margem direita considerou-se o valor "0" para altitudes abaixo de 120 m e "1" para elevações acima.

### 4.3.1.1.1 Método Index Overlay (MIO)

Nesse método, cada imagem (SRTM, eTh/K e eU/K) tem um peso diretamente relacionado à hipótese avaliada. Os pesos pertencem a uma progressão geométrica de razão 2 ($A_n = 2^{n-1}$): ((eU/K + 2*eTh/K + 4*SRTM)/7). Nesta primeira hipótese a altimetria (SRTM) tem peso maior considerando sua relação com platôs. Para a margem esquerda a equação aplicada, foi distinta: 2 ($A_n = 2^{n-1}$) ((eU/K + 2*SRTM + 4*eTh/K)/7). Nesta segunda hipótese atribui-se maior peso à gamaespectrometria, pois os lateritos associados a platôs não são expressivos, diminuindo consequentemente a importância da altimetria (SRTM).

O resultado final é o mapa com classes que variam entre 0 e 1 as quais indicam áreas com menor (0) e maior probabilidade (1) de ocorrência de lateritos e fragmentos derivados de sua desagregação, assim como latossolos. Em todo caso, a combinação de pesos possibilitou diferenciar classes favoráveis ou desfavoráveis, permitindo a visualização de cada uma, e respectiva individualização das variáveis ou suas combinações.

### 4.3.1.2 Lógica Fuzzy

Na lógica *fuzzy* foram utilizadas as mesmas variáveis da lógica booleana. Os dados foram rasterizados e então simplificados usando a fuzzificação, o que permitiu o reescalonamento em graus de variabilidade ou pertinência entre "0" (menor favorabilidade) e "1" (maior favorabilidade). O reescalonamento dos dados considerou os valores próximos a "1" aqueles relacionados ao alto intemperismo (altas razões U/K e Th/K, ou seja, maiores que $\bar{X} + 1\sigma$) e para tanto foi utilizada a função *large* que tende a ressaltar os altos valores. No que diz respeito a altimetria (SRTM) optou-se apenas por manter os dados fuzzificados utilizando-se a função linear que reescalona os dados entre 0 e 1 mas não ressalta nenhum intervalo de dados específico. Os produtos fuzzificados foram utilizados em três etapas principais: i) Na geração do *Fuzzy Algebraic Product Operator* – FAPO; ii) Na geração do *Fuzzy Algebraic Sum Operator* – FASO; e iii) Na geração do *fuzzy gamma operator* – FGO.

**4.3.2 Área Sul**

*4.3.2.1 Lógica Booleana*

O procedimento realizado na lógica booleana considerou os mesmos produtos utilizados na área norte, ou seja, as razões eTh/K, eU/K e dados altimétricos (SRTM). Os valores considerados altos ($\bar{X}$ + 1,5σ) de eTh/K e eU/K foram vinculados a maior potencialidade de ocorrência de lateritos e, portanto, transformados em "1" e aqueles menores foram transformados em "0", gerando novas imagens reclassificadas (0 e 1) para ambas as razões.

Para o modelo digital de elevação, a abordagem foi distinta daquela realizada na área norte devido às características geomorfológicas diferenciadas. Assim como citado no capítulo 2, atribuiu-se valor 1 para altitudes abaixo de 300 m e acima de 500 m, e valor "0" para as elevações entre 301 e 499 m. As altitudes abaixo de 300 m estão associadas às coberturas sedimentares indiferenciadas e a alguns afloramentos lateríticos, enquanto as altitudes acima de 500 m estão principalmente associadas aos arenitos da Bacia dos Parecis e secundariamente a ocorrências de crostas lateríticas.

*4.3.2.1.1 Método Index Overlay (MIO)*

Neste método, Iza *et al.* (2016a) propôs inicialmente quatro hipóteses considerando a combinação de três variáveis (eTh/K, eU/K, e SRTM). Nas diferentes hipóteses as variáveis receberam pesos iguais (caso 1), ou eTh/K ou o SRTM receberam os maiores pesos (casos 3 e 4). Nos casos 2, 3 e 4 o eU/K recebeu o menor peso. Os casos estudados representaram uma progressão geométrica de razão 2 exatamente como seguido por Herrera (2016). Em cada um dos resultados as classes variaram de 0 a 1 e indicaram áreas com menor e maior potencial de ocorrência de lateritos, respectivamente.

Os casos 3 e 4 foram aqueles que mostraram os melhores resultados entre todos os casos apresentados por Iza *et al.* (2016a). Foi escolhido o caso 3 como o mais significativo para a previsão de lateritos (eU/K + 2*SRTM + 4*eTh/K)/7) pois atribuiu à razão Th/K o maior peso devido os altos valores (altas razões Th/K) serem frequentes em um contexto de alto intemperismo.

*4.3.2.2 Lógica Fuzzy*

Na lógica *fuzzy* foram utilizadas as mesmas variáveis da lógica booleana. Os procedimentos do método *fuzzy* foram exatamente os mesmos realizados na área norte e considerou, portanto, a geração dos mesmos produtos (FAPO, FASO e FGO).

## 4.4 PRINCIPAIS RESULTADOS

### 4.4.1 Área Norte

O modelo booleano, por meio do método *index overlay* (MIO), permitiu a geração de 8 classes de favorabilidade para a presença de lateritos e fragmentos derivados de sua desagregação, assim como latossolos. Na região centro-leste (margem direita do rio Madeira) os domínios considerados como potenciais representam aproximadamente 6% do total da área. Esses domínios são aqueles com influência da altimetria (SRTM) (classe 4), do SRTM com o eU/K (classe 5), do SRTM com o eTh/K (classe 6) e de todas as variáveis somadas (classe 7).

A utilização da respectiva metodologia na porção oeste da área (margem esquerda do rio Madeira) gerou resultados inconclusivos, pois a ausência de platôs interferiu na definição das áreas potenciais, portanto, a altimetria mostrou-se menos importante como variável discriminante para a ocorrência de lateritos. Desse modo, Herrera (2016) optou por atribuir peso 4 à razão Th/K. Assim, as classes consideradas com maior potencial têm influência da razão eTh/K e de suas combinações com a razão eU/K, com o SRTM, e com todas as variáveis supracitadas (classes 5, 6 e 7). Essa reorganização dos pesos gerou resultados extremamente satisfatórios e destacou 0,5% da área total como favorável. O somatório das áreas favoráveis, para a ocorrência de lateritos, da margem esquerda (0,5%) e direita do rio Madeira (6%) totalizam aproximadamente 6,5% da área total (Figura 4.5).

A aplicação do método *fuzzy* na área norte mostrou-se ineficiente para a identificação dos lateritos e produtos derivados. Os resultados incluíram praticamente toda a área de estudo e não contribuíram na delimitação de áreas com maior potencial para a presença de lateritos.
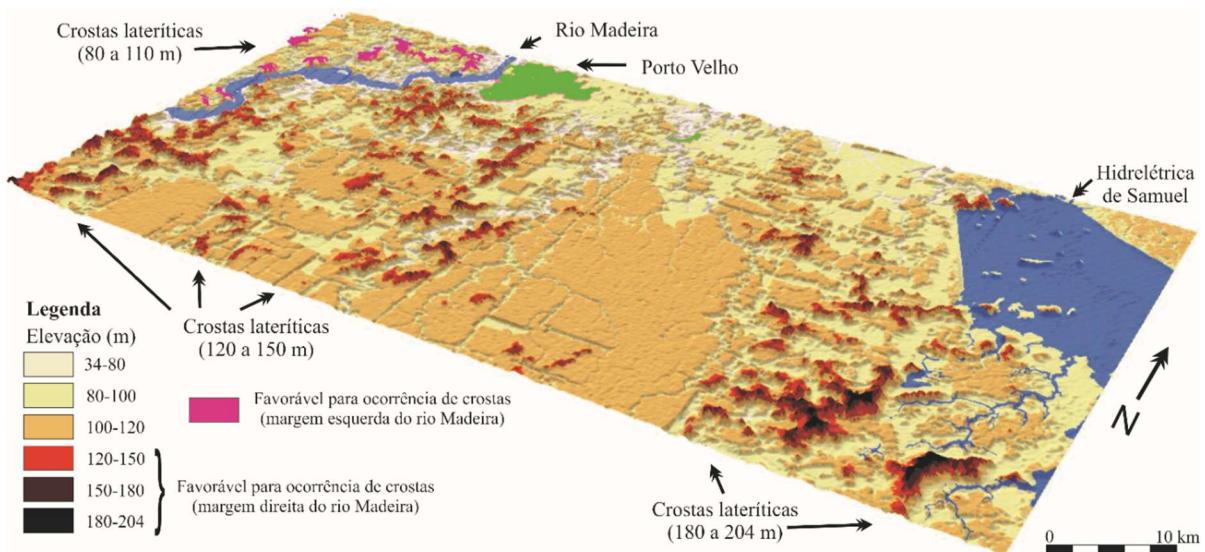


Figura 4.5 – Mapa de previsibilidade de presença de lateritos e fragmentos derivados de sua desagregação, assim como latossolos, por meio do método *index overlay*.

### 4.4.2 Área Sul

Na área sul tanto o modelo booleano quanto o modelo *fuzzy* mostraram-se eficientes na delimitação das áreas previsionais para a presença de lateritos. O modelo booleano, por meio do método *index overlay* (MIO), assim como na área norte, proporcionou a obtenção de 8 classes de favorabilidade. O referido modelo foi utilizado para toda a área sul e delimitou 7,84% de áreas potenciais para a presença de lateritos e fragmentos derivados de sua desagregação, assim como latossolos. As áreas consideradas com alto potencial têm influência pelo menos da razão eTh/K (classe 4) e de suas combinações com a razão, eU/K e altimetria (classes 5, 6 e 7), (figura 4.6).

O método *fuzzy*, ao contrário da área norte, mostrou-se extremamente eficiente na delimitação de áreas potenciais para a presença de lateritos. Nele foram utilizados o produto (FAPO) e a soma algébrica (FASO) que apresentaram diferentes respostas em relação a delimitação das respectivas áreas potenciais. Os resultados subestimaram ou superestimaram as áreas potenciais (em relação aos dados de campo) e por este motivo foi utilizado o operador *fuzzy* gamma (FGO), que contribui para balancear os resultados e delimitou cerca de 10,71% da área como potencial para a ocorrência de lateritos. O operador *fuzzy* gamma 0,7 foi sobreposto ao modelo digital de terreno e corresponde ao resultado mais otimista para a ocorrência de lateritos e fragmentos derivados de sua desagregação, assim como latossolos. (Figura 4.7). As áreas destacadas (extremamente favoráveis) são referentes aos valores iguais ou superiores à média mais uma vez e meia o desvio padrão ($\bar{X} + 1,5\sigma$) dos dados e estão fortemente relacionadas às superfícies de aplanamento superior (SAS) e inferior (SAI).
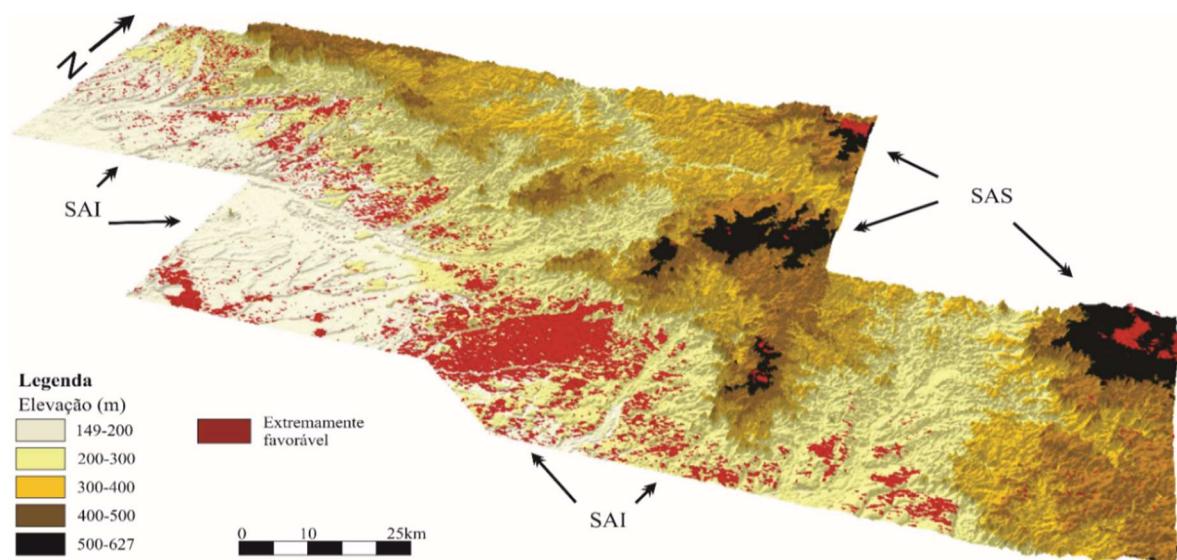


Figura 4.6 - Mapa de previsibilidade de presença de lateritos e fragmentos derivados de sua desagregação, assim como latossolos por meio do método booleano (*index overlay*).
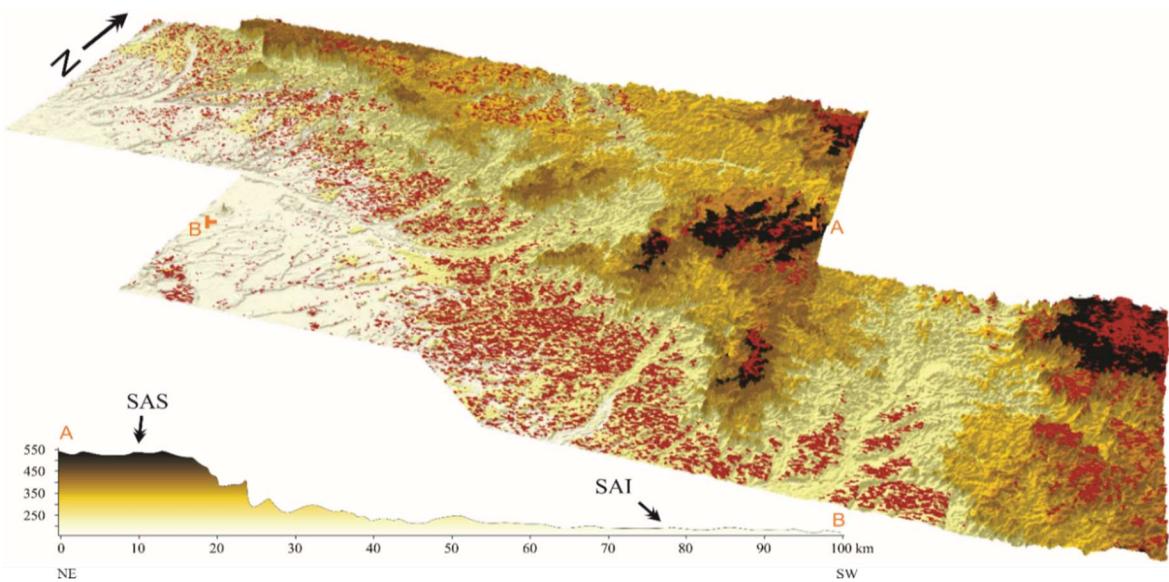
Figura 4.7 - Mapa de previsibilidade de presença de lateritos e fragmentos derivados de sua desagregação, assim como latossolos por meio do operador *fuzzy* gamma (γ = 0.7).

## 4.5 AVALIAÇÃO E COMPARAÇÃO DOS MODELOS E RESPECTIVOS RESULTADOS

As áreas norte e sul apresentam diferenças geomorfológicas e as principais discrepâncias entre os modelos estão relacionadas principalmente a esta variável. Em termos gamaespectrométricos a área norte apresentou razões eTh/K e eU/K mais altas do que as da área sul. Na área sul o parâmetro de corte ($\bar{X} + 1,5\sigma$) delimitou de forma coerente a ocorrência de lateritos. Na área norte o parâmetro de corte também foi eficiente, mas foi menos restritivo, ou seja, considerou valores um pouco mais baixos ($\bar{X} + 1\sigma$) na correlação com a presença de lateritos.

Na área norte os lateritos estão restritos a três intervalos altimétricos bem definidos sendo o primeiro entre 80 e 110 m (margem esquerda do rio Madeira) e os outros 120 e 150 m e 180 e 204 m, esses dois últimos associados a platôs, o que favorece a eficácia do modelo booleano especialmente no domínio centro-leste da área (Figura 4.5).

Na área sul o método booleano gerou bons resultados, mas a ausência de platôs isolados e a maior variedade altimétrica (<300 e > 500 m) contribuiu com resultados um pouco menos eficientes do que os observados na área norte e no método *fuzzy*. Portanto, no método booleano adotado há a necessidade de um rígido controle da variável altimétrica.

O método *fuzzy* utilizado na área norte mostrou-se menos eficiente e não destacou satisfatoriamente todas as áreas com lateritos, provavelmente devido ao seu modo de ocorrência e à existência de 3 intervalos altimétricos em três domínios distintos da área, além de apresentar

respostas radiométricas localmente diferentes para os mesmos produtos (lateritos). Trabalhos futuros realizados em porções mais restritas (subáreas) ou com auxílio de filtros, tais como Pi-shaped, Pi-shaped invertido, etc. podem contribuir com resultados mais animadores.

Em todo caso, na área sul, os intervalos de ocorrência de lateritos são mais amplos e contínuos, e portanto, menos restritivos quando comparados com a área norte. Além disso, os padrões radiométricos são mais homogêneos. Desse modo, os resultados apresentados por meio do método *fuzzy* foram mais representativos (otimistas) para a ocorrência de lateritos.

No geral, o método booleano é indicado quando os lateritos se destacam em platôs e/ou quando o intervalo altimétrico de ocorrência de lateritos é bem definido e/ou restrito. Na ausência de platôs isolados, amplos intervalos altimétricos de ocorrência de lateritos e/ou intervalos pouco conhecidos, a indicação é pelo uso do método *fuzzy*. Em termos gerais, os modelos apresentados contribuíram na discriminação das áreas de ocorrência de lateritos, contudo, fica evidente que cada área possui características únicas (geológicas, geomorfológicas, altimétricas, etc.) que devem ser consideradas no modelamento. A tabela 1 destaca os principais resultados e discrepâncias entre os modelos.

Table 4.1 – Principais discrepâncias entre os modelos previsionais (Herrera 2016 e Iza *et al*. 2016a)

|  | Área Norte | Área Sul |
|---|---|---|
| Área previsional de lateritos | 6,6% (booleano) | 10,71% (máximo-FGO) |
| Razão eTh/K | 355-2020 (X + 1 σ) | 254-1148 (X + 1,5 σ) |
| Razão eU/K | 45-174 | 29-111 |
| Geomorfologia | Platôs isolados | Planície / Planalto |
| Altimetria dos lateritos | 80 a 110 m* / 120 a 150 m / 180 a 204 m | < 300 m e > 500 m |
| Eficiência dos métodos | Booleano (muito bom) | Booleano e fuzzy (muito bom) |

Onde $\bar{X}$ é a média e σ é o desvio padrão. *Margem esquerda do rio Madeira.

# CAPÍTULO 5 - CONSIDERAÇÕES FINAIS

## 5.1 CONSIDERAÇÕES FINAIS

No domínio sudoeste do cráton amazônico os perfis lateríticos são tipicamente imaturos e podem variar desde poucos centímetros de espessura até 6 metros. Os perfis são completos ou incompletos e as melhores exposições podem ser observadas nos topos dos platôs e bordas de escarpas, tanto no sul do Estado de Rondônia quanto no norte, nas cercanias de Porto Velho. Os lateritos são principalmente vermiformes, celulares e pisolíticos a nodulares e frequentemente apresentam estruturas colunares a megacolunares. Essas últimas são mais facilmente observadas no norte de Rondônia. Os lateritos não aflorantes são normalmente cobertos por latossolos que podem atingir cerca de 3 metros de espessura, especialmente na superfície de aplanamento inferior.

A definição de áreas potenciais para a presença de lateritos, por meio da integração de dados multifonte mostrou-se eficiente. Ficou patente que o modelo previsional para a presença de lateritos deve considerar as características locais (geofísica, geomorfologia, altimetria, etc.) de cada área. Nesse ponto de vista, não há um modelo único representativo de toda e qualquer área de estudo, e sim modelos adaptados a cada área/contexto de acordo com suas peculiaridades. Iniciativas como as apresentadas por este trabalho além daquelas desenvolvidas por Carrino *et al.* (2011), Wilford (2012), Arhin *et al.* (2015), Mota e Faria Junior (2016), entre outros, corroboram as asserções supracitadas e ratificam a eficiência dos métodos e da integração multifonte para o mapeamento do regolito.

Apesar das crostas lateríticas macroscopicamente apresentarem características similares em diversas partes do mundo (mineralogia, textura, estrutura, etc.), a correlação entre o CIA e o WIP evidenciou diferenças geoquímicas importantes entre elas. A correlação entre os respectivos índices de intemperismo pode ainda servir como parâmetro para trabalhos futuros que busquem eventuais correlações entre dados gamaespectrométricos e padrões geoquímicos.

O índice de intensidade de intemperismo mostrou-se uma ferramenta robusta e perfeitamente adequada à região amazônica. Nesse aspecto, apesar da gamaespectrometria atuar em profundidades de até 45 cm, contribuiu significativamente para a própria construção do índice de intemperismo e do índice laterítico e consequentemente para o mapeamento dos lateritos e latossolos (determinação de áreas potenciais para a presença de ambos).

O índice laterítico não considera dados altimétricos, mas é respaldado pela forte relação de enriquecimento de Th e U e perda de K no processo intempérico. Nesse sentido, constitui-se em uma ferramenta complementar, mas do mesmo modo eficiente para a delimitação de domínios lateríticos. Por outro lado, a elaboração do LI exige apenas dados

gamaespectrométricos ao contrário do WII que, além da aerogeofísica, exige dados altimétricos e trabalhos de campo.

Os dados de geoquímica de solo, sedimento de corrente, assim como litoquímica dos lateritos, mostraram excelentes correlações com o WII, LI e MI. As associações geoquímicas relacionadas aos elementos alcalinos e alcalinos terrosos igualmente evidenciaram excelentes correlações com as áreas de menor índice de intemperismo e/ou exposição do embasamento pouco ou nada alterado. Por outro lado, as associações dos elementos Al, Ce, Ga, La, Th, U, V e Zr evidenciaram boas correlações com os domínios lateríticos.

Os resultados geoquímicos não destacaram, na área de estudo, anomalias significativas a tal ponto de gerar alvos de interesse metalogenéticos associados a processos supergênicos. Em todo caso, foi fundamental para o apoio e correlação com os dados geofísicos e para as interpretações subsequentes.

Em termos gerais, existem entendimentos equivocados na literatura em relação à gênese e descrições pouco claras dos lateritos, que contribuem negativamente na individualização cartográfica correta das unidades lateríticas. Por outro lado, há escassez de dados geoquímicos sistemáticos integrados a dados geofísicos e principalmente geocronológicos de unidades lateríticas no Brasil. Além disso, a ausência de mapas do regolito contribui negativamente para as discussões relacionadas aos aspectos evolutivos e sua individualização mais criteriosa como unidade geológica/regolítica.

Nesta perspectiva, os resultados aerogeofísicos, geoquímicos e geomorfológicos apresentados nesta pesquisa permitiram a reinterpretação das áreas mapeadas como coberturas sedimentares indiferenciadas para simplesmente lateritos e latossolos associados. Nesse sentido, as áreas associadas aos processos supergênicos foram ampliadas abrindo novas perspectivas de prospecção na porção sudoeste do cráton amazônico, especialmente associadas ao Sn, Au, Ni, Mn, entre outros.

O mapa preliminar do regolito gerado a partir de dados aerogeofísicos, altimétricos, geológicos, geomorfológicos, pedológicos e de campo permitiu o reconhecimento do regolito e dos principais materiais associados. O WII, o modelo previsional para a presença de lateritos, o LI e MI, assim como citado anteriormente, também representam ferramentas importantes para o entendimento do regolito, e para o próprio mapeamento dos lateritos.

As razões gamaespectrométricas (eTh/K, eU/K) evidenciam padrões distintos entre os produtos residuais e aqueles transportados, fato que reforça a importância de sua utilização nas etapas pré-campo e campo. Por outro lado, nas etapas de campo, sugere-se a realização de

descrições e mapeamento dos lateritos sempre vinculados ao processo de intemperismo (residual) e formação do solo (pedogênese). As descrições associadas aos fragmentos derivados de sua desagregação que passaram por algum tipo de transporte local, como aqueles associados a colúvios, devem ser descritos dentro dos próprios colúvios e cartografados de acordo com a escala e área de exposição. Os mapeamentos de detalhe devem se referir a tais colúvios como "constituídos por produtos derivados da desagregação de lateritos" ou simplesmente "constituídos por fragmentos de lateritos". Portanto, os lateritos (autóctones) devem ser referenciados como depósitos residuais e relacionados a processos pedogenéticos (*in situ*) que frequentemente estão vinculados a relevo de topo tabular por vezes associados a colúvios e nunca tratada como produtos sedimentares.

Em todo caso a integração multifonte focada em estudos do regolito deve, especialmente na região amazônica e em áreas de difícil acesso, seguir um protocolo mínimo de acordo com o apresentado na figura 5.1.
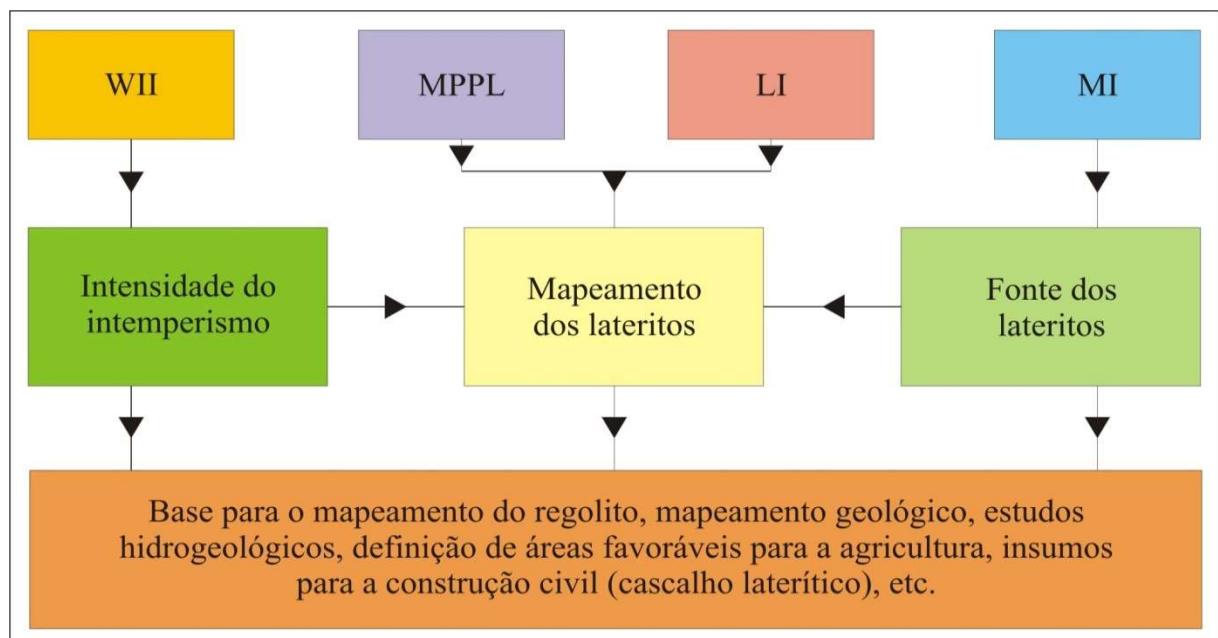


Figura 5.1– Principais produtos gerados neste trabalho e respectivas aplicabilidades. WII – Índice de intensidade de intemperismo. MPPL – Modelo Previsional para a Presença de Lateritos. LI – Índice Laterítico. MI – Índice Máfico

Nessa perspectiva, o mapa do regolito e os demais produtos gerados nesta pesquisa podem ser aplicados com diferentes fins, dentre eles destacam-se:

1) No planejamento das atividades de coleta de amostras (rocha, solo, sedimento de corrente);
2) Em estudos hidrogeológicos, no caso da identificação de áreas com embasamento exposto, solos, etc.;

3) Na determinação de áreas potenciais para a ocorrência de insumos para a construção civil, tais como, cascalho laterítico e outros agregados;

4) No apoio ao mapeamento geológico, geomorfológico, pedológico e do regolito; e

5) No apoio à determinação de áreas favoráveis ou não para agricultura (uso e ocupação do solo). Ex.: áreas com ocorrência de lateritos podem inviabilizar o cultivo devido a sua resistência mecânica e/ou impor a necessidade de significativo uso de corretivos agrícolas (latossolos associados).

Por fim, a integração multifonte apresentada e os diversos produtos gerados constituem procedimentos/produtos que contribuem para garantir um bom nível de confiabilidade do planejamento das atividades de campo e das respectivas interpretações (geológica, geomorfológica, pedológica, etc.), representando um avanço para diversos estudos realizados especialmente na região amazônica e em outras áreas ínvias.

# REFERÊNCIAS

Adamy, A., 2010. Geodiversidade do estado de Rondônia. Porto Velho: CPRM.

An, P.; Moon, W. M.; Rencz, A., 1991. Application of fuzzy set theory to integrated mineral exploration. Canadian Journal of Exploration Geophysics, v. 27, p. 1-11.

Anand R.R., Smith R.E. 1993. Regolith distribution, stratigraphy and evolution in the Yilgarn Craton -implications for exploration. In: Williams P.R. & Haldane J.A. eds. Kalgoolie 93, An International Conference on Crustal Evolution, Metallogeny and Exploration of the EasternGoldfields Extended Abstracts, AGSO Record 1993/54, 187-193.

Anand, R.R.; Paine, 2002. M. Regolith geology of Yilgarn Craton, western Australia: Implication for exploration. Australian Journal of Earth Sciences, 49, 3-162.

Arhin, E.; Jenkin, G.R.T.; Cunningham, D.; Nude, O. 2015. Regolith mapping of deeply weathered terrain in savannah regions of the Birimian Lawra Greenstone Belt, Ghana. Journal of Geochemical Exploration, 159, 194-207.

Beauvais, A., 1999, Geochemical balance of lateritization processes and climatic signatures in weathering profiles overlain by ferricrete in Central Africa. Geochimica et Cosmochimica Acta, 63(23/24): 3939-3957.

Bigarella, J. J.; Becker, R. D.; Passos, E.; Hermann, M. L. P.; Mendonça, M.; Santos, G. F.; Carvalho, S. M. C.; Coitinho, J. B. L. 1996. Estrutura e Origem das Paisagens Tropicais e Subtropicais. Vol. II. Florianópolis, Editora da UFSC.

Bonham-Carter, G.F., 1994. Geographic Information Systems for Geoscientists: Modelling with GIS. Computer Methods in the Geosciences. 13. Pergamon Publications, Oxford.

Büdel, J. 1982. Climatic geomorphology. Princeton: Princeton University Press.

Butt, C. R. M.; Zeegers, H. (Eds.). 1992. Regolith exploration geochemistry in tropical and subtropical terrains. Amsterdam: Elsevier, 607 p. v.4. (Handbook of Exploration Geochemistry).

Carranza, E. J. M. 2009. Knowledge-driven modeling prospectivity. In: _____.Geochemical anomaly and mineral prospectivity mapping in GIS, v 11. Amsterdam: Elsevier. Cap 7. p. 189-246.

Carrino, T. A.; Silva, A.M.; Botelho, N.F.; Silva, A.A.C. 2011. Discriminação de áreas de espesso regolito do leste do Estado do Amazonas usando estatística multivariada, algoritmo hiperespectral e modelagem de dados espaciais. Revista Brasileira de Geofísica, v. 29, n. 1, p. 155-172.

Castro, R.T., 2015. A lateritização na Amazônia Ocidental: Sul de Roraima e norte e noroeste de Rondônia, Manaus. Dissertação (Programa de Pós Graduação em Geociências, Universidade Federal do Amazonas.

Christofoletti, A. Geomorfologia. 2 ed. São Paulo: Edgard Blücher, 1980.

Costa, M.L. 1991. Aspectos geológicos dos lateritos da Amazônia. Rev. Bras. de Geociências, 21, 146-160.

Costa, J.B.S; Bemerguy, R.L; Hasui, Y; Borges, M.S; Ferreira Júnior, C.R.P; Bezerra, P.E.L, Costa, M.L; Fernandes, J.M.G. 1996 Neotectônica da Região Amazônica: Aspectos Estruturais, Tectônicos, Geomorfológicos e Estratrigráficos. Geonomos, 4 (2): 23-44.

Costa, ML. 1997. Lateritisation as a major process of ore deposit formation in the Amazon region. Explor. Mining Geol, 6, 79-104.

Costa, M.L., Fernandez, O.J.C. Requelme, M.E.R., 2005. Depósito de manganês do Azul, Carajás: estratigrafia, mineralogia, geoquímica e evolução geológica. In: J. Marini, E. T. Queiroz e B.W. Ramos (eds.) Caracterização de depósitos minerais em distritos mineiros da Amazônia. DNPM, FINEP, ADIMB, Brasília, p.227-333.

Costa, M.L. 2008. Introdução ao intemperismo laterítico e à laterização In: Licht, O.A.B.; Mello, C.S.B.; Silva, C.R. Prospecção geoquímica:Depósitos Minerais Metálicos, Não-metálicos, Óleo e Gás p. 199-244

CPRM - Serviço Geológico Do Brasil. 2006. Projeto Aerogeofísico Sudeste de Rondônia: relatório final de levantamento e processamento dos dados magnetométricos e gamaespectrométricos. Rio de Janeiro: Lasa Engenharia e Prospecções; Prospectors Aerolevantamentos e Sistemas, 27 v., v. 1.

CPRM - Serviço Geológico Do Brasil. 2010. Projeto Aerogeofísico Rondônia Central: relatório final de levantamento e processamento dos dados magnetométricos e gamaespectrométricos. Rio de Janeiro: Lasa Engenharia e Prospecções; Prospectors Aerolevantamentos e Sistemas, 27 v., v. 1.

Della-Justina, E.E., 1994. Retrato Social da Exploração de Recursos Minerais no Município de Porto Velho-Rondônia. O caso dos lateritos. Monografia (Especialização em Geografia) – Amazônia, questão Regional e Ambiental, Universidade Federal de Rondônia.

Freyssinet, Ph., Butt, C.R.M., Morris, R.C. & Piantone, P. 2005, Ore-forming processes related to lateritic weathering. Economic Geology, 100th Aniversary Volume, 681-722.

Guerra A.T. 1952. Formação de lateritos sob a floresta equatorial amazônica (Território Federal do Guaporé). Revista Brasileira de Geografia, 4, 33-52.

Guerra, A.T. 1953. Observações geográficas sobre o Território do Guaporé. Revista Brasileira de Geografia, 2, 183-302.

Herrera, I.L.I.E. 2016. Utilização de dados altimétricos, geomorfológicos e gamaespectrométricos para a identificação de crostas lateríticas em uma área da porção norte do estado de Rondônia. 2016. Dissertação (Mestrado em Geografia). Universidade Federal de Rondônia. Porto Velho.

Herrera, I.L.I.E, Da Silva Filho, E.P, Iza, E.R.H.F, Horbe, A.M.C. 2016a. Cartografia geológica e geomorfológica de crostas lateríticas na porção norte do estado de Rondônia. Revista Brasileira de Geomorfologia. V.17, n1. http://dx.doi.org/10.20502/rbg.v17i1.880.

Herrera, I.L.I.E.; Silva Filho, E.P.; Iza, E.R.H.F.; Horbe, A.M.C. 2016b. Utilização de dados gamaespectrométricos no apoio à cartografia geomorfológica. In: SIMPOSIO NACIONAL DE GEOMORFOLOGIA, 11, 15-21 set. 2016, Maringá. Anais... Maringá: UGB, 2016b. http://sinageo.org.br/2016/trabalhos/6/6-42-1551.html

IBGE. Mapas interativos, 2006. Disponível em: ftp://geoftp.ibge.gov.br/mapas_interativos/ Acessado em: 20 de junho de 2015.

IBGE. Mapas interativos, 2013. Disponível em: ftp://geoftp.ibge.gov.br/mapas_interativos/ Acessado em: 20 de junho de 2015.

Iza, E.R.H.F; Horbe, A.M.C; Silva, A.M. 2016a. Boolean and fuzzy methods for identifying lateritic regoliths in the Brazilian Amazon using gamma-ray spectrometric and topographic data. Geoderma. V. 269, 27-38.

Iza, E.R.H.F; Horbe, A.M.C; Herrera, I.L.I.E, 2016b. Use of gamma spectrometric and altimetric data to map lateritic crusts on the Western portion of the Brazilian Amazon. Anais do Simpósio Brasileiro de Exploração Mineral – Simexmin. Ouro Preto, Minas Gerais-Brasil.

Lagacherie, P. 2005. An algorithm for fuzzy pattern matching to allocate soil individuals to pre-existing soil classes. Geoderma, n. 128, p. 274-288.

McBratney, A. B.; Mendonça Santos, M.L.; Minasny, B. 2003. On digital soil mapping. Geoderma, v. 117, n. 2. p. 3-52.

McNeil, M., 1978. Lateritic Soils in distinct Tropical Environments: Southern Sudan and Brazil. The Careless Technology.

Moreira, F. R. S.; Almeida-Filho, R.; Camara, G. 2003. Spatial analysis techniques applied to mineral prospecting: an evaluation in the Poços de Caldas Plateau. Revista Brasileira de Geociências, v. 33, n. 2, p. 183-190.

Mota, J.G., Faria Junior, I.R. 2016. A mineral potential mapping approach for supergene nickel deposits in southwestern São Francisco Craton, Brazil. Brazilian Journal of Geology, 46(2): 261-273.

Moss, R.P., 1965 Slope development and soil morphology in a part of south-west Nigeria, Journal of Soil Science 16, 192-209.

Nascimento, T.C.N., 2011. A natureza e aplicação dos materiais lateríticos entre Porto Velho e Morrinhos: relação morfológica e aplicação. Dissertação (Programa de Pós Graduação Mestrado em Geografia – Universidade Federal de Rondônia, Porto Velho).

Nascimento, T.C.N., Maniesi, V., Adamy, A., Nogueira, A., 2012. A natureza e aplicação dos materiais lateriticos na área urbana e entorno de Porto Velho. Rev. Geonorte, Edição Especial, V.2, p.11 – 19.

Oliveira, C.E.S., E Filho, R.S. 2013. Materiais de Construção Civil da Folha Porto Velho (SC.20-V-B-V). Porto Velho, CPRM.

Penteado, M. Mª 1978. Fundamentos de geomorfologia. 2. ed. Rio de Janeiro: IBGE. 154 p.

Pires, A.C.B., Moraes, R.A.V. (2006). New processing Technologies applied do airborne geophysical data: impact on interpretation. *II Simpósio Brasileiro de Exploração Mineral – Simexmin*. Ouro Preto, Minas Gerais-Brasil.

Quadros, M. L. do E.S.; Rizzotto, G.J. (Orgs.). 2007. Geologia e recursos minerais do Estado de Rondônia: texto explicativo do mapa geológico e de recursos minerais do Estado de Rondônia-escala 1:1.000.000. Porto Velho: CPRM. 116 p. Programa Geologia do Brasil-PGB.

Quadros, M.L do E.S.P.; Palmeira, L.C.M.; Castro, C.C. 2011. Geologia e Recursos Minerais da Folha Rio Machadinho SC.20-X-C.

Rizzotto, G. J. (Org.). 2010. Geologia e recursos minerais da folha Pimenteiras SD.20-X-D: Sistema de Informações Geográficas-SIG: texto explicativo do mapa geológico e de recursos minerais da folha Pimenteiras, escala 1:250.000. Porto Velho: CPRM 136 p. il. color.

Rizzotto, G. J. (Org.). 2012. Geologia e recursos minerais da folha Vilhena (SD.20-X-B): Sistema de Informações Geográficas-SIG: texto explicativo do mapa geológico e de recursos minerais da folha Vilhena, escala 1:250.000. Porto Velho: CPRM. 177 p. il. color.

Rondônia, Secretaria de Estado do Planejamento. Plano agroflorestal e Pecuário de Rondônia – Planafloro (bando de dados geográfico). Porto Velho, 2002. Disponível em: <http://www.sedam.ro.gov.br/index.php/component/content/article/109-cogeo/168-acervo-tecnico>. Acessado em 20 de junho de 2015.

Smith, R.E; Anand, A.R.R; Alley, N.F. 2000. Use and implications of paleoweathering surfaces in mineral exploration in Australia. Ore Geology Reviews 16 _2000. 185–204

Tardy, Y.; Roquin, C., 1998, Derive des continents, Paléoclimats et altérations tropicales. Èditions BRGM. Orléans. 473p. 1-33.

Taylor, G.; Eggleton, R. A. 2001. Regolith geology and geomorphology. Chichester: John Wiley.

Thomas, M. F. 1974. Tropical geomorphology: a study of weathering and landform development in warm climates. New York: John Wiley & Sons.

Vasconcelos, P.M; Reich, M; Shuster, D.L. 2015. The paleoclimatic signatures of supergene metal deposits. Elements, v. 11, no. 5, p. 317-322. DOI: 10.2113/gselements.11.5.317

Wilford, J., 2012. A weathering intensity index for the Australian continent using airborne gamma-ray spectrometry and digital terrain analysis. Geoderma 183-184, 124–142. http://doi.org/10.1016/j.geoderma.2010.12.02.

Zimmermann, H. J. 1985. Fuzzy set theory and its applications. Boston: Kluwer-Nijhoff, 363 p.